

DISSERTATION

PROTEOMIC ANALYSIS OF THE EFFECT OF METABOLIC ACIDOSIS ON THE
APICAL MEMBRANE OF THE RENAL PROXIMAL CONVOLUTED TUBULE

Submitted by

Scott J. Walmsley

Graduate Degree Program in Cell and Molecular Biology

In partial fulfillment of the requirements

For the Degree of Doctor of Philosophy

Colorado State University

Fort Collins, Colorado

Spring 2011

Doctoral Committee:

Advisor: Norman Curthoys

Jennifer Deluca

Karen Dobos

Paul Laybourne

Jessica Prenni

ABSTRACT

PROTEOMIC ANALYSIS OF THE EFFECT OF METABOLIC ACIDOSIS ON THE APICAL MEMBRANE OF THE RENAL PROXIMAL CONVOLUTED TUBULE

Metabolic acidosis is a physiological disturbance which results in a decrease in blood and extracellular pH and HCO_3^- . The renal response to this disturbance is initiated in the proximal convoluted tubule (PCT) of the kidney. At the PCT, the brush border membrane facilitates solute reabsorption and excretion of acid during acidosis. However, the extent of the global remodeling of proteins at the brush border remains mostly unknown. Therefore a proteomic investigation of the remodeling of these proteins during metabolic acidosis at the brush border was completed. First, using LTQ mass spectrometry and spectral counting, an enrichment method was tested that analyzed brush border membrane vesicles (BBMV) from cortex versus those which were derived from purified proximal convoluted tubules. From these results we detected and hypothesized that enzymes of glucose metabolism localized at the brush border would be altered in abundance during acidosis at the PCT brush border. Next, we performed a quantitative analysis of the temporal response to metabolic acidosis during 1-d, 3-d and 7-d acidosis using Q-TOF mass spectrometry and spectral counting. As expected, the results indicated a decrease of enzymes of glucose metabolism including Fructose-1,6-

bisphosphatase 1 and Enolase A. Aldolase A was found to be transiently decreased during 1-d and 3-d acidosis. In addition, the Na⁺-glucose transporter 2 was found to be transiently increased during 1-d and 3-d acidosis. Finally, to confirm these abundance changes detected using spectral counting, an accurate mass and time tag method was developed. Using this method, we successfully developed an AMT database of the previously identified spectra. This database was used to match peptides detected using QTOF-LC-MS to the previously identified peptides. Peptide abundance by spectral counting was validated using the more accurate peak intensities and were generally in concordance with those abundance measurements using spectral counting. The developed model suggested a mechanism for internalization of these enzymes of glucose metabolism in support of glutamine metabolism, which is central to the cellular response to acidosis by the PCT.

ACKNOWLEDGEMENTS

I would like to extend my greatest thanks to my committee members Dr. Norm Curthoys, Dr. Jennifer Deluca, Dr. Karen Dobos, Dr. Paul Laybourn, Dr. Jessica Prenni and Dr. Ken Reardon for their advice, guidance and optimism. I would like to extend a special thanks to my advisor Dr. Norm Curthoys for his patience, support and the warm-felt welcome he always has given me under his guidance. By a strange twist of fate after certain family events, I felt compelled to perform my doctoral research for Norm. To this day, I am glad I did. I especially would like to thank Dr. Jessica Prenni and Dr. Corey Broeckling, who both provided technical support for our mass spectrometry experiments, and who always provided a wonderful forum for discussion- whether it was scientific or related to malt beverages. Thank you to Dr. Ann Hess for her help with statistics and our great discussions about proteomics and statistics. Thanks to Brian Cranmer for training with the QTOF mass spectrometer. I also would like to thank the members of the Curthoys Lab who have provided a source of friendship, discussion, and support. I would especially like to thank my family, especially my wife Amanda, who has provided me with the greatest of support. To my community here in Fort Collins, some of whom I have known for over 15 years, they were always there for the greatest of challenges always providing their support...and some of who made for the greatest adventures. And to my Father, who was always watching over me.

TABLE OF CONTENTS

Preliminaries

Abstract	ii
Acknowledgements	iv
Table of contents	v
List of figures and tables	ix
List of abbreviations	xi

Chapter 1. Introduction

1.1 Introduction and historical background	1
1.2 Definition and Causes of metabolic acidosis	3
1.3 Glutamine and renal metabolism during normal physiology	4
1.4 Glutamine catabolism during acidosis	5
1.5 PCT response to metabolic acidosis	9
1.6 Proximal tubular physiology	10
1.7 Proximal convoluted tubular brush border membrane physiology	11
1.8 Brush border membrane physiology during acidosis	12
1.9 Current status of proteomic studies of proximal convoluted tubules	14
1.10 Enrichment of brush border membranes from PCT	17

Chapter 2. Proteomic tools for the study of renal physiology

2.1 Introduction	18
2.2 2D-PAGE proteomics	18
2.3 Shotgun proteomics	19
2.4 Mass spectrometry instrumentation	21
2.5 Quantitative proteomics using labeled peptides	23
2.6 Label-free quantitative proteomics: spectral counting	25

2.7 Label-free quantitative proteomics: precursor ion peak intensity and AMT	26
Statement of Problem and Aims	30
Chapter 3. Proteomic analysis of brush border membrane vesicles isolated from purified proximal convoluted tubules	
3.1 Abstract	33
3.2 Introduction	34
3.3 Materials and Methods	36
3.3a Materials	36
3.3b Purification of proximal convoluted tubules	37
3.3c Isolation of brush border membrane vesicles	37
3.3d γ -Glutamyltranspeptidase assay and immunoblot analysis	38
3.3e Sample preparation and mass spectrometric analysis	39
3.3f Bioinformatic analysis	40
3.3g Enrichment of gene functional annotations	42
3.4 Results and discussion	42
3.4a Enrichment of BBMVs from cortex and from proximal convoluted tubules	42
3.4b Proteomic analysis of BBMVs _{CTX} and BBMVs _{PCT}	43
3.4c Quantitative analysis of protein abundance in BBMVs _{CTX} and BBMVs _{PCT}	53
3.5 Acknowledgements	66
Chapter 4. Proteomic Analysis of the Effect of Metabolic Acidosis on the Apical Membrane of the Renal Proximal Convoluted Tubule	
4.1 Abstract	76
4.2 Introduction	77
4.3 Materials and methods	80
4.3a Animals	80
4.3b Purification of proximal convoluted tubules	81
4.3c Isolation of brush border membrane vesicles	81
4.3d γ -Glutamyltranspeptidase assay	82

4.3e	Sample preparation and mass spectrometric analysis	82
4.3f	Bioinformatic analysis	83
4.3g	Spectral counting	84
4.3h	Cluster analysis and heat maps	85
4.3i	Statistical Analysis	85
4.3j	Enrichment of Functional Annotations	86
4.4	Results	86
4.4a	Purification of Proximal Convoluted Tubules and BBMVs	86
4.4b	Proteomic analysis of BBMVs _{PCT} from control, 1-d, 3-d and 7-d acidotic rats	87
4.4c	Quantitative analysis of changes in protein abundance in BBMVs _{PCT} during onset of acidosis	95
4.5	Discussion	107
4.5a	Proteins involved in carbohydrate transport and metabolism.	107
4.5b	Cytoskeletal, scaffolding and trafficking proteins	110
4.5c	Amino acid transport and metabolism	111
4.5d	Relevance to brush border membrane physiology	111
4.6	Acknowledgements	112
Chapter 5. Validation by AMT and LC-MS Mass Spectrometry		
5.1	Introduction	118
5.2	Materials and methods	120
5.2a	Materials	120
5.2b	AMT database preparation	120
5.2c	LC-MS analysis	120
5.2d	LC-MS peptide feature finding and matching to the AMT database	121
5.2e	Quantitation of relative abundance changes	121
5.2f	Additional statistical analysis	122
5.3	Results	122
5.3a	Mass distribution of interpreted tandem mass spectra and uniqueness statistics	122

5.3b Development of the AMT database and matching to LC-MS features	127
5.3c Data normalization	130
5.3d Significance analysis for peptide level changes in abundance	130
5.3e Significance analysis for protein level changes in abundance	137
5.3f Comparison of measurements of abundance by LC-MS vs SpC	142
5.3g Western blot data of SC5A2 and GLUT2 changes during MA	142
5.4 Discussion	147
Chapter 6. Conclusions and Future Directions	
6.1 Overview	149
6.2 SGLT2., GLUT2, ENOA and FBP1 altered abundances during metabolic acidosis	152
6.3 Future directions	155
6.4 Conclusions	157
References	158

LIST OF FIGURES AND TABLES

Figure 1.1 Overview of GLN metabolism in response to chronic acidosis at the proximal convoluted tubule	7
Figure 2.1 Digital 2-D map of C18-NSI-MS data	28
Figure 3.1 Enrichment of γ -glutamyltranspeptidase activity in isolated BBMV	45
Figure 3.2 Western blot analyses of the purity of the BBMV _{CTX} and BBMV _{PCT}	47
Figure 3.3 Proteomic Analysis of BBMV _{CTX} and BBMV _{PCT}	49
Figure 3.4 Comparison of the total spectral counts associated with the 20 most abundant proteins identified in the combined BBMV _{PCT} and BBMV _{CTX}	51
Figure 3.5 Scatter plots of total spectral counts in replicate samples	56
Figure 3.6 Statistical analysis of differences in abundance of the proteins identified in the BBMV _{CTX} and BBMV _{PCT} samples	58
Figure 3.7 Functional classification of the proteins that are significantly enriched in the BBMV _{PCT} (Panel A) and the BBMV _{CTX} (Panel B) samples	60
Figure 3.8 Comparison of the total spectral counts associated with proteins that are significantly enriched in the BBMV _{PCT} or BBMV _{CTX} sample	62
Figure 3.9 Validation of the enrichment in BBMV _{CTX} of proteins that are preferentially expressed in the S3 segment of the proximal tubule	64
Table S1 List of proteins identified by the proteomic analysis in chapter 3.	67
Figure 4.1 Onset of acidosis causes an increase in γ -glutamyltranspeptidase activity in isolated BBMV _{PCT}	88
Figure 4.2 Work flow for analysis of peptides using a QTOF mass spectrometer	90
Figure 4.3 Functional classification of proteins identified in control and acidotic BBMV _{PCT} samples	93
Figure 4.4 Correlation of overall proteomic data obtained from control,	96

1-d, 3-d and 7-d acidotic rats.

Figure 4.5	Cluster analysis of the spectral count data.	99
Figure 4.6	Statistical analysis of spectral count data	101
Figure 4.7	Global analysis of significant changes in protein abundance	103
Table 4.1		113
Table 4.2		116
Figure 5.1	Effect of proteotypic peptide distribution on uniqueness statistics	123
Figure 5.2	Mass versus retention time plots	125
Figure 5.3	Analysis by normalized elution times for the AMT identified and filtered peptide features	128
Figure 5.4	Boxplots of the peptide abundances for each LC-MS injection replicate	131
Figure 5.5	Principle components analysis of the peptides identified using AMT	133
Figure 5.6	Peptide level volcano plots of log 2 fold change of abundance versus pvalue	135
Figure 5.7	Peptide level abundance analysis of fructose-1,6-bisphosphatase -1 (FBP1).	138
Figure 5.8	Log fold changes of selected markers identified using AMT	140
Figure 5.9	Correlation of log 2 fold changes for selected markers using SpC versus AMT	143
Figure 5.10	Immunoblot analysis of SGLT2 and Glut2 expression. 20ug of cortical homogenate was probed for PCT specific markers SGLT2 and GLUT2 expression.	145
Table 5.1	Proteins altered during MA	148
Figure 6.1	Model for internalization of FBP1 and ENOA	163

LIST OF ABBREVIATIONS

1DE	One dimensional electrophoresis
2DE	Two dimensional electrophoresis
2D- PAGE	Two dimensional poly acrylamide gel electrophoresis
AMT	Accurate mass and time tag
ANOVA	Analysis of variance
BBMV	Brush border membrane vesicles
BBMV _{CTX}	Brush border membrane vesicles from cortex
BBMV _{PCT}	Brush border membrane vesicles from PCT
C18-ESI-MS/MS	Reversed phase ESI tandem mass spectrometry
C18-NSI-MS	Reversed phase nanospray mass spectrometry
CID	Collisionally induced dissociation
CTX	Kidney cortex
DIGE	Two dimensional difference gel electrophoresis
DTT	Dithiothreitol
ENOA	Enolase A
ESI	Electrospray ionization
FBP1	Fructose-1,6- <i>bis</i> phosphatase
FDR	False discovery rate
FTICR	Fourier transform ion cyclotron resonance
GLN	Glutamine
GLUT2	Glucose transporter 2
HPLC	High performance liquid chromatography
iCAT	Isotope-coded affinity tags
iTRAQ	Isobaric tags for relative and absolute quantitation
LC-MS	Liquid chromatography mass spectrometry
LC-MS/MS	2--dimensional liquid chromatography/mass spectrometry
LTQ	Linear ion trap mass spectrometer
MA	Metabolic acidosis
MAPK	Mitogen activating protein kinase
MS	Mass spectrometry
MS/MS	Tandem mass spectrometry
MUDPIT	multidimensional protein identification technology
m/z	Mass over charge ratio
NPT2	Na ⁺ dependent phosphate transporter 2
NSI	Nanospray ionization
PEPCK	Phospho <i>enol</i> pyruvate carboxykinase
PCK1	PEPCK gene
PCT	Proximal convoluted tubule
qRT-PCR	Quantitative real time PCR
RSc	Ratio of spectral counts

RT	Retention time
QQQ	Triple quadrupole mass spectrometer
QTOF	Quadrupole time of flight mass spectrometer
SCX	Strong cation exchange
SGLT2	Na ⁺ facilitated glucose transporter 2
SILAC	Stable isotope labeling with amino acids in cell culture
SpC	Spectral counting
TMD	Transmembrane domain

CHAPTER 1

Introduction

1.1 Introduction and Historical Background

Metabolic acidosis is a physiological disturbance which results in a decrease in blood and extracellular pH and HCO_3^- . The renal response to this disturbance is initiated in the proximal convoluted tubule (PCT) of the kidney. The PCT cell is the primary site of NH_4^+ and HCO_3^- ion synthesis that contributes to the maintenance of blood pH during the onset of acidosis. Current techniques and methodologies can give exciting and new insight into the molecular mechanisms that regulate this response. However, basic research into the understanding of the mechanisms of acid-base homeostasis extends over a century. In 1902, Barcroft first described a method to measure carbonic acid, H_2CO_3 , in blood[1]. However, it was Hasselbalch who first described the relationship of the levels of CO_2 in blood with pH leading to the well known Henderson-Hasselbalch equation and its application to the determination of blood pH [2]. In 1923, La Mer described the measurement of CO_2 as a direct measurement of pH[2]. These landmark experiments, among others, lead to the suggestion that the rapid dissociation of carbonic acid contributed to buffering of blood pH. Ammonium ions, which provide a measure of the acid excreted during metabolic acidosis, was first measured with precision using the Folin-Denis method[3]. Using this method, Nash and Barcroft, in 1921, described that

the kidney produces the ammonium ions it excretes. In 1943, Van Slyke observed in dogs that GLN extracted from blood could account for 60% of the total ammonium excreted by the kidneys during acidosis[4]. Later observations by Kennan *et al.* suggested that increases in the concentrations of glutamine (GLN) in blood occur in diabetic ketoacidosis [5]. Kennan realized that glutamine concentration increased as acidosis increased. As such, these observations linked the production of GLN with a decrease in blood pH. However, it was an ¹⁵N metabolic tracer experiment that definitively linked GLN synthesis in the liver with GLN catabolism and ammonium production in the kidney during chronic metabolic acidosis [6]. Later, it was Goorno who suggested that gluconeogenesis was a metabolic pathway that was stimulated concurrent with ammonium production[7, 8]. Later studies elucidated the interorgan relationship for controlling blood ammonia levels through GLN production and established accurate blood and urinary measurements for metabolic intermediates for the response to acidemia[9, 10]. Physiological and anatomical studies and their measurements of filtrate and blood aided in the determination of the response along the nephron of the kidney [11]. These experiments subsequently determined the significance of renal proximal tubular contribution to acid-base regulation. Elucidation of the mechanisms for transcriptional activation of phosphoenolpyruvate carboxykinase 1 (PCK1) and mitochondrial glutaminase followed. In these experiments, activation of p38 mitogen activating protein kinase (MAPK) during onset of acidosis induced PEPCK expression[12, 13]. More recently, selective stabilization of PCK1 and mitochondrial glutaminase mRNAs were shown to contribute to the renal response to acidosis[14-18]. Taken together, these many years of experiments outlined how glutamine catabolism is

related to the excretion of ammonia and the production and reabsorption of bicarbonate in response to acidosis. However many of the regulatory, metabolite and pH sensing, and signal transduction mechanisms remain to be elucidated.

1.2 Definition and causes of metabolic acidosis

Metabolic acidosis is a physiological disturbance which results in a decrease in blood and extracellular pH and HCO_3^- . The condition is caused by a decrease of available bicarbonate (HCO_3^-), the primary buffer in blood, or an increase in acid[19]. Bicarbonate and the partial pressure of dissolved arterial CO_2 (pCO_2) tightly regulate blood pH. Metabolic acidosis is also characterized with a decrease in hepatic urea production and an increase in renal ammonium ion production[20]. Additionally, increased glutamine (GLN) synthesis in both perivenous hepatocytes and in skeletal muscle tissue lead to an increase in blood GLN concentration [9, 21]. The proximal tubule cell in kidney responds to the increase in blood concentration of glutamine by activating the catabolism of glutamine.

Generally, physiological disturbances which cause a significant decrease in plasma pH and blood are called acidemia. Those disturbances which are metabolic in origin are called metabolic acidosis (MA). Physiological disturbances which can cause MA include diabetes, chronic obstructive pulmonary disorder, cancer, alcoholism, starvation, digestive abnormalities (diarrhea) and genetic disorders such as the renal Fanconi syndrome. These disturbances are ubiquitously characterized by decreased blood pH ($\text{pH} < 7.35$) and by a decrease in bicarbonate buffering capacity. However, the

mechanism by which metabolic acidosis progresses is as varied as the primary disturbance causing MA. These include:

- 1) Loss of bicarbonate due to diarrhea and other conditions that cause rapid water loss
- 2) Increased use of bicarbonate due to buffering of increased organic acids in the blood due to lactic acidosis (cancer) or ketoacidosis (diabetes, cancer, chronic obstructive pulmonary disorder, starvation)
- 3) Loss of renal capacity to reabsorb bicarbonate (renal Fanconi syndrome)

As such, the primary disturbance can typically be determined by profiling of urinary and blood solutes. Electrolytes in blood (Na^+ , K^+ , HCO_3^- , Cl^-) help to determine the underlying cause of MA. This can determine if the MA is caused by bicarbonate buffering of organic acids leading to an increased anion gap, which is typical of those conditions where acid production increase. Alternatively, these measurements can also determine if the MA is due to a loss of bicarbonate ions, such as is typical in patients with chronic diarrhea.

1.3 Glutamine and renal metabolism during normal physiology

Glutamine serves as a primary carrier for nitrogen transport between the organs. It's high abundance (0.5 - 1.0mM) in blood together with it's high relative abundance in the tissues other than kidney ensure a readily releasable pool for use during stress[21]. As a metabolite, GLN is consumed as a fuel in liver, the digestive tract, and brain. Production of GLN occurs by the ATP-dependent glutamine synthetase, an enzyme highly enriched in perivenous hepatocytes and skeletal muscle[22]. Glutamine

catabolism supports additional metabolic processes such as ureagenesis and gluconeogenesis in periportal hepatocytes and ammoniogenesis and gluconeogenesis in the kidney.

During normal physiology, GLN enters the filtrate and is extracted from the lumen of the nephron but very little is catabolized by the kidney[21]. The apical B⁰AT1 transporter aids the Na⁺-dependent facilitated transport into the PCT, followed by the basolateral transport of GLN by the system L type heteromeric transporter, LAT2[23, 24]. Additionally, a small proportion of the recovered GLN (~10%) is catabolised by the PCT in a mechanism central to acid-base maintenance. Specifically, GLN enters the mitochondria by an unidentified transporter and is subsequently deamidated by mitochondrial glutaminase (GA) to glutamate. Subsequent deamination by glutamate dehydrogenase produces α -ketoglutarate, which then enters the citric acid cycle. These deamidation steps result in the production of two NH₄⁺ ions which are eventually excreted in the urine.

1.4 Glutamine catabolism during acidosis

PEPCK is a rate limiting step required for the entrance of phosphoenolpyruvate into the gluconeogenic pathway. Immunohistochemistry has shown PEPCK to be highly expressed in liver, intestinal enterocytes, and the PCT of the kidney[25]. Treatment of porcine PCT cells with acidotic medium leads to *PCK1* gene activation possibly by the activation of p38 mitogen activated protein kinase (MAPK) signaling pathway[12]. While PEPCK controls the rate of entrance into gluconeogenesis, fructose-1,6 bisphosphatase 1 (FBP1) is also a rate limiting step in the pathway. Porcine kidney LLC-

PK1 cells lack endogenous FBP1 and the ability to produce glucose. Selection of cells by glucose starvation produced a line of cells that express FBP1 and are gluconeogenic [26, 27]. In mammals, enzyme activity assays have determined that PEPCK and FBP1 are highly enriched in the PCT when compared to the more distal portions of the nephron [28, 29]. As such, FBP1 and PEPCK are important regulators of gluconeogenesis during acidosis.

During acute acidosis (less than one day), blood GLN concentration ([GLN]) increases significantly [14]. This leads to an increase in the [GLN] found in glomerular filtrate. To handle the increases in blood and glomerular filtrate, transport of GLN into the proximal tubule increases at both the apical brush border and basolateral sides of the cell. Approximately one-third of the GLN in the blood that enters the cell is deamidated by mitochondrial glutaminase and then deaminated by Glutamate dehydrogenase resulting in a pronounced increase in NH_4^+ produced from the GLN that enters the cell (Figure 1.1). The increased GLN utilization and NH_4^+ excretion are supported by increased levels of mitochondrial glutaminase and Glutamate dehydrogenase protein. α -ketoglutarate conversion to succinyl CoA by α -KG-dehydrogenase produce one HCO_3^- molecule. Subsequent metabolic steps lead to the production of malate. The malate is then transported to the cytosol and consumed in the synthesis of glucose [30, 31]. Following conversion in the cytosol to oxaloacetate by cytosolic malate dehydrogenase, another HCO_3^- is released during conversion to phosphoenolpyruvate by PEPCK.

As a result of GLN catabolism during MA as outlined during these steps, a net of two NH_4^+ ions and two HCO_3^- ions are produced to help restore blood pH.

Figure1.1 Overview of GLN metabolism in response to chronic acidosis at the proximal convoluted tubule. The proximal tubule responds by increasing synthesis of genes involved in ammoniagenesis, bicarbonate production and gluconeogenesis. Red arrows indicate increased abundance of gene products. Green arrows indicate increased metabolic byproducts. Adapted from Weiner, 2007[32].

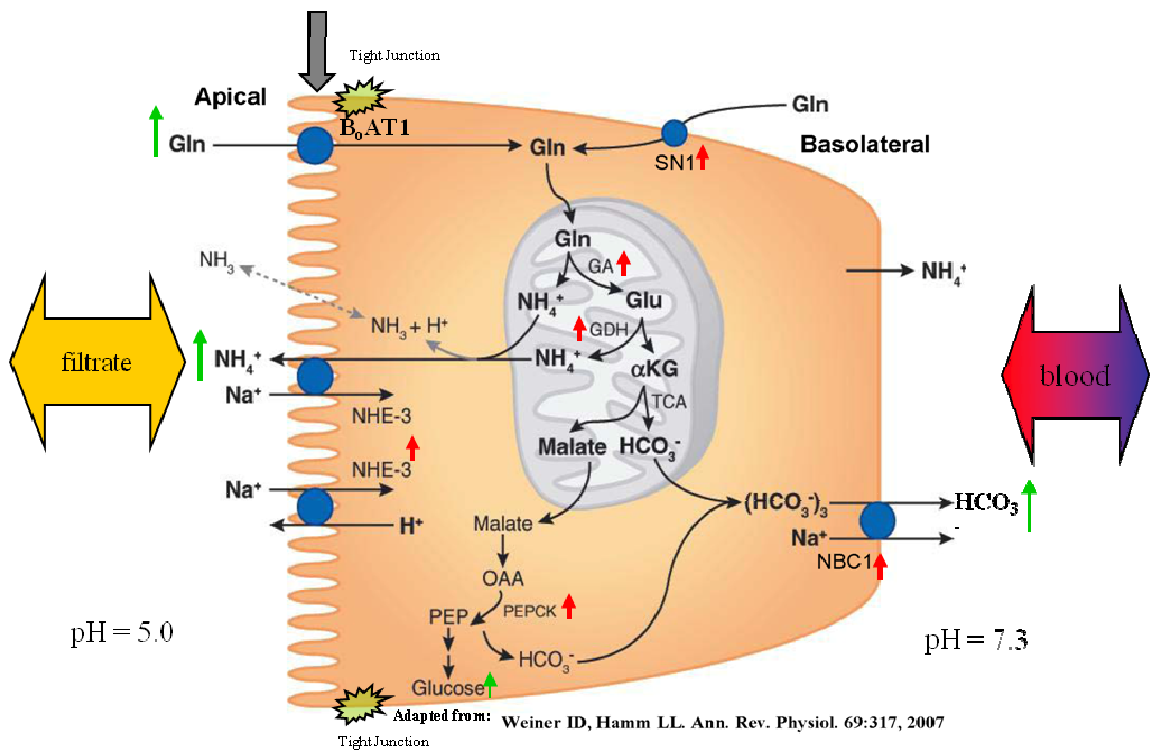


Figure 1.1

Additionally, for each GLN metabolized, a net $\frac{1}{2}$ glucose molecule is produced during gluconeogenesis.

1.5 PCT response to metabolic acidosis

During acute (<1 days) MA, renal GLN extraction rapidly increases. As plasma GLN increases, renal extraction of GLN from the filtrate increases. Additionally, the abundances of PEPCK and mitochondrial glutaminase are increased due to the increased transcription of their mRNAs. Subsequently, PEPCK, mitochondrial glutaminase and Glutamate dehydrogenase mRNAs are stabilized by cytosolic factors possibly aiding in the chronic response to acidosis. The increases in mRNA half lives lead to a long term increase in protein levels during chronic metabolic acidosis[18, 33-36]. These in turn probably aid the increased catabolism of GLN.

During chronic (> 1 day) acidosis, the transcription and/or stability of several mRNAs increase to handle the increased influx of cellular GLN. The mitochondrial phosphate dependent glutaminase (KGA), glutamate dehydrogenase, and phosphoenolpyruvatecarboxy kinase (PEPCK) all increase in abundance. To aid with flux across the proximal tubule cell membrane, the abundances of the electrogenic $\text{Na}^+/\text{3CO}_3^-$ cotransporter 1 (NBCe1), system N glutamine transporter 1 (SN1), and the apical Na^+/H^+ cotransporter 3 (NHE3) all increase [37-40]. Increased influx of GLN is aided by the SN1 transporter. Ammonium excretion to the lumen is facilitated by the NHE3 antiporter leading to a general acidification of the urine, while NBCe1 aid in the recovery of HCO_3^- [39]. Overall, the increased abundances of these proteins contribute to the ability of the proximal tubule cell to increase flux and metabolism of glutamine in

the cell, the net excretion of acid from the body as ammonium salts, and the attempt to restore blood pH by production of bicarbonate [41].

1.6 Proximal Tubular Physiology

The proximal convoluted tubule (PCT) is the earliest part of the nephron after the glomerulus. The cells are polarized epithelia containing an apical brush border which aid with the reabsorption of solutes that pass through the glomerulus. Typical glomerular filtrate contains salts (Na^+ , Cl^- , K^+), phosphate, urea, and glucose in addition to peptides (<10kDa). The large surface area of the brush border aids in the selective reabsorption of most of these solutes during normal cell function. In addition, the PCT aids in the maintenance of physiologic function including acid-base homeostasis, regulation of blood glucose and recovery of protein. Recoverable ions and other small molecules are transported via vectorial transport processes usually in a Na^+ -dependent manner. These include recovery of glucose by the Na^+ -dependent glucose symporter (SGLT2) [42, 43] and amino acids by various solute carrier family members whose gradient potentials are maintained by the basolateral Na^+/K^+ ATPase [44, 45]. Larger peptides and molecules are recovered by the cell's megalin, cubulin and Disabled Homologue 2 (DAB2) endocytic machinery [46] and supply an important mechanism for protein recovery during normal normal condition and during stress such as renal failure [47, 48].

Recently, there has been an increase in the interest of controlling the glucose reabsorptive process by selectively inhibiting SGLT2 [49, 50]. This process has been considered important for aiding in altering the proximal tubular function during type 2 diabetes. In these studies, selective inhibitors of SGLT2 successfully decreased blood

glucose levels by modulating the ability to excrete glucose into the urine (glucosuria). While further validation of the total physiological effects of these selective inhibitors remains to be determined, the importance of further elucidating the markers of the PCT brush border membrane during pathology is evident. This is due to the important role the PCT contributes toward the recovery of solutes from filtrate and the maintenance of acid-base during such pathologic events such as diabetes and MA. This suggests that studying the effect of acidosis on the brush border membrane can give insight into potential novel mechanisms for the MA response in concordance with the causative disease.

1.7 Proximal convoluted tubular brush border membrane physiology

The PCT apical membrane supports multiple functions. One such function is the reabsorption of organic solutes passively filtered by the glomerulus. This filtrate includes peptides, organic solutes (glucose, amino acids), phosphate, inorganic ions and water. Of these solutes, the PCT actively recovers nearly all the glucose present (> 90%) through a process that is facilitated by the sodium glucose transporter 2[42, 43]. Such processes are typically accomplished by facilitated co-transport with Na^+ as the counter ion, via a Na^+ concentration gradient that is maintained by the basolateral Na^+/K^+ ATPase. The Na^+ gradient also contributes to the acidification of luminal fluid, a process that requires Na^+ coupled H^+ transport via the apical sodium hydrogen exchanger 3. A vacuolar H^+ -ATPase (V- H^+ ATPase) also contributes to the acidification of the luminal fluid[51]. Additional functions of the brush border include peptidase activities via dipeptidyl peptidase 4, glutathione metabolism via γ -glutamyltranspeptidase 1 (GGT1) activity, and

Megalyn and Disabled homologue 2 (Dab2) mediate the endocytic mechanism for receptor mediated endocytic recovery of molecules into the PCT[52-56].

1.8 Brush border membrane physiology during acidosis

Glutamine uptake and ammonium and bicarbonate ion release from the proximal tubule is handled by transport processes at both the basolateral and apical membranes. In recent studies of two and seven days acidotic mice, the SN1, NHE3, and NBCe1 transporters all increased in abundance as indicated by quantitative real time PCR (qRT-PCR) and validated by Western blot and immunofluorescence [37, 40, 57]. Additionally, the heterodimeric cationic L type amino acid transporter 1 (y^+ LAT1) decreased in abundance. Most interestingly, SN1 expression, which is found predominately in the S3 segment or proximal straight tubule cells during normal acid-base balance, increases during chronic acidosis in the basolateral membrane of the S1 and S2 segments of the proximal convoluted tubule [40]. It was suggested that as a result of this response, glutamine was preferentially transported into the cell from the basolateral surface for subsequent phosphate-dependent glutaminase activity. However, previous data produced by Foreman *et. al* indicated that glutamine is also extracted from the lumen via an alternate apical transport mechanism during acidosis[58].

In 1983, Foreman isolated brush border and basolateral membranes from kidneys of 10 day acidotic rats. These were assayed for [14 C]-L-glutamine transport in the presence of NaCl. The results indicated little change in the transport of glutamine in basolateral membranes for the acidotic versus control group. However, the brush border membrane vesicles showed a 1.9 fold increase in V_{max} for glutamine in acidotic rats (V_{max} = 4.8 control versus 9.8 acidotic expressed as nmol / 15s / mg protein). The studies

completed by Moret utilized mRNA and membrane protein isolated from total kidney whereas the study by Foreman utilized brush border membrane vesicles (BBMV) isolated from dissected cortex. Both studies elucidated mechanisms for GLN uptake by both basolateral and apical sides of the cell. Additionally, the data produced in both studies was strongly influenced by cell type heterogeneity that was introduced by the source of the sample being assayed. The samples produced in both studies were from cortical homogenates which contain PCT (S1 and S2), proximal straight tubules (S3), and partial segments of the thick ascending limb and collecting duct.

In addition to transport function, the apical membrane in proximal tubules may contain additional uncharacterized proteins that may initiate a response to acidosis. For example, the endothelin receptor mediates the increase in NHE3 transcription and protein abundance [59, 60]. In addition, NHE3 mRNA and protein abundance are reduced upon parathyroid hormone (PTH) stimulation in cultured opossum kidney cells. [61, 62]. NHE3 function is also modulated by its interaction partners in a 9 protein complex including NHERF1/2 [63, 64]. These altered abundances and interactions could be detected further elucidated using a global expression profiling technique.

During pathogenesis of metabolic acidosis, the PCT brush border membrane responds by increasing the abundance of NHE3 to handle the increased excretion of ammonium ions by aiding in the acidification of the urine [65-67]. The primary transport mechanisms for handling the increased ammonium ion, bicarbonate ion, and glucose production during MA are well understood [40, 68, 69]. However, little is known about the additional metabolic constraints, the cellular signaling pathways and concordant changes in protein abundances that are induced by MA. Additionally, recent mRNA

transcript microarray, qRT PCR, and protein abundance measurements have suggested additional metabolic intermediates are required for maintaining the flux required to aid the PCT response to chronic metabolic acidosis[70-72]. However, such experiments have not always been clearly defined with anatomical precision and, due to the heterogeneity of the assays, are not considered specific to the PCT. Thus, proteomic studies of PCT specific samples are ideally suited to aid in the rapid discovery of additional mechanisms to the response to MA. The isolation of PCT cells from the S1 and S2 segments may provide a more specific approach to elucidate the response to acidosis specifically within the proximal tubule brush border membrane.

1.9 Current status of proteomic studies of proximal convoluted tubules

While the literature for ‘omics’ studies (transcriptomics, proteomics, genomics) of renal physiology and pathophysiology is extensive, such studies of the proximal tubule have been limited. The earliest such study by Cheung *et al.*[73] utilized Percoll density gradient isolated PCTs to discover mechanisms about the PCT response to a low phosphate diet. Bandara *et al.* later described the PCT stress response to the necrotic inducing factors 4-aminophenol (4-AP), D-serine and cisplatin. However, Bandara used correlation of macroscopic inspection of PCTs with an indirect proteomic analysis of the plasma markers[74]. Both of these studies relied on two dimensional gel electrophoresis (2-DE) analysis.

A later publication by Cutillas revealed insight into the urinary proteome during a form of Fanconi Syndrome known as Dent’s disease[75]. Such patients lack sufficient proximal tubular reabsorption caused by a chloride proton antiporter 5 (*Clc5*) mutation.

This subsequently abolishes the megalin mediated PCT endocytosis and recovery of peptides from the urinary filtrate. Complementary proteomic approaches (one dimensional gel electrophoresis (1DE) and two dimensional gel electrophoresis (2DE)) were used to screen urine samples from Dent's patients. A few additional studies followed which attempted to determine the effects of diabetes (etiological to MA) and an angiotensin converting enzyme (ACE) inhibitor on sodium uptake[76-79]. However, none of these studies specifically attempted to profile the PCT response to acidosis.

In 2007, Curthoys *et al.* described a proteomic approach to study the proteome of proximal tubule cells for 0 and 7 day acidotic rats[33]. Proximal tubules from rat were first isolated by Percoll density equilibrium centrifugation and then analyzed using two dimensional difference gel electrophoresis (DIGE). The results identified several known markers for acidosis including PEPCK, Glutamate dehydrogenase, and GA. In addition, novel proteins were identified as potential markers of the acidotic response. Most interestingly, such proteins included those involved in glycine metabolism, fatty acid utilization, calcium sensing mechanisms and pyruvate utilization. However the identifications were generally lacking for the identification of proteins of the plasma and mitochondrial membranes. This was due to the method of extraction and subsequent conditions for isoelectric focusing of the proteins. Specifically, the first dimension of DIGE subjects proteins to isoelectric focusing. This step required the use of mild non-ionic detergents to maintain charge necessary for isoelectric focusing. As such, integral and associated membrane proteins were not routinely identified. But the DIGE method is advantageous due to the multiplexing of samples resulting in more accurate normalization and subsequent abundance measurements between the samples. Potential

markers identified by the DIGE method were validated by western blot, and in general, exhibit a positive linear correlation.

In 2008, Nowik et al. completed a microarray analysis of 0, 2, and 7 day acidotic mice[71]. The study utilized whole genome mouse DNA arrays hybridized with digoxigenin-UTP labeled cRNAs. cRNAs were synthesized from total RNA from mouse kidney. Results were validated by traditional biochemical methods including qRT-PCR, and western blot. Results paralleled previously characterized changes in transcripts for genes involved in glutamine metabolism, ammoniogenesis and bicarbonate production identified with the Curthoys approach. In addition, several transcripts whose abundances changed or were differentially regulated were identified as novel markers for acidosis. Genes involved in cytoskeletal organization, cell proliferation, cell differentiation, and apoptosis were identified. Collectively, the results from Curthoys and Nowik indicate an increased role in cellular processes other than the primary GLN metabolism response during acidosis.

The microarray studies by Nowik (2007) did identify several genes that are specific to proximal tubules. However, the cRNAs used in their study were synthesized from whole kidney RNA, whereas the protein used for validation was from dissected proximal tubules. Such an approach would indicate the response of several cell types in the kidney, and as such, are not specific to the PCT.

The outlined studies revealed new insight into the MA response by the PCT. But the specificity of this response at the membrane can be limited by the heterogeneity of the sample in addition to the extraction methods. As such, first purifying the PCT for a, 'omics' experimental approach would be ideal. Additionally, fractionating the PCT cell

into respective compartments such as the mitochondria, cytosol, basolateral and apical membranes would lead to not only inferences of cellular function by the changes in abundance, but also by subcellular location.

1.10 Enrichment of brush border membranes from PCT

For the analysis described in this dissertation, we chose to focus specifically on the apical membrane. A method using Mg^{2+} /EGTA precipitation of brush border membrane vesicles (BBMV) was previously developed[80, 81]. This method by Biber *et al.* is advantageous due to its simplicity and suggested specificity for brush border membranes from PCT (BBMV_{PCT}). BBMV from a cortical homogenate can be enriched due to the negative charge of the sialic acid modified surface moieties present in the luminal surface of the proximal tubule lumen at physiological pH. Cutillas recently completed a proteomic analysis of cortical BBMV using this method[82]. In his experiment, a proteomic investigation was completed using denaturing conditions together with reversed phase (C18) - electrospray ionisation tandem mass spectrometry (C18-ESI-MS/MS). The study elucidated a 'snap-shot' inventory of proteins present at the brush border which also included the identification of many integral and membrane associated proteins. However, no inferences were made to the relative distribution by abundance of the identified proteins and were not profiled for changes during any pathophysiology. As such, our analysis would be novel to the pathophysiology of the response of the apical membrane of the PCT to MA.

CHAPTER 2

Proteomic Tools for the Study of Renal Physiology

2.1 Introduction

Proteomics in renal research has been utilized for many years, even during the earliest years of the discipline[83]. Concurrent with the technological advancements of the 1990's, many challenges for instrument sensitivity, data acquisition and analysis have advanced at a rapid pace. Such advancements have contributed to the identification of broad changes in proteins in the kidney. These include rapidly improving instrumentation and the production of large data sets, which often cannot be met due to the cost of data storage and instruments. Regardless, since 1994, when 'proteomics' was first described by Marc Wilkins, the number of publications for proteomics in renal nephrology have seen a meteoric rise[84, 85]. After the first renal study in 1997 by Taylor *et al.* which sought to study the trans-golgi of MDCK cells by 2D PAGE, the annual publications have risen to almost 350 publications in 2009, and are trending with an increase in annual publications[86].

2.2 2D-PAGE proteomics

2D- PAGE methods separate proteins based on their net charge followed by molecular weight based separation using SDS-PAGE. This technique resolves intact

proteins which can also be quantified by their relative intensities when stained in the gel. Traditional stains, such as silver and coomassie based methods, have been used in the various studies. Other stains target phosphor-containing proteins and can indicate the quantitative-phosphorylative state of the protein. To identify the samples, "plugs" or spots are cut from the regions of interest, then digested with trypsin and analyzed by mass spectrometry. One caveat to the 2D-PAGE methods is that they require exhaustive work on the part of the researcher to prepare, focus, resolve and analyze the sample, often requiring days to obtain the results. Another issue that arose from development of the technique was that using 2-DE identifies mostly soluble proteins (not membrane bound). An alternative set of methods known as "shotgun" proteomics can reveal valuable data by including less soluble proteins such as membrane bound proteins in the analysis consistent with the premise for our experiments.

2.3 Shotgun proteomics

In Shotgun proteomics, proteins of a complex mixture are digested into peptides with an endopeptidase such as trypsin. The peptides are subsequently separated by high performance liquid chromatography (HPLC) and then analyzed using a mass spectrometer. Fragmentation of the peptide bonds produce a spectra representing the entire amino acid sequences and are matched to theoretical amino acid sequences contained in a protein sequence database[87]. One of the original challenges of such an approach was matching an identified sequence with it's theoretical match in a sequence database, which were usually derived from arduous cloning and sequencing efforts. Such databases were incomplete, and relied on similarity searches across taxonomy to interpret

the results. In 1986, Hunt *et. al* described site specific cyano bromide or trypsin digestion and the subsequent analysis by HPLC coupled to triple quadrupole mass spectrometry [88]. In concordance with the predictability of peptide fragmentation into m/z values that represented the charged sub-peptide amino acid masses, the sequences could be matched by the differences of mass of the produced y and b ions. However, the ability to identify peptides in a sample of complexity (100's-1000's of proteins versus 10-15 for the study by Hunt *et. al*) together with the computational capability to make that match was a huge challenge. With the improvements in genomic sequencing technologies dependent on the computing age, one of the earliest advancements was made in 1994 by Eng *et.al* and in 1995 by Yates *et.al* [89, 90]. Following Eng and Yates' initial experiments that matched selected digested proteins by MALDI-MS/MS to the Protein Information Resource database[91], these studies successfully matched uninterpreted MS/MS spectra derived from lysate of *E. coli* or *S. cerevisiae*. In addition, these experiments introduced the statistical spectra-sequence matching method still commonly in use today known as SEQUEST.

Since the earliest days of proteomics, the limitations of chromatographic and mass resolution of the available instrumentation together with the complex combination of proteins from tissue and cellular samples have indicated the need to simplify the sample mixture. Often, this is accomplished using methods which combine two dimensions of separation. These usually include strong cation (SCX) or anion exchange followed by reversed phase (C₁₈) high performance liquid chromatography (HPLC). Combining these methods has the advantage of increasing peptide identifications from a sample while improving the capability of the spectra matching algorithms due to the decreased

noise produced in the spectra. One negative aspect of this approach is the inclusion of an additional sample processing step to enable compatibility of the mobile phase for the first separation (containing salts) with those of the second separation step (typically organic solvents). There has been success at combining these stationary phases into a single column known as multidimensional protein identification technology (MUDPIT)[92]. This method reduces the sample loss between separation phases. However, typical applications of this technology utilize two separate columns on an automated HPLC coupled directly to a mass spectrometer. The sample must flow through two separate circuits to bind and elute from the first column (SCX) prior to binding and being eluted from the second column (C18). The alternative to this method is to perform the first separation using offline HPLC (not eluting directly into the mass spectrometer) or microfuge columns with the appropriate stationary phase. Both of these methods reduce the sample complexity and increase the peptide and protein identifications by MS/MS. However, these separation techniques subsequently lead to loss of sample and /or a decrease in chromatographic resolution as detected at the mass spectrometer. Regardless of these issues, shotgun proteomic methods provide the largest potential for increased protein identification if these challenges can be met.

2.4 Mass spectrometry instrumentation

There are a wide array of instruments available for use in proteomics. For shotgun based methods, instruments with an attached HPLC elute samples directly into the instrument through an emitter spray tip known as electrospray ionization (ESI). During ESI, sample is ionized by a voltage potential as the molecules partition to the

surface of the droplets. These droplets then desolvate until only the charged particles are left and then enter the mass spectrometer. The peptides are acidified usually with TFA or formic acid prior to chromatography. Once these charged and ionized peptides enter the instrument, they are subjected to precursor ion detection and selection followed by collision induced dissociation (CID) or "fragmentation" of the precursor ion to produce uninterpreted MS/MS spectra. Two such instruments that accomplish this are the Thermo-Finnigan linear ion trap mass spectrometer (LTQ) and the Agilent 6520 quadrupole time of flight (QTOF) mass spectrometer (MS).

The principal mode of operation of the LTQ MS is the trapping of ions in an electromagnetic field[93]. As ions enter the instrument, a magnetic field traps the ions between four magnetic poles and has an ejection path axial to the poles alignment[94]. Upon capture of the precursor ions, 2 dimensional radiofrequency fields are used to filter peptides based on the peptide ions' polarity and mass to charge ratios (m/z). Subsequently, the charged peptides are selected for fragmentation, typically by CID followed by detection using a mass analyzer and amplification of the signal using an electron multiplier. The LTQ also has the advantage of the ability to trap ions from the entering sample, leading to selective amplification of the detected signal.

The QTOF instrument filters ions by m/z in a manner similar to the LTQ. However, the QTOF continually ejects ions into a second quadrupole for further selection by m/z of the precursor ions prior to CID. The instrument is continually switching from detection of MS precursor ions in the first quadrupole (Q1) to filtering and CID of the selected precursor by the second quadrupole (Q2). Both MS and MS/MS scans are resolved by the time of flight tube followed by detection with the aid of a reflectron to

condense the selected ions into a smaller time space[95]. The Agilent QTOF has a mass error for the precursor ions of $\sim \pm 5-7$ ppm (as produced in our lab) and a mass resolution of $\sim 10-15,000$. As such, it is considered a high mass accuracy instrument and can resolve the natural $^{12}\text{C}/^{13}\text{C}$ isotopic distribution over the mass range typical for peptides (150-3000 m/z). Additionally, the TOF portion of the instrument can detect peptides and larger proteins over a larger selection of mass ranges (25-200,000 Da). Both instruments have similar duty cycle times for switching between selecting precursors for fragmentation, performing the fragmentation, and collecting the data. The described instrumentation is ideal for performing a 'snapshot' inventory of the peptides present in a sample, but are also ideally suited for analysis of relative abundance between samples.

2.5 Quantitative proteomics using labeled peptides

While shotgun proteomics can identify peptides by matching MS/MS spectra to a sequence database, sequence information alone is insufficient for abundance measurements. Several methods exist to aid in the determination of relative abundance measurements. These include chemical labeled and non-labeled techniques.

Isobaric tags for relative and absolute quantitation (iTRAQ) reagents are commercially available (AB Sciex) compounds that allow the simultaneous determination of the relative abundance of proteins from different samples[96]. The labels are covalently linked to the N- terminus of each peptide. Prior to fragmentation of peptides in the mass spectrometer, the reporter ion plus the cleaved tag all have the same mass (are isobaric). Upon selected fragmentation, the isobaric tags are cleaved to liberate a reporter molecule of which the intensity can be measured. The selective mass range of

the tags (114-118 Da) is below the working mass range of the LTQ. Therefore, detecting the labeled peptides requires switching fragmentation energies for shorter time periods to selectively fragment the tag followed by CID of the peptide itself[97]. The intensity measurement of the tag is used to measure the abundance of the peptide. Inferences of protein abundance are made by combining peptide abundance measurements per protein. Similarly, isotope-coded affinity tags (ICAT) and (+)-biotinyl-iodoacetamidyl-3,6-dioxaoctanediamine (iodoacetyl-PEO-biotin) can be used to label the cysteine residues of peptides[98]. These biotinylated labels, when conjugated to the cysteine residue, can be selectively enriched by avidin-biotin affinity purification. Such labels enable the simultaneous identification of peptides from multiple sample groups (4-8 for iTRAQ, and 2 for ICAT) mixed into one sample for analysis (multiplexing). Stable isotope labeling with amino acids in cell culture (SILAC) utilizes ^{13}C or ^{15}N labeled amino acids that are metabolically incorporated into the proteins[99]. This method was developed for use with cell culture. However, recent work has shown some success at breeding rats which were fed a diet enriched in ^{15}N [100]. These labeled methods are advantageous due to the multiplexing which can reduce instrument time. They also permit the direct detection of abundance ratios from a single mass spectrometry experiment that are reliable down to a 1.5 fold change over a dynamic range of 1.5-1000 fold[101-103]. However, the labels are expensive, are limited to a subset of peptides (ICAT) and require testing for chemical labeling efficiency (in the case of ICAT or iTRAQ) or metabolic incorporation (SILAC).

2.6 Label-free quantitative proteomics: Spectral Counting

By far spectral counting has become the *de facto* standard for non-labeled relative quantitative proteomics in the basic sciences. Spectral counting relies on the random sampling of spectra by the mass spectrometer producing a pseudo-count for each time a peptide is identified[104]. Larger and more abundant proteins are proteotypically represented in an experiment by more MS to MS/MS transitions which identify that protein. By altering the dynamic data acquisition of the instrument, the counts per peptide (and thus, the protein) can be optimized. In 2004, Liu *et. al* tested standards spiked in a yeast lysate. The results produced data that were linear over 2 orders of magnitude. In a later study by Old *et. al*, abundance ratios determined by spectral counting(SpC) of spike in standards in a complex background of protein were shown to positively correlate with analysis by peak area ($r=0.96$) and gel band intensity measurements ($r=0.90$)[103]. In yet another study by Hendrickson *et. al*, SpC abundance ratios were shown to positively correlate to results produced using SILAC, but with reduced sensitivity for detecting a 2-fold change[105]. Since SpC data is count data, it typically is not normally distributed and therefore presents a challenge to successfully infer significance of altered abundance. This is partly due to the dependency on the mass spectrometer's dynamic selection of MS precursors together with the sample complexity. Additionally, count data is not an actual measurement of abundance such as peak intensity. These limitations combine to make SpC data more difficult to assess abundance changes when the SpC are low. A promising approach to circumvent these issues is to combine the count data from multiple injection replicates of the same sample. This can increase the SpC per protein increasing the sensitivity to detect a change in abundance. By increasing the SpC per protein, the

variability of the SpC per protein decreases. SpC data can be sensitive enough to detect 2 fold changes with a high enough sensitivity that is nearly 80% when the SpC per protein is a minimum of 10 for a total of 3 replicates [106]. Thus, increasing SpC per protein together with the number of replicates increases the sensitivity for detection of abundance measurements.

Spectral counting is advantageous due to the simplicity of its use. There are no extra sample handling steps as required with chemical labeling which may result in sample loss. More time on the instrument is required to inject the multiple samples for a comparison study. However, the statistical power of the technique can be acquired with careful planning and experimental design.

2.7 Label-free Quantitative proteomics: precursor ion peak intensity and AMT

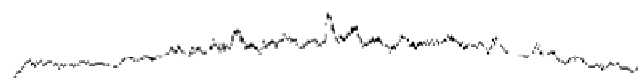
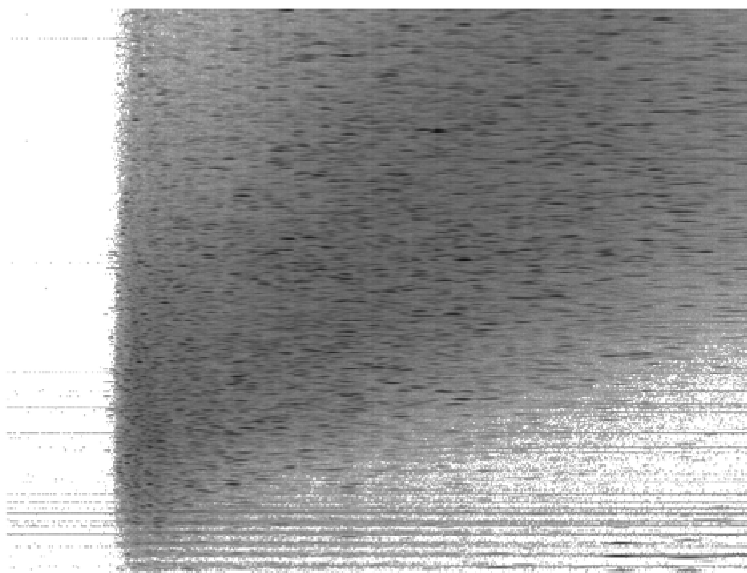
Another label free method is to measure the peak intensities of the precursor ions using LC-MS. Using this method, MS peaks can be visualized with a 2D digital map comparing retention time versus m/z (figure 2.1). The maps obtained from multiple samples can then be aligned by non linear regression. This alignment can be accomplished by a number of different software packages including OpenMS, msInspect, and XCMS[107-110]. The abundance measurements are then compared for the aligned maps. There are two primary methods for the LC-MS based approaches. In the first method, a targeted list of peptides from aligned LC-MS maps are later identified using MS/MS[111]. This method provides validation of the LC-MS features while still allowing the more accurate abundance measurement of MS alone. The other method similarly aligns LC-MS features, but identification is inferred from separate LC-MS/MS

injections. The basis for this approach is the reproducibility of the detection of a peptide by its hydrophobicity (retention time) together with its monoisotopic mass [112]. If the mass accuracy of the mass spectrometer is high enough, the RT and m/z can provide an accurate identification of the peptide feature. Additional confidence can be assigned to the mass tag if hydrophobicity of the peptide is calculated[113]. Decreasing the elution time using reversed phase HPLC from 60 minutes to as little as 5 minutes can still result in highly reproducible observed hydrophobicities when using AMT[114]. ESI-TOF with ± 15 ppm error of the matched feature was sufficient for these rapid 2-5 minute chromatography separations when resolving ~ 120 proteins. Additionally, the utility of ultra performance liquid chromatography toward AMT has been determined[115]. Shen *et. al* showed that using 50 μ m inner diameter capillary C18 HPLC could produce 250 to 550 protein identifications by MS/MS in 8-20 minutes. These early experiments used ESI, whereas nanospray technology is more commonly in use today.

The methods using accurate mass and time tag (AMT) technology have been limited in use, probably due to the general availability and expense of mass spectrometers with a high mass accuracy. The complexity of a typical whole cell lysate contains 10,000 potentially detectable tryptic peptides. Additionally, the typical mammalian rat and human genome contains millions of theoretical peptides that a feature could be matched against. Taken together, these indicate it is necessary to reduce the sample complexity together with the use of the highest mass accuracy instrument available if the experimenter wishes to utilize AMT technology.

Figure 2.1. Digital 2-D map of C18-NSI-MS data. A) The collected data is visualized in two dimensions, retention time (x axis) versus m/z . Relative intensity is a measurement of abundance for a peptide. trace at the bottom is of total ion current. B) m/z scan for a peptide. The mono-isotopic $^{12}\text{C}/^{13}\text{C}$ distribution of peaks are shown. C) Extracted ion chromatogram for the peptide in B as eluted over the duration of several seconds.

A.



B.



C.

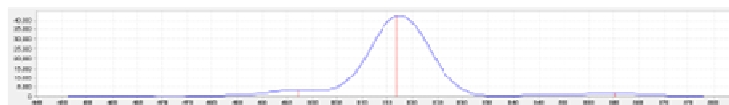


Figure 2.1

Statement of Problem and Aims

To date, only a few 'omics analysis of the response to metabolic acidosis have been completed. Studying the proximal convoluted tubular response to metabolic acidosis would increase the knowledgebase for further hypothesis driven research while revealing novel mechanisms for the response. Furthermore, the analysis at the brush border membrane would reveal the effect of compartmentalization of this response within the cell. Such an effect could be masked if the total abundance of proteins in the cell. To reveal these changes at the brush border membrane, the following experiments will be completed:

1. Characterize the inventory of proteins at the brush border membrane of proximal convoluted tubule cells. Determine the reproducibility and purity of the enriched brush border membrane samples and then perform a shotgun proteomic analysis using ion trap mass spectrometry and spectral counting.
2. Profile the global abundance changes that occur at the brush border membrane during 1-d, 3-d, and 7-d metabolic acidosis. Using QTOF mass spectrometry and spectral counting, test the relative changes in abundance of the proteins detected. In addition, establish the reproducibility of the peptides elution profiles obtained from multiple

injection and biological replicates to determine if accurate mass and time tags can be developed from the identified peptides.

3. Perform more accurate relative quantification of the profiled peptides using liquid chromatography QTOF mass spectrometry. Using the AMT database and spectral counts developed in 2, peptide level quantification will be performed and then compared to the protein level abundance measurements that are determined by spectral counting.

CHAPTER 3

Proteomic Analysis of Brush Border Membrane Vesicles Isolated from Purified Proximal Convoluted Tubules

**This chapter describes work published in the *American Journal of Physiology: Renal
Physiology*
Scott J. Walmsley *et. al*, 2010**

Walmsley SJ, Broeckling C, Hess A, Prenni J, Curthoys NP. Proteomic analysis of brush-border membrane vesicles isolated from purified proximal convoluted tubules. *Am J Physiol Renal Physiol*. 2010 Jun;298(6):F1323-31.

3.1 Abstract

The renal proximal convoluted tubule is the primary site of water, electrolyte and nutrient reabsorption and of active secretion of selected molecules. Proteins in the apical brush border membrane facilitate these functions and initiate some of the cellular responses to altered renal physiology. The current study uses 2-dimensional liquid chromatography/mass spectrometry to compare brush border membrane vesicles isolated from rat renal cortex (BBMV_{CTX}) and from purified proximal convoluted tubules (BBMV_{PCT}). Both proteomic data and western blot analysis indicate that the BBMV_{CTX} contain apical membrane proteins from cortical cells other than the proximal tubule. This heterogeneity was greatly reduced in the BBMV_{PCT}. Proteomic analysis identified 194 proteins common to both samples, 20 proteins unique to BBMV_{CTX}, and 57 proteins unique to BBMV_{PCT}. Spectral counts were used to quantify relative differences in protein abundance. This analysis identified 42 and 53 proteins that are significantly enriched (p values ≤ 0.001) in the BBMV_{CTX} and BBMV_{PCT}, respectively. These data were validated by measurement of γ -glutamyltranspeptidase activity and by western blot analysis. The combined results establish that BBMV_{PCT} are primarily derived from the proximal convoluted tubule (S1 and S2 segments), whereas BBMV_{CTX} include proteins from the proximal straight tubule (S3 segment). Analysis of functional annotations indicated that BBMV_{PCT} are enriched in mitochondrial proteins and enzymes involved in glucose and organic acid metabolism. Thus, the current study reports a detailed proteomic analysis of the brush border membrane of the rat renal proximal convoluted tubule and provides a database for future hypothesis driven research.

Key Words: rat kidney, apical membrane, spectral counting, membrane proteins

3.2 Introduction

The proximal tubule is the most abundant segment of the nephron within the renal cortex [116]. It is composed of polarized epithelial cells and consists of three sub-segments (S1, S2, and S3) that differ in protein composition and function. The primary functions of the entire proximal tubule are the recovery of approximately 80% of the fluid and electrolytes from the glomerular filtrate, the reabsorption of > 99% of the filtered glucose and other nutrients, and the active secretion of selected molecules. These processes are facilitated by a unique set of largely Na⁺-independent transporters in the basolateral membrane that promote exchange of solutes with blood and a separate set of primarily Na⁺-dependent transporters in the apical brush border membrane that facilitate exchange with the glomerular filtrate. In addition, the brush border membrane also contains multiple hydrolases and proteins involved in receptor-mediated signaling.

Previous analyses of the brush border membrane have primarily utilized brush border membrane vesicles (BBMV) that were isolated by MgCl₂ precipitation from renal cortical homogenates [81]. Such studies have included the functional characterization of transporters such as the Na⁺-dependent glucose [42] and phosphate [117] transporters, of NHE3, the apical Na⁺/H⁺ exchanger [118], and of various peptidases and disaccharidases [119]. While these studies sought to characterize the function of a single protein, a recent analysis utilized a shotgun approach to define the proteome of BBMV isolated from rat renal cortex [82]. This approach offers the potential of creating a comprehensive inventory of the protein composition of the brush border membrane. In addition, a thorough proteomic characterization of highly purified brush border membranes would

provide additional insight into the processes mediated by the proximal tubule during normal physiology. It would also provide the basis to characterize alterations in the proteome that are associated with the loss of specific functions during pathological conditions such as hypoxic or toxic injury to the proximal tubule.

However, due to the presence of multiple cell types and the subtle differences between the segments of the proximal tubule, it may be difficult to accurately define the protein composition using BBMVs isolated from renal cortex. For example, BBMV prepared from micro-dissected proximal convoluted and proximal straight tubules exhibit differences in kinetic parameters of glucose uptake, indicative of cell specific expression of different isoforms [120]. In addition, immunofluorescence studies have demonstrated that numerous proteins are preferentially expressed in the individual segments of the proximal tubule. For example, γ -glutamyltranspeptidase expression is greater in the proximal straight tubule (S3 segment) than in the proximal convoluted tubule (S1 and S2 segments) [54, 121, 122]. Together, these results demonstrate that an accurate assessment of the localization of specific proteins by proteomic analysis may require the further enrichment of BBMV from specific segments of the proximal tubule.

In this study, 2-dimensional liquid chromatography/mass spectrometry (LC-MS/MS) was used to compare the proteome of BBMV prepared from rat renal cortex (BBMV_{CTX}) and from isolated proximal convoluted tubules (BBMV_{PCT}). This approach, along with immunoblot analysis of marker proteins, indicated that the BBMV_{CTX} preparation also contains apical membranes that are derived from cells of the renal cortex other than the proximal tubule. However, the initial isolation of proximal convoluted tubules by Percoll gradient centrifugation was sufficient to remove the identified contaminants from the

BBMV_{PCT} preparation. The comparative proteomic analysis also revealed significant differences between the two samples. This analysis, along with the observed differences in γ -glutamyltranspeptidase activity, indicates that the BBMV_{PCT} are derived primarily from the S1 and S2 segments of the proximal tubule. Conversely, only the BBMV_{CTX} contain proteins that are expressed solely in the S3 segment and exhibit higher levels of proteins that are enriched in the proximal straight tubule. Finally, an analysis of functional annotations indicates that BBMV_{PCT} are enriched in enzymes of glucose metabolism, organic acid catabolism, and mitochondrial proteins. Therefore this study provides the first detailed proteomic analysis of the brush border membrane of the rat renal proximal convoluted tubule.

3.3 Materials and methods

3.3a Materials

Rabbit polyclonal antibodies versus GLUT2 and Calnexin (H-70) were purchased from Chemicon International (Billerica, MA) and from ABCAM Inc. (Cambridge, MA), respectively. A mouse monoclonal antibody to the 70 kDa subunit of succinate dehydrogenase was from Mitosciences (Eugene, OR). Rabbit polyclonal antibodies raised against aquaporin-2, thiazide-sensitive Na^+Cl^- co-transporter and $\text{Na}^+\text{K}^+2\text{Cl}^-$ co-transporter-2 were kindly provided by Dr. Mark Knepper (NIH, Bethesda, MD). Mouse monoclonal antibodies to Na^+/H^+ exchanger-3 were kindly provided by Dr. Orson Moe (Southwestern Medical Center, Dallas, TX). Male Sprague-Dawley rats (~200g) were obtained from Charles River Laboratories (Kingston, NY) and were fed rodent chow

(Harlan-Teklad, Madison, WI) and tap water. All procedures were approved by the Institutional Animal Care and Use Committee at Colorado State University.

3.3b Purification of proximal convoluted tubules

Rat renal proximal convoluted tubules were isolated by Percoll density gradient centrifugation [33]. Briefly, approximately 1 mm³ pieces of excised kidney cortex were incubated in phosphate-buffer saline (PBS) containing 5 mM glucose, 1 mg/ml bovine serum albumin, 0.1 mg/ml DNase, 2 mg/ml collagenase B (Roche Diagnostics, Mannheim), 1 mM heptanoic acid, 1 mM phenylmethylsulfonyl fluoride, and 1 mM sodium orthovanadate. The resulting tubules were washed twice in PBS containing 5 mM glucose to remove collagenase and then resuspended in an osmotically and pH balanced PBS solution containing 5 mM glucose, 45% Percoll (Sigma Life Sciences), and 10 mM Hepes, pH 7.4. After centrifugation, the tubules were recovered from a band that formed near the bottom of the gradient and were washed twice with PBS containing 5 mM glucose to remove the Percoll.

3.3c Isolation of Brush Border Membrane Vesicles

Brush border membranes vesicles (BBMV) were prepared using the standard method of MgCl₂ precipitation [80, 81]. Excised kidney cortex or purified proximal convoluted tubules were resuspended in 10 volumes (vol./wet wt.) of a solution containing 300 mM mannitol, 5 mM EGTA, 1 mM phenylmethylsulfonyl fluoride, 1 mM sodium orthovanadate and 12 mM Hepes, pH 7.1. After Polytron homogenization (90 sec, setting 5), the homogenate was diluted 2-fold with H₂O and then MgCl₂ was added to yield a

final concentration of 12 mM. The mixture was then incubated on ice for 15 min with intermittent and gentle mixing. Following centrifugation at 3,000 x g for 10 min at 4°C to remove mitochondria and cellular debris, the resultant supernatant was centrifuged at 30,000 x g for 40 min at 4°C to pellet the BBMV. The pellet was then resuspended in 1 volume of 150 mM mannitol, 2.5 mM EGTA, and 6 mM Hepes, pH 7.1 and homogenized with 15 passes of a glass Teflon homogenizer. The BBMV were again precipitated by addition of 12 mM MgCl₂ and repetition of the incubation and centrifugation steps. The final pellet was resuspended in the previous mannitol buffer and the BBMV were stored at -80°C.

3.3d γ -Glutamyltranspeptidase assay and immunoblot analyses

Aliquots of cortical homogenate and the isolated BBMV were assayed for protein [123] and γ -glutamyltranspeptidase activity [124]. The specific activity ($\mu\text{mol}\cdot\text{min}^{-1}\cdot\text{mg}^{-1}$) was determined by quantifying the liberation of p-nitroaniline from γ -glutamyl-p-nitroaniline (Sigma-Aldrich) with glycylglycine (Sigma-Aldrich) as the acceptor. For immunoblot analyses, samples containing 20 μg of protein were separated by 7% or 10% SDS-PAGE. Following transfer to PVDF membranes (Immobilon-FL, Millipore), the blots were incubated overnight with either mouse monoclonal or rabbit polyclonal antibodies. Either 680 or 800 Dylight conjugated goat anti-mouse or goat anti-rabbit IgG (Pierce) was used as secondary antibody (1:10,000 (v/v)). The resulting complexes were visualized and quantified using an Odyssey Infrared Imager (LI-COR Biosciences, Lincoln, NE).

3.3e Sample Preparation and Mass Spectrometric Analysis

Aliquots of BBMV containing 100 µg of protein were denatured by heating at 95°C for 5 min. After cooling to room temperature, the samples were dried and reconstituted to 3 mg/ml in 8 M urea. The ultra-sonicated samples were reduced (14 mM dithiothreitol, 30 min, 37°C) and alkylated (5 mM iodoacetamide, 1 h, 37°C) and then diluted 5-fold with 100 mM ammonium bicarbonate, pH 8.0. Sequencing grade modified trypsin was added (1:30, enzyme:protein) and the samples were incubated for 16 h at 37°C. The resulting peptides were desalted on a PepClean-C18 spin column (Thermo Scientific), normalized by measuring the absorbance at 220 nm (Nanodrop), and fractionated by strong cation exchange (SCX) chromatography. For SCX fractionation, the peptides were bound to a Polysulfoethyl-A microspin TopTip (Glygen) and eluted stepwise with 20 µl volumes of increasing ammonium acetate (20, 40, 60, 80, 120, 160 and 200 mM) in 20% acetonitrile, pH 2.9-3.8 to yield a total of 7 fractions. The peptides were then dried (SpeedVac) and reconstituted in 30 µl of 0.1% formic acid/3% acetonitrile. Each fraction was analyzed in triplicate by injecting 7 µl aliquots onto a Biobasic C-18 PicoFrit reverse phase nanospray column (74 µm ID x 10 cm, New Objective). Peptides were eluted directly into an LTQ mass spectrometer (Thermo Scientific) using a 90 min linear gradient of 15%-45% acetonitrile in 0.1% formic acid at a flow rate of 300 nl/min. MS spectra were collected over an m/z range of 200-2000 Da. MS/MS spectra were collected for the 5 most abundant ions in each MS scan using a dynamic exclusion limit of 2 MS/MS spectra of a given mass for 30 sec with an exclusion duration of 90 sec. Compound lists of the resulting spectra were generated using Bioworks 3.0 software (Thermo Scientific) with an intensity threshold of 5,000 and 1 scan/group.

3.3f Bioinformatic analysis

The resulting mass spectra were searched against the Rat-IPI database (v.3.57) using SEQUEST and X!Tandem (v.2008.12.01) search engines [90, 125, 126]. Each search was performed with a mass tolerance of 2.5 Da for MS and 1.0 Da for MS/MS spectra and with settings for tryptic peptides with up to 2 missed cleavages and carbamidomethylation of cysteine as a fixed modification and oxidation of methionine as a variable modification. Peptide false discovery rates (FDR) were determined by a target decoy approach using a reversed database concatenated to the parent forward database [127, 128]. The results of the searches were combined and protein identifications were validated using Scaffold (Proteome Software). Protein identifications with delta Cn values ≥ 0.2 and Xcorr scores ≥ 2.0 (z^{+1}), ≥ 2.4 (z^{+2}), and ≥ 3.7 (z^{+3}) for SEQUEST and Expect scores ≥ 1.0 for X!Tandem were entered in Scaffold (v.2.02) to produce a FDR of $\leq 1\%$. Lists of total proteins were assembled using a minimum of 2 identified peptides in at least one of the biological replicates of each BBMV preparation as an additional threshold for protein identification.

The relative abundance of the identified proteins in the BBMV isolated from cortex (BBMV_{CTX}) or from purified proximal convoluted tubules (BBMV_{PCT}) was determined by spectral counting (32). Similarity of sampling across injections was tested by comparing the spectral counts (SpC) for each analysis. SpC were also compared by summing each of the SCX fractions from a single sample. A test for correlation between injections and between each of the biological samples was completed using the Pearson moment correlation function with the R statistics package (v.2.8.1) (<http://www.r->

project.org). The spectral data were compared for variance by analyzing several diagnostic variables. These included total spectra, total identified spectra, % of total spectra above the search engine threshold cutoffs, and total proteins identified. The diagnostics were calculated for each biological sample. Once the similarity and variance between the biological samples were determined, the significance of the differences in SpC was calculated.

Significant changes between the $BBMV_{CTX}$ and $BBMV_{PCT}$ samples were calculated using the total SpC for the two biological replicates and the Fisher Exact Test [129, 130] to calculate p values. The p value distribution was corrected for the false positive rate using the method of Benjamini and Yeuketieli [131]. An adjusted p value ≤ 0.001 and a minimum of two identified peptides per protein were used as the cutoff for a significant change in protein abundance between the $BBMV_{CTX}$ and $BBMV_{PCT}$ samples. For each protein, the ratio of the spectral counts (R_{SC}) in the $BBMV_{PCT}$ samples to the $BBMV_{CTX}$ samples was calculated using Eq. 1 [103, 132], where n_{CTX} and n_{PCT} are the total spectral counts in the $BBMV_{PCT}$ and $BBMV_{CTX}$ samples, respectively, and t is the total spectral counts for all of the identified proteins in each of the two samples.

$$(Eq. 1) \quad R_{SC} = \log_2 \left[\frac{(n_{PCT} + 0.5)}{(n_{CTX} + 0.5)} \right] + \log_2 \left[\frac{(t_{CTX} - n_{CTX} + 0.5)}{(t_{PCT} - n_{PCT} + 0.5)} \right]$$

Once significant differences were determined, the R_{SC} values were plotted versus the total spectral counts for each protein in the combined $BBMV_{CTX}$ and $BBMV_{PCT}$ samples. The corrected p values were then used to visualize the distribution of the proteins that were significantly enriched in either $BBMV$ preparation.

3.3.g Enrichment of Gene Functional Annotations

A list of Gene Identifier accession numbers corresponding to each IPI accession was created using Microsoft Access software. The list of Gene Identifiers for the two samples (BBMV_{CTX} and BBMV_{PCT}) were then used to upload the proteins into the DAVID 2008 Bioinformatics Resources web server (<http://david.abcc.ncifcrf.gov/>) for analysis [133, 134]. Lists of total proteins per sample were tested for enrichment of functional annotations using the suggestions of Huang *et al*, [134]. *Rattus norvegicus* was used as the background species to test for enrichment of Gene Ontology and Kegg Pathway terms. Biological process, cellular component, and molecular function were tested separately. Functional annotations were selected based on known inferences of cell function for our samples (*ie.*, brush border membrane, proximal tubule function, glycolysis, etc.). Lists of interest were assembled based on these inferences and then expanded by manually evaluating proteins whose functional annotations were incomplete.

3.4 Results and discussion

3.4a Enrichment of BBMV from cortex and from proximal convoluted tubules

Initially, BBMV_{CTX} were prepared by selective MgCl₂ precipitation from a homogenate of rat renal cortex [80]. Compared to the cortical homogenate, the isolated BBMV_{CTX} exhibit a 15-fold increase in specific activity of γ -glutamyltranspeptidase, an apical membrane marker for the proximal tubule (Fig. 3.1). Western blot analysis (Fig. 3.2A) also indicated that the BBMV_{CTX} are highly enriched in the apical Na⁺/H⁺ exchanger (NHE3), but contain greatly reduced levels of the basolateral glucose

transporter (GLUT2), the mitochondrial succinate dehydrogenase (SDH), and the endoplasmic reticulum marker, calnexin (CNX). These data are in agreement with previous results [80] and are consistent with the removal of other subcellular membranes. However, the isolated BBMV_{CTX} exhibit increased levels of markers for the apical membranes of the collecting duct (aquaporin-2), the thick ascending limb, ($\text{Na}^+\text{K}^+2\text{Cl}^-$ cotransporter-2), and the distal tubule (thiazide-sensitive Na^+Cl^- cotransporter) (Fig. 3.2B). These data indicate that the classical preparation of BBMV also contains the apical membranes from cortical cells other than the proximal tubule.

3.4b Proteomic analysis of BBMV_{CTX} and BBMV_{PCT}

Duplicate biological samples of BBMV_{CTX} and BBMV_{PCT} were analyzed by 2-dimensional LC-MS/MS. Each sample was initially separated by off-line SCX chromatography to produce 7 fractions. Triplicate samples from each of the SCX fractions were further fractionated by on-line C18-chromatography coupled directly to an LTQ mass spectrometer via a nanoelectrospray source. The SEQUEST and X!Tandem search engines were used to match the recorded MS/MS spectra from the 84 mass spectrometric analyses against the current rat IPI database.

Of the total identified proteins, 22% are integral membrane proteins and an additional 18% are peripheral membrane proteins. However, the single largest group of identified proteins is those involved in metabolism. Functional analysis of the 214 proteins identified in the BBMV_{CTX} samples indicated a slightly greater proportion of membrane transporters and a decreased level of mitochondrial proteins (Fig. 3.3C) compared to the

BBMV_{PCT} samples. A complete list of the identified proteins is provided in supplemental Table S1.

A comparison of the relative abundance of the 20 most abundant proteins in the combined BBMV_{PCT} and BBMV_{CTX} samples, as determined by spectral counts (SpC), is illustrated in Fig. 3.4. The 12 most abundant proteins are well characterized apical membrane proteins: α and β subunits of the Na⁺/K⁺-ATPase-1, actin, aminopeptidase N, low density lipoprotein receptor-2, Na⁺/H⁺-exchanger regulatory factor-3, an amino acid transporter (rBAT), dipeptidylpeptidase-4, maltase-glucoamylase, ezrin, villin-1, and Na⁺/glucose co-transporter-2.

The resulting identifications were validated in Scaffold using stringent criteria that produced a false discovery rate of $\leq 1\%$. This analysis identified 194 proteins common to both preparations of BBMV, 57 proteins unique to the BBMV_{PCT} and 20 proteins unique to the BBMV_{CTX} (Fig. 3.3A). Functional analysis of the 251 proteins contained in the BBMV_{PCT} indicated that nearly 30% of the identified proteins are transporters, peptidases and cytoskeleton proteins that are typical of the brush border membrane (Fig. 3.3B). An additional 12% of the proteins are membrane receptors and proteins involved in signal transduction. For the most part, this set of proteins produced a similar number of SpC in the two samples. However, a few proteins, such as rBAT and γ -glutamyltranspeptidase, appear to be more abundant in the BBMV_{CTX} than in the BBMV_{PCT}. By contrast, aldolase-B, α -actinin-4, and NHE3 regulatory factor-1 appear to be more abundant in the BBMV_{PCT}. Therefore, a statistical analysis of the SpC associated with the proteins

Figure 3.1 Enrichment of γ -glutamyltranspeptidase activity in isolated BBMV. Crude homogenates of rat renal cortex and of isolated BBMV_{CTX} and BBMV_{PCT} were assayed for γ -glutamyltranspeptidase activity and protein. The fold increases in specific activity are plotted as a bar graph +/- the standard deviation for 3 separate samples.

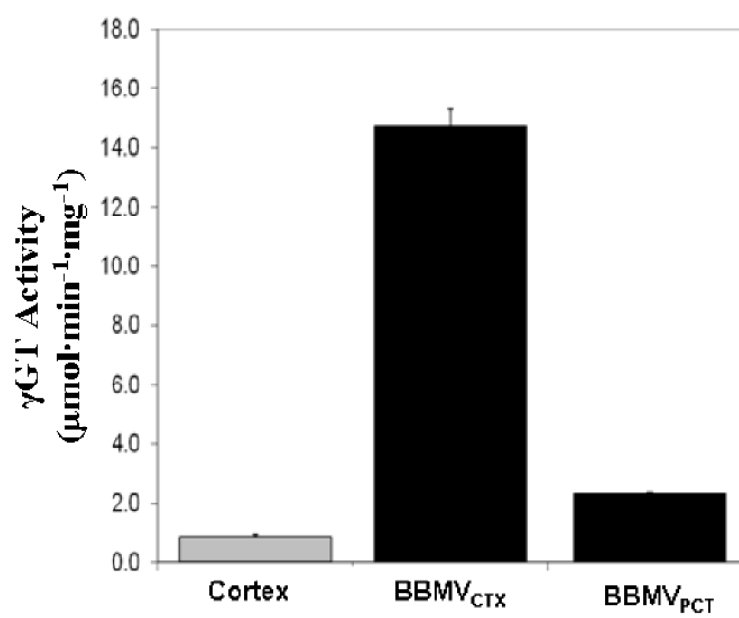


Figure 3.1

Figure 3.2 Western blot analyses of the purity of the BBMV_{CTX} and BBMV_{PCT} . Panel A. Analysis of contaminating organelle and basolateral membranes. Samples containing 20 μg of crude homogenates of rat renal cortex and BBMV_{CTX} were separated by SDS-PAGE and probed with antibodies that are specific for the apical (BBM) Na^+/H^+ exchanger (NHE3), the basolateral (BLM) glucose transporter (GLUT2), the mitochondrial (MITO) succinate dehydrogenase (SDH), and the endoplasmic reticulum (ER) marker, calnexin (CNX). Panel B. Analysis of contaminating apical membranes. Samples containing 20 μg of renal cortex, isolated proximal convoluted tubules (PCT), and purified BBMV were probed for proteins that, within the cortex, are expressed only in the proximal tubule (PT), Na^+/H^+ exchanger (NHE3); the thick ascending limb (TAL), $\text{Na}^+\text{K}^+2\text{Cl}^-$ -cotransporter-2 (NKCC2); the distal tubule (DT), thiazide-sensitive Na^+Cl^- co-transporter (TSC); and the collecting duct (CD), aquaporin 2 (AQP2).

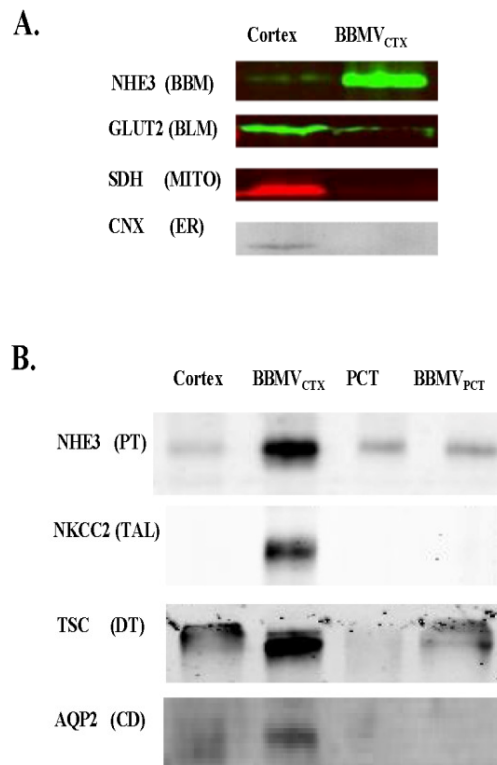
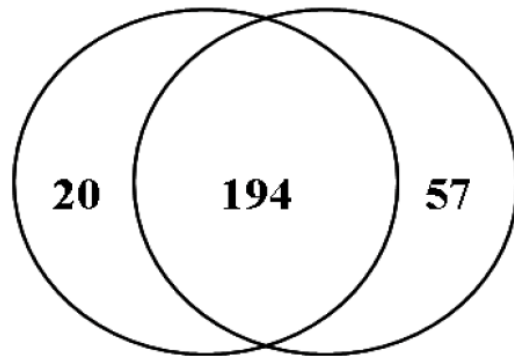


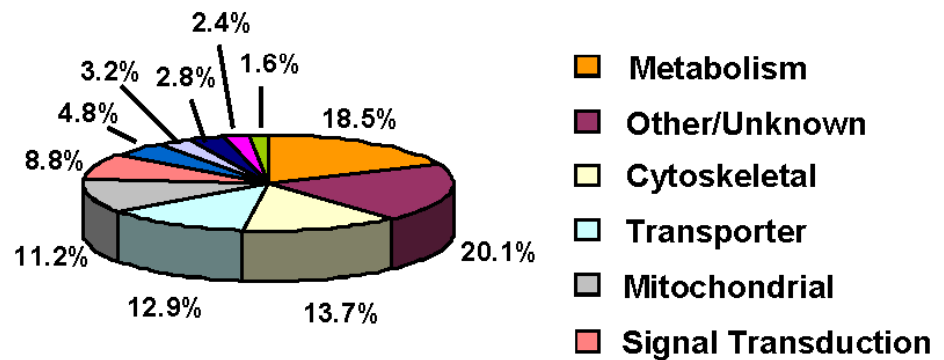
Figure 3.2

Figure 3.3 Proteomic Analysis of BBMV_{CTX} and BBMV_{PCT} . Panel A. Venn diagram of total proteins identified in the two BBMV samples. Panel B. Functional classification of the 251 proteins identified in the BBMV_{PCT} sample. Panel C. Functional classification of the 214 proteins identified in the BBMV_{CTX} samples.

A. BBMV_{CTX} BBMV_{PCT}



B. BBMV_{PCT}



C. BBMV_{CXT}

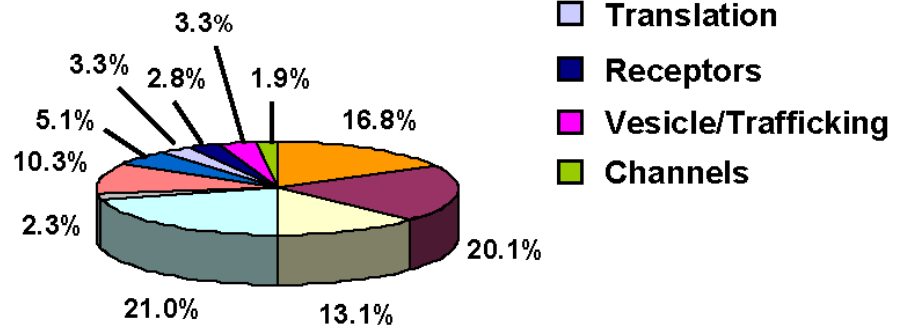


Figure 3.3

Figure 3.4 Comparison of the total spectral counts associated with the 20 most abundant proteins identified in the combined BBMV_{PCT} and BBMV_{CTX} samples. The total spectral counts (SpC) determined for each protein in the BBMV_{PCT} and BBMV_{CTX} samples are illustrated by the solid bar and the hatched bar, respectively.

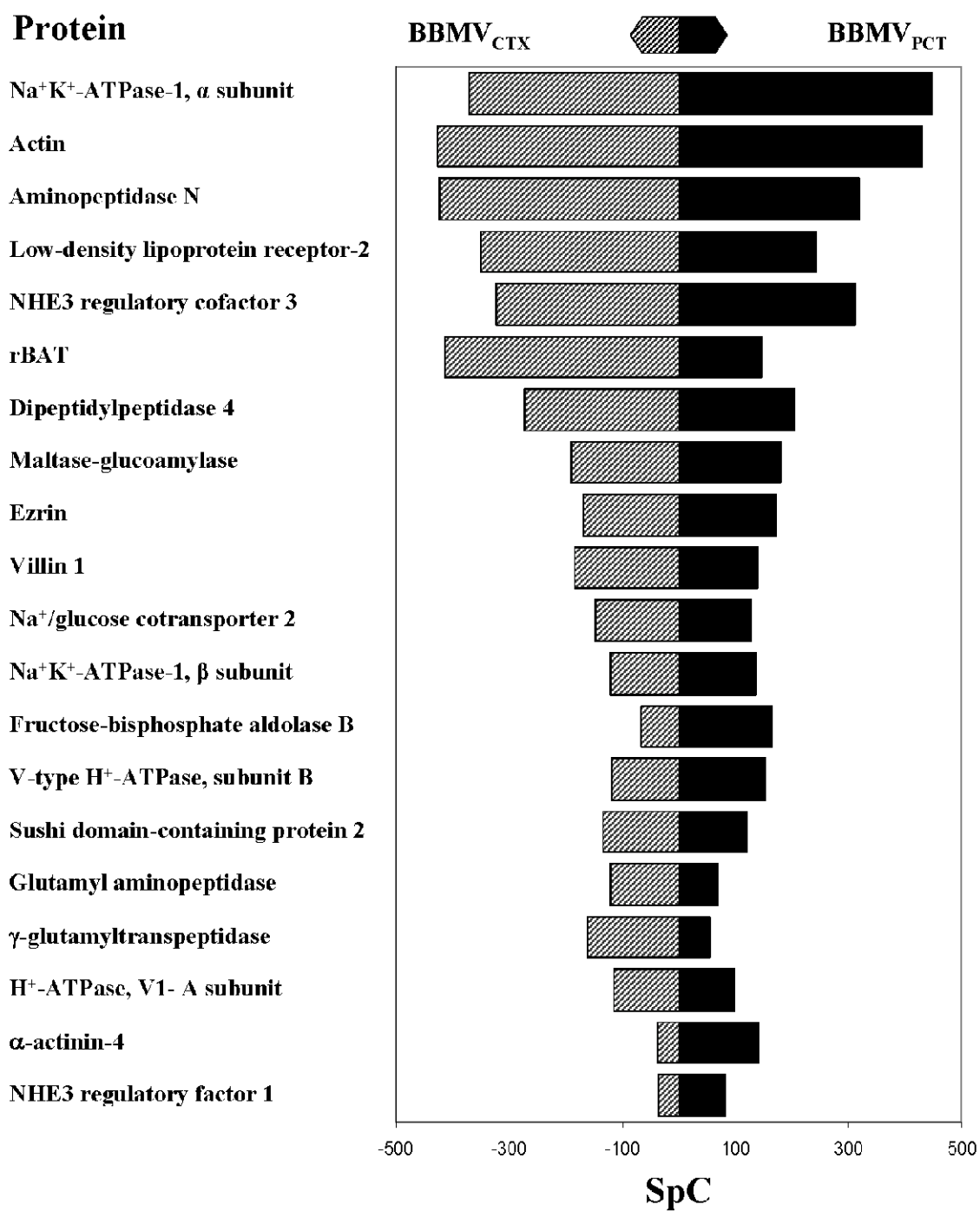


Figure 3.4

identified in the $BBMV_{PCT}$ and $BBMV_{CTX}$ samples was performed to verify the differences in the two preparations.

3.4c Quantitative analysis of protein abundance in $BBMV_{CTX}$ and $BBMV_{PCT}$

The spectral counts (SpC) collected for an individual protein increase in proportion to its abundance [135]. As a result, spectral counting has become the preferred method of quantification due to its ease of implementation compared to alternative methods that require chemical modification of peptides or labeling with heavy isotopes. However, to utilize the SpC to quantify the differences in protein abundance, the samples must be carefully normalized to each other and an analysis of the data should ensure that no significant loss of proteins or peptides occurred during the sample preparation. For the reported data, the standard deviation of the total identified SpC for each of the four biological samples expressed as a percent of the mean was only 5.6%. The same analysis for total spectra (unidentified and identified), percent of total spectra identified, and the number of protein identifications yielded values of 2.6%, 6.5%, and 7.5%, respectively. The highest variance was between the two $BBMV_{CTX}$ samples. This is probably due to the heterogeneity introduced by the dissection of renal cortex.

To further assess the consistency of replicate samples, the total SpC for each of the identified proteins was compared between individual injections (Fig. 3.5A) and between the sum of all injections (Fig. 3.5B). As expected, the greatest dissimilarity was observed in the SpC measured for the less abundant proteins. However, the data had Pearson's correlation coefficients of $r = 0.97$ between representative injections and $r = 0.94$ and $r = 0.95$ for the replicate $BBMV_{CTX}$ and $BBMV_{PCT}$ samples, respectively.

Therefore, the SpC measured in the multiple injections and the biological replicates were highly reproducible. The Fisher's exact test [129] was used to identify significant changes in protein abundance between the BBMV_{CTX} and BBMV_{PCT} samples (Fig. 3.6A). The resulting p values were further refined using the Benjamini-Yeuketeli correction [131]. The criteria for identifying a significant change was set as a ≥ 2 -fold change in total SpC and a corrected p value of ≤ 0.001 . The normalized ratios of spectral counts (R_{SC}) for the 271 proteins identified in the two BBMV samples were plotted versus the total SpC and color coded to identify proteins that are significantly enriched in either BBMV preparation (Fig. 3.6B). This analysis identified 42 proteins that were significantly enriched in the BBMV_{CTX} and 53 proteins enriched in the BBMV_{PCT} . The proteins that are significantly enriched in the two samples are italicized in supplemental Table S1.

The compiled data revealed significant enrichment of several interesting proteins in both the BBMV_{CTX} and BBMV_{PCT} preparations. Functional analysis of the data indicates that membrane transporters constitute 45% of the proteins enriched in the BBMV_{CTX} (Fig 3.7A), but only 21% of the total proteins identified in the BBMV_{CTX} (Fig. 3.3C).

Some of the proteins that are significantly enriched in the BBMV_{CTX} are illustrated in Fig. 3.8. The R_{SC} values are the \log_2 of the normalized ratios of SpC in the BBMV_{PCT} to the BBMV_{CTX} samples. Included in this list are the thiazide-sensitive Na^+Cl^- cotransporter and the $\text{Na}^+\text{K}^+2\text{Cl}^-$ co-transporter-2 that are derived from the apical membranes of the distal tubule and the thick ascending limb, respectively. These data are validated by the previous western blot analysis (Fig. 3.2B) and strongly support the conclusion that the BBMV_{PCT} are essentially free of contaminating apical membranes

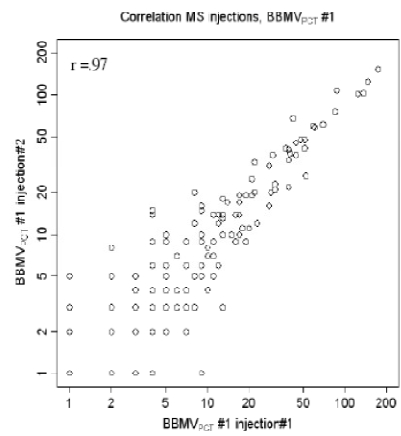
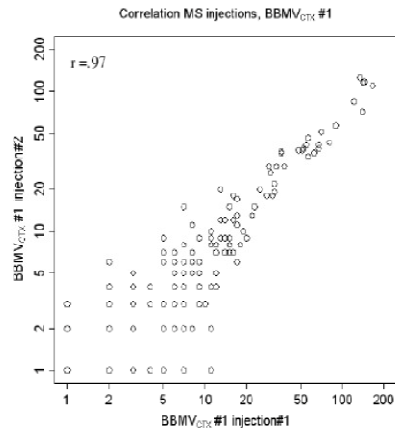
from non-proximal tubule cells. The BBMV_{CTX} samples are also significantly enriched for meprin, neprilysin, the amino acid transporter: rBAT, glutamine synthetase, and γ -glutamyltranspeptidase.

Of particular interest is the identification of neprilysin, which is not expressed in the S1 and S2 segments of the proximal tubule [136, 137]. In addition, the amino acid transporter, rBAT [138], glutamine synthetase [139], and γ -glutamyltranspeptidase [54] are proteins that are primarily expressed in the S3 segment. The increases in rBAT and γ -glutamyltranspeptidase quantified by spectral counting were confirmed by western blot analysis (Fig. 3.9). Thus, the observed increase in their abundance in the BBMV_{CTX} further validates the conclusion that the BBMV_{PCT} are derived primarily from the proximal convoluted tubule.

Functional analysis of the proteins that were enriched in the BBMV_{PCT} group revealed an increased abundance of enzymes of metabolism and mitochondrial proteins (Fig. 3.6B). The former group constitutes 39% of the proteins that are significantly enriched, but only 19% of the total proteins identified in the BBMV_{PCT} (Fig 3.3B). This group contains 11 proteins (Table S1) involved in glucose metabolism including aldolase and fructose 1,6-bisphosphatase-1 (Fig. 3.8). Aldolase was previously reported to co-localize with the vacuolar H^+ -ATPase in the apical membrane and the submicrovillar zone of endocytic vesicles [140]. This interaction is essential for the assembly and the activity of the proton pump [141, 142]. Immunofluorescence studies demonstrated that fructose 1,6-bisphosphatase-1 is also concentrated in the apical region of the rat renal proximal convoluted tubule [143]. As a result of their localization, aldolase and fructose -

Figure 3.5 Scatter plots of total spectral counts in replicate samples. Panel A. Correlation of total SpC between replicate injections. Pearson's product indicated a correlation of $r = 0.97$ between typical examples of replicate injections. Panel B. Correlation of total SpC between biological replicates. Pearson's product indicated correlations of $r = 0.94$ and $r = 0.95$ between the replicate BBMV_{CTX} and BBMV_{PCT} samples, respectively.

A.



B.

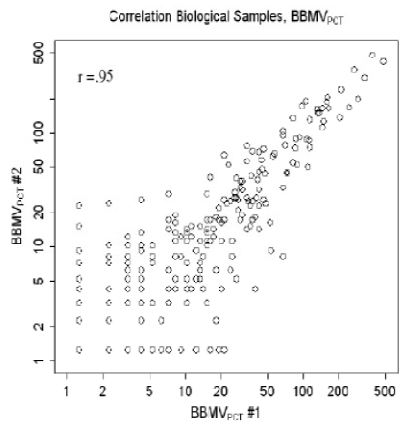
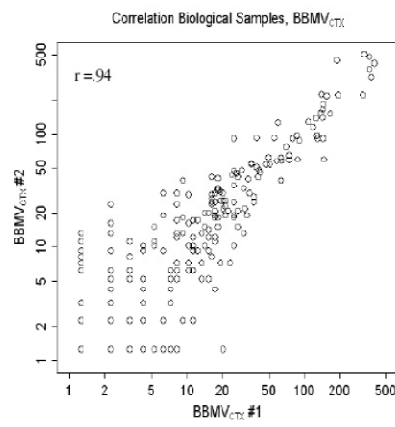


Figure 3.5

Figure 3.6 Statistical analysis of differences in abundance of the proteins identified in the BBMV_{CTX} and BBMV_{PCT} samples. The analysis is illustrated as a plot of \log_2 of the normalized ratio of SpC (R_{SC}) versus the total SpC for all of the identified proteins. Solid green and red circles represent proteins increased in either the BBMV_{PCT} or BBMV_{CTX} samples, respectively. Open green and red circles represent the proteins from the BBMV_{PCT} and BBMV_{CTX} samples that meet only the cutoff of $p \leq 0.001$. Black asterisks represent proteins with a p value ≤ 0.01 . Solid black circles represent the remaining proteins that were not significantly different in the two samples.

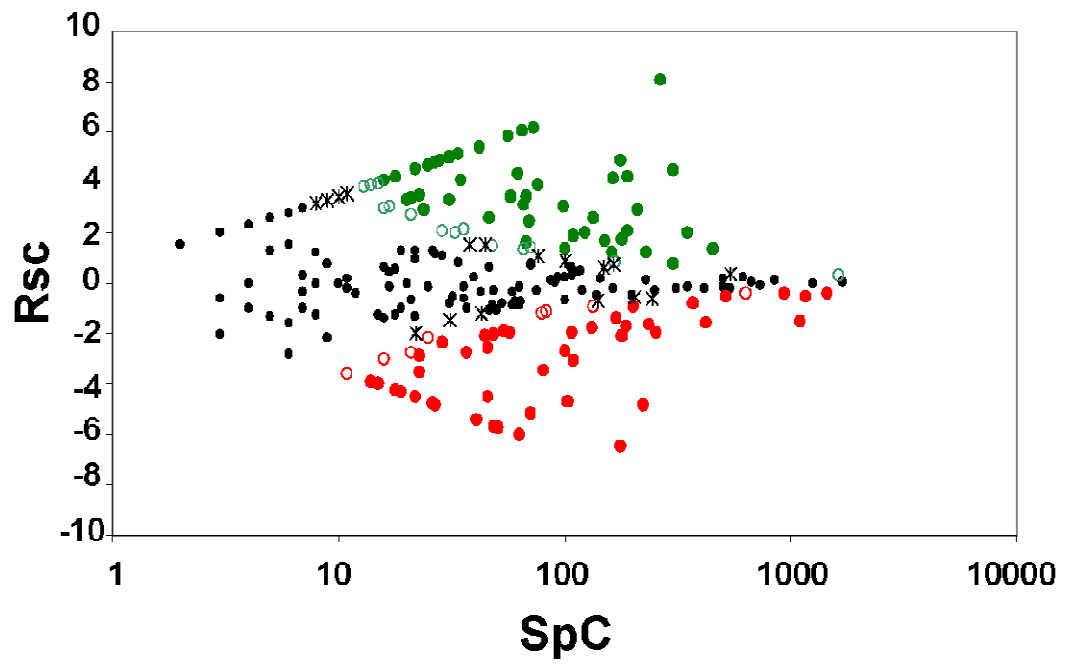


Figure 3.6

Figure 3.7 Functional classification of the proteins that are significantly enriched in the BBMV_{PCT} (Panel A) and the BBMV_{CTX} (Panel B) samples.

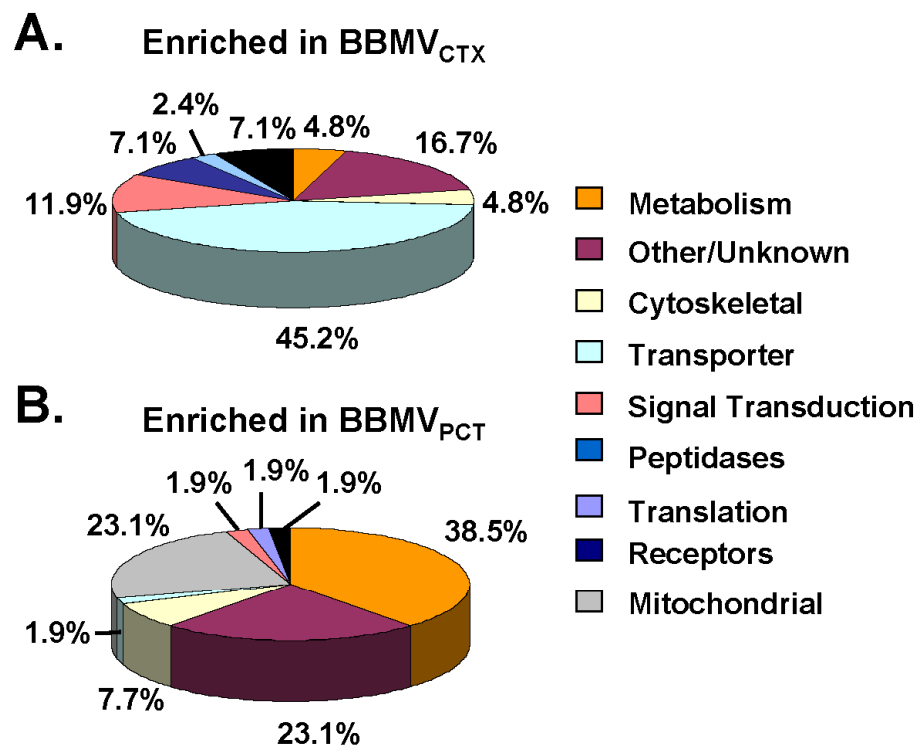


Figure 3.7

-1,6-bisphosphatase-1 may be trapped in the BBMV_{PCT} that are formed during homogenization of isolated proximal convoluted tubules. The enrichment of multiple enzymes of glucose metabolism also supports the concept that the enzymes form a complex that facilitates the channeling of intermediates of glycolysis and/or gluconeogenesis [144]. The positioning of this complex adjacent to the brush border membrane may facilitate the catabolism of glucose that is reabsorbed from the glomerular filtrate. Alternatively, following an overnight fast [145] or the onset of acidosis [146], this complex could facilitate the net renal synthesis of glucose from reabsorbed gluconeogenic precursors.

Mitochondrial proteins constitute 23% of the proteins that are enriched in the BBMV_{PCT} but only 11% of total identified proteins. The proteins enriched in the BBMV_{PCT} included components of the mitochondrial ATP synthase, including the α , β and oligomycin-binding subunits (Fig. 3.8). The mitochondria within the proximal convoluted tubule are larger, more elongated, and more abundant than those within the proximal straight tubule [116]. In addition, the mitochondria in the S1 and S2 segments are positioned in close proximity to the well developed endocytic apparatus immediately underneath the brush border membrane. By contrast, the small circular mitochondria found in the S3 segment are more evenly distributed throughout the cytosol. As a result, mitochondrial proteins, released during homogenization, may be preferentially trapped in the BBMV_{PCT} .

In summary, the reported data establish that sequential isolation of proximal tubules by Percoll gradient centrifugation and MgCl_2 aggregation yields a highly enriched

Figure 3.8 Comparison of the total spectral counts associated with proteins that are significantly enriched in the BBMV_{PCT} or BBMV_{CTX} sample. The total spectral counts (SpC) determined for each protein in the BBMV_{PCT} and BBMV_{CTX} samples are illustrated by the solid bar and the hatched bar, respectively. The R_{SC} value is the \log_2 of the normalized ratio of the total SpC in the BBMV_{PCT} to the BBMV_{CTX} samples.

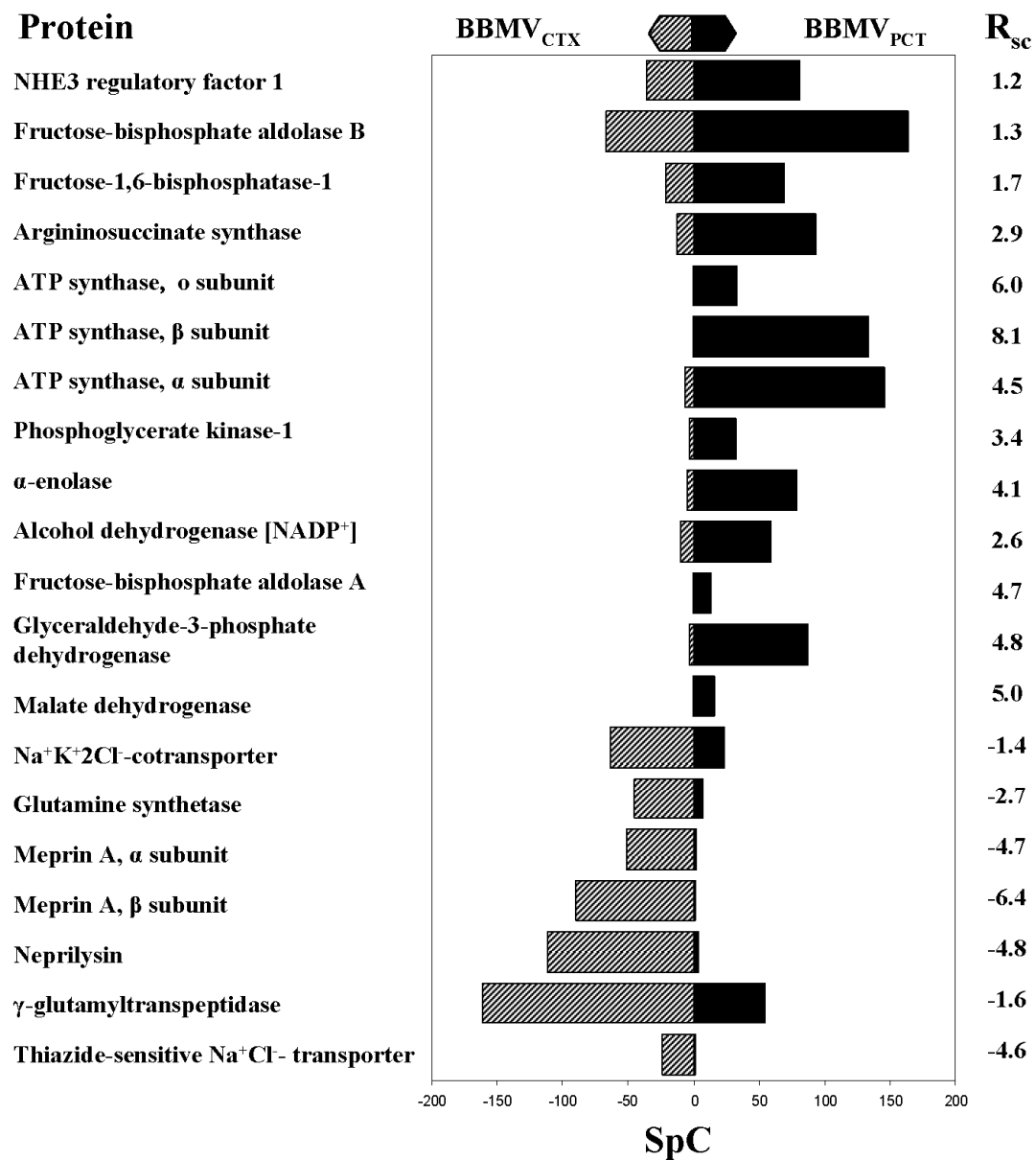


Figure 3.8

Figure 3.9 Validation of the enrichment in BBMV_{CTX} of proteins that are preferentially expressed in the S3 segment of the proximal tubule. Panel A. The levels of rBAT and γ -glutamyltranspetidase (γ GT) in homogenates of kidney cortex (CTX), of isolated proximal convoluted tubules (PCT), and of BBMV_{CTX} and BBMV_{PCT} samples were assessed by western blot analysis. Panel B. The fold enrichment of rBAT and γ GT in the BBMV_{CTX} to BBMV_{PCT} samples was calculated from the ratio of spectral counts (SpC) and by western blot analysis (WB) and illustrated as a bar graph.

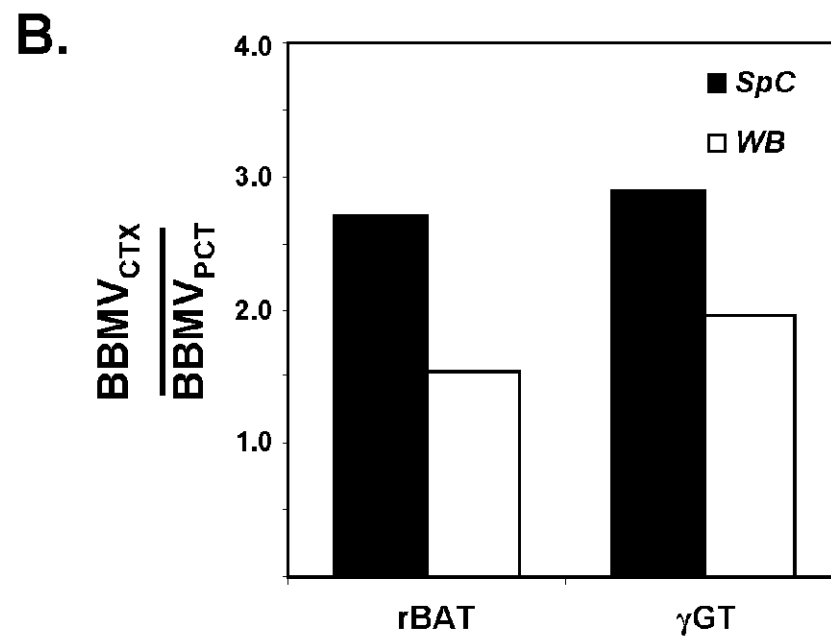
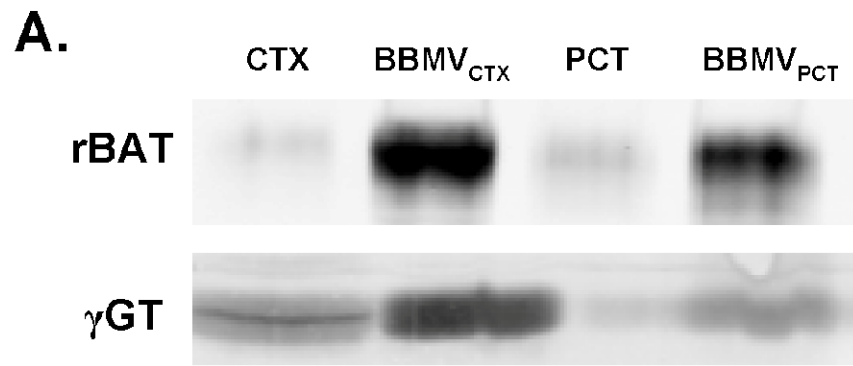


Figure 3.9

preparation of BBMV that are derived preferentially from the S1 and S2 segments of the proximal convoluted tubule. Comparison of the reported proteomic data to those of Cutillas, *et al.* [82] also indicates that this preparation contains a similar level of intracellular contaminants as observed with BBMV purified by capillary free flow electrophoresis. However, the reported protocol is simpler and utilizes equipment that is more generally available. Thus, the reported protocol and database provide the basis for a comprehensive analysis of the temporal changes in the brush border membrane that occur in response to various physiological adaptations or pathological conditions.

3.5 Acknowledgements

This research was supported in part by National Institutes of Diabetes and Digestive and Kidney Diseases Grants DK-37124 and DK-75517 awarded to N. P. Curthoys.

Table S1. List of Proteins Identified by the Proteomic Analysis. Proteins are sorted by the calculated R_{SpC} value as described in the text. Proteins determined to be enriched in the analysis are italicized. Red and green shaded boxes are those proteins enriched in the $BBMV_{PCT}$ and $BBMV_{CTX}$ groups, respectively. MW: molecular weight in kDa, TMD: predicted number of transmembrane domains, SpC: Spectral counts of the identified proteins for each biological sample, Σ_{SpC} : the sum of the SpC for each group, p: the FET calculated p values, BY: the adjusted p values using the method of Benjamini and Yekutieli (2001).

Protein	Gene	IP	MW	TMD	SpC				ΣSpC		R_{SpC}	p	BY _p
					$BBMV_{CTX1}$	$BBMV_{CTX2}$	$BBMV_{PCT1}$	$BBMV_{PCT2}$	$BBMV_{CTX}$	$BBMV_{PCT}$			
<i>ATP synthase subunit beta</i>	<i>Atp5b</i>	<i>IPI00551812</i>	56	0	0	0	96	171	0	267	8.1	0.0000	0.0000
<i>Hydroxyacid oxidase 2</i>	<i>Hao2</i>	<i>IPI00231245</i>	39	0	0	0	66	7	0	73	6.2	0.0000	0.0000
<i>ATP synthase subunit O</i>	<i>Atp5o</i>	<i>IPI00195123</i>	23	0	0	0	26	39	0	65	6.0	0.0000	0.0000
<i>p55 protein</i>	<i>LOC652956</i>	<i>IPI00464886</i>	51	0	0	0	34	22	0	56	5.8	0.0000	0.0000
<i>Cytochrome b-c1 complex subunit Rieske</i>	<i>Uqcrfs1</i>	<i>IPI00362949</i>	29	0	0	0	14	28	0	42	5.4	0.0000	0.0000
<i>Rat alpha-2u-globulin</i>	<i>LOC298116</i>	<i>IPI00464885</i>	21	0	0	0	24	10	0	34	5.1	0.0000	0.0000
<i>NADH dehydrogenase (ubiquinone) 1 alpha subcomplex 10-like</i>	<i>Ndufa10f1</i>	<i>IPI00189759</i>	41	0	0	0	15	16	0	31	5.0	0.0000	0.0000
<i>Malate dehydrogenase, cytoplasmic</i>	<i>Mdh1</i>	<i>IPI00198717</i>	36	0	0	0	24	7	0	31	5.0	0.0000	0.0000
<i>Glyceraldehyde-3-phosphate dehydrogenase</i>	<i>Gapdh</i>	<i>IPI00555252</i>	36	0	0	5	85	88	5	173	4.8	0.0000	0.0000
<i>Ribonuclease UK114</i>	<i>Hrsp12</i>	<i>IPI00231292</i>	14	0	0	0	23	5	0	28	4.8	0.0000	0.0000
<i>A kinase (PRKA) anchor protein 2</i>	<i>Akap2</i>	<i>IPI00364858</i>	96	0	0	0	3	25	0	28	4.8	0.0000	0.0000
<i>Glutathione peroxidase 1</i>	<i>Gpx1</i>	<i>IPI00192301</i>	22	0	0	0	14	13	0	27	4.8	0.0000	0.0000
<i>Fructose-bisphosphate aldolase A</i>	<i>Aldoa</i>	<i>IPI00231734</i>	39	0	0	0	15	10	0	25	4.7	0.0000	0.0000
<i>Cytochrome b-c1 complex subunit 1</i>	<i>Uqcrc1</i>	<i>IPI00471577</i>	53	0	0	0	7	18	0	25	4.7	0.0000	0.0000
<i>ATP synthase, H₊ transporting, F0 complex, subunit G</i>	<i>Atp5l</i>	<i>IPI00421711</i>	11	0	0	0	7	15	0	22	4.5	0.0000	0.0000
<i>NADH dehydrogenase [ubiquinone] flavoprotein 2</i>	<i>Ndufv2</i>	<i>IPI00367152</i>	27	0	0	0	6	16	0	22	4.5	0.0000	0.0000
<i>ATP synthase subunit alpha</i>	<i>Atp5a1</i>	<i>IPI00396910</i>	60	0	0	12	130	161	12	291	4.5	0.0000	0.0000
<i>44 kDa protein, enolase 1, (alpha) isoform 1</i>	<i>Eno1a</i>	<i>IPI00782342</i>	44	0	2	0	36	24	2	60	4.3	0.0000	0.0000
<i>Isocitrate dehydrogenase [NADP] cytoplasmic</i>	<i>Idh1</i>	<i>IPI00194045</i>	47	0	0	0	12	6	0	18	4.2	0.0000	0.0002
<i>Rab GDP dissociation inhibitor beta</i>	<i>Gdi2</i>	<i>IPI00197568</i>	51	0	0	0	17	1	0	18	4.2	0.0000	0.0002
<i>Nucleoside diphosphate kinase B</i>	<i>Nme2</i>	<i>IPI00325189</i>	17	0	0	0	18	0	0	18	4.2	0.0000	0.0002
<i>similar to glyceraldehyde-3-phosphate dehydrogenase</i>	<i>RGD1565368</i>	<i>IPI00554039</i>	36	0	1	8	92	91	9	183	4.2	0.0000	0.0000
<i>Alpha-enolase</i>	<i>Eno1</i>	<i>IPI00464815</i>	47	0	6	2	108	49	8	157	4.1	0.0000	0.0000
<i>91 kDa protein, Erythrocyte protein band 4.1-like 3</i>	<i>Epb4.1f3</i>	<i>IPI00558692</i>	91	0	0	1	17	17	1	34	4.1	0.0000	0.0000
<i>Histidine triad nucleotide-binding protein 1</i>	<i>Hint1</i>	<i>IPI00231146</i>	14	0	0	0	12	4	0	16	4.1	0.0000	0.0005
<i>ATP synthase gamma chain</i>	<i>Atp5c1</i>	<i>IPI00454288</i>	68	0	0	0	9	6	0	15	4.0	0.0001	0.0010
<i>Isoform 1 of Catechol O-methyltransferase</i>	<i>Comt</i>	<i>IPI00210280</i>	30	1	0	0	11	4	0	15	4.0	0.0001	0.0010
<i>Calcium-binding mitochondrial carrier protein Aralar2</i>	<i>Slc25a13</i>	<i>IPI00358163</i>	74	0	0	0	3	12	0	15	4.0	0.0001	0.0010
<i>Cytochrome c oxidase subunit 4 isoform 1</i>	<i>Cox4i1</i>	<i>IPI00194222</i>	20	1	0	0	0	14	0	14	3.9	0.0001	0.0019
<i>Isoform 2 of Electrogenic sodium bicarbonate cotransporter 1</i>	<i>Slc4a4</i>	<i>IPI00679235</i>	116	9	3	1	22	51	4	73	3.9	0.0000	0.0000

Protein	Gene	IPI	MW	TMD	SpC				ΣSpC		Rsc	p	BY _p
					BBMV _{CTX1}	BBMV _{CTX2}	BBMV _{PCT1}	BBMV _{PCT2}	BBMV _{CTX}	BBMV _{PCT}			
Isoform 1 of Kynurenine--oxoglutarate transaminase 1	Ccbl1	IPI00411232	52	0	0	0	9	4	0	13	3.8	0.0002	0.0037
Aromatic-L-amino-acid decarboxylase	Ddc	IPI00567511	54	0	0	0	11	0	0	11	3.6	0.0010	0.0126
hypothetical protein LOC304650	RGD1310262	IPI00371643	23	0	0	0	3	8	0	11	3.6	0.0010	0.0126
Cytochrome c oxidase subunit 6A	Cox6a	IPI00192246	16	0	0	0	2	9	0	11	3.6	0.0010	0.0126
Cytochrome b-c1 complex subunit 2	Uqcrc2	IPI00188924	48	0	0	1	9	13	1	22	3.5	0.0000	0.0001
Isoform 2 of Basigin	Bsg	IPI00193425	30	1	3	1	41	13	4	54	3.4	0.0000	0.0000
NADH dehydrogenase (ubiquinone) 1 beta subcomplex, 10	Ndufb10	IPI00202238	21	0	0	0	1	9	0	10	3.4	0.0020	0.0241
Phosphoglycerate kinase 1	Pgk1	IPI00231426	45	0	1	4	41	22	5	63	3.4	0.0000	0.0000
transketolase	Tkt	IPI00231139	71	0	1	0	20	0	1	20	3.4	0.0000	0.0004
Peptidyl-prolyl cis-trans isomerase A	Ppia	IPI00387771	18	0	2	0	19	10	2	29	3.3	0.0000	0.0000
Phenylalanine-4-hydroxylase	Pah	IPI00193258	52	0	0	1	8	11	1	19	3.3	0.0000	0.0007
Phosphate carrier protein	Slc25a3	IPI00562259	39	2	0	0	2	7	0	9	3.3	0.0039	0.0469
Isoform 2 of Tropomyosin alpha-3 chain	Tpm3	IPI00210941	29	0	0	0	2	7	0	9	3.3	0.0039	0.0469
Phosphoglycerate mutase 1	Pgam1	IPI00421428	29	0	0	0	6	2	0	8	3.1	0.0078	0.0892
C-1-tetrahydrofolate synthase, cytoplasmic	Mthfd1	IPI00231356	101	0	0	0	1	7	0	8	3.1	0.0078	0.0892
cytochrome c-1	Cyc1	IPI00366416	35	0	0	0	1	7	0	8	3.1	0.0078	0.0892
ATP synthase subunit d	Atp5h	IPI00230838	19	0	0	0	1	7	0	8	3.1	0.0078	0.0892
Isoform Mitochondrial of Peroxiredoxin-5	Prdx5	IPI00205745	22	0	0	0	0	8	0	8	3.1	0.0078	0.0892
L-lactate dehydrogenase B chain	Ldhb	IPI00231783	37	0	5	1	52	8	6	60	3.1	0.0000	0.0000
Protein DJ-1	Park7	IPI00212523	20	0	1	0	14	2	1	16	3.1	0.0003	0.0041
ADP/ATP translocase 2	Slc25a5	IPI00200466	33	2	0	10	46	43	10	89	3.0	0.0000	0.0000
Aminoacylase-1A	Acy1	IPI00464791	46	0	1	0	15	0	1	15	3.0	0.0005	0.0071
60 kDa protein, carboxylesterase ES-4	rCG_44273	IPI00558164	60	0	0	1	11	4	1	15	3.0	0.0005	0.0071
D-amino-acid oxidase	Dao	IPI00326225	39	0	0	1	3	12	1	15	3.0	0.0005	0.0071
Probable oxidoreductase C10orf33 homolog	Pyroxd2	IPI00470325	63	0	0	0	3	4	0	7	3.0	0.0156	0.1669
NADH-ubiquinone oxidoreductase 75 kDa subunit	Ndufs1	IPI00358033	79	0	0	0	2	5	0	7	3.0	0.0156	0.1669
Succinate dehydrogenase [ubiquinone] flavoprotein subunit	Sdha	IPI00200659	72	0	0	0	1	6	0	7	3.0	0.0156	0.1669
Cofilin-1	Cfl1	IPI00327144	19	0	0	2	17	5	2	22	2.9	0.0000	0.0006
Argininosuccinate synthase	Ass1	IPI00211127	46	0	12	12	112	74	24	186	2.9	0.0000	0.0000
Keratin, type II cytoskeletal 1	Krt11	IPI00421857	65	0	0	0	5	1	0	6	2.8	0.0313	0.3138
Cytoplasmic aconitate hydratase	Aco1	IPI00207003	98	0	0	0	4	2	0	6	2.8	0.0313	0.3138
Mitochondrial 2-oxoglutarate/malate carrier protein	Slc25a11	IPI00231261	34	0	0	0	0	6	0	6	2.8	0.0313	0.3138
Integrin beta-1	Irgb1	IPI00191681	88	1	1	1	9	10	2	19	2.7	0.0002	0.0035
Alcohol dehydrogenase [NADP+]	Akr1a1	IPI00230859	37	0	12	6	72	44	18	116	2.6	0.0000	0.0000

Protein	Gene	IPI	MW	TMD	SpC					ΣSpC		Rsc	p	BY _p
					BBMV _{CTX1}	BBMV _{CTX2}	BBMV _{PCT1}	BBMV _{PCT2}	BBMV _{CTX}	BBMV _{PCT}				
Sorbitol dehydrogenase	Sord	IPI00760137	38	0	6	0	38	3	6	41	2.6	0.0000	0.0000	
NADH dehydrogenase [ubiquinone] 1 alpha subcomplex subunit 5	Ndufa5	IPI00231997	13	0	0	0	3	2	0	5	2.6	0.0625	0.5694	
ADP,ATP carrier protein 2	Slc25a5	IPI00561209	22	0	0	10	29	31	10	60	2.4	0.0000	0.0000	
Xaa-Pro dipeptidase	Peptd	IPI00364304	65	0	0	0	4	0	0	4	2.3	0.1251	1.0000	
similar to procollagen, type IV, alpha 5	Col4a5	IPI00367440	161	0	0	0	3	1	0	4	2.3	0.1251	1.0000	
similar to aldehyde dehydrogenase family 7, member A1	Aldh7a1	IPI00208917	69	0	0	0	2	2	0	4	2.3	0.1251	1.0000	
Prohibitin-2	Phb2	IPI00190557	33	0	0	0	1	3	0	4	2.3	0.1251	1.0000	
ATP synthase subunit b	Atp5f1	IPI00196107	29	0	0	0	1	3	0	4	2.3	0.1251	1.0000	
Isoform 1 of Brain-specific angiogenesis inhibitor 1- protein 2	Baiap2	IPI00203614	69	0	0	0	0	4	0	4	2.3	0.1251	1.0000	
Brain acid soluble protein 1	Basp1	IPI00231651	22	0	6	0	26	4	6	30	2.1	0.0001	0.0012	
Heat shock cognate 71 kDa protein	Hspa8	IPI00208205	71	0	16	20	84	72	36	156	2.1	0.0000	0.0000	
Cytochrome P450 2C23	Cyp2c23	IPI00327991	66	1	3	2	10	14	5	24	2.0	0.0006	0.0076	
Spectrin alpha chain, brain	Spta2	IPI00209258	285	0	1	23	43	57	24	100	2.0	0.0000	0.0000	
Triosephosphate isomerase	Tpi1	IPI00231767	27	0	5	1	16	11	6	27	2.0	0.0003	0.0048	
Collagen alpha-1(I) chain	Col1a1	IPI00188909	138	0	0	0	1	2	0	3	2.0	0.2501	1.0000	
60S ribosomal protein L3	Rpl3	IPI00395295	46	0	0	0	1	2	0	3	2.0	0.2501	1.0000	
78 kDa glucose-regulated protein	Hspa5	IPI00208624	72	0	0	0	1	2	0	3	2.0	0.2501	1.0000	
ankyrin 3, epithelial isoform 2	Ank3	IPI00199445	284	0	0	0	0	3	0	3	2.0	0.2501	1.0000	
ATP synthase-coupling factor 6	Atp6j	IPI00204316	12	0	0	0	0	3	0	3	2.0	0.2501	1.0000	
Alpha-actinin-4	Actn4	IPI00213463	105	0	32	39	134	148	71	282	2.0	0.0000	0.0000	
Non-erythrocyte beta-spectrin	Spibn1	IPI00373419	251	0	7	16	32	55	23	87	1.9	0.0000	0.0000	
Fructose-1,6-bisphosphatase 1	Fbp1	IPI00231745	40	0	29	12	87	51	41	138	1.7	0.0000	0.0000	
Elongation factor 1-alpha 1	Eef1a1	IPI00195372	50	0	7	29	45	71	36	116	1.6	0.0000	0.0000	
Superoxide dismutase [Cu-Zn]	Sod1	IPI00231643	16	0	12	4	27	25	16	52	1.6	0.0000	0.0003	
11 kDa protein, Histone H4	H4	IPI00231340	11	0	1	8	19	10	9	29	1.6	0.0017	0.0212	
ATP-dependent dihydroxyacetone kinase/FAD-AMP lyase	Dak	IPI00372498	69	0	1	0	5	0	1	6	1.6	0.2188	1.0000	
Acyl-coenzyme A synthetase ACSM2	Acsm2	IPI00198641	64	0	0	0	0	2	0	2	1.6	0.5000	1.0000	
similar to FLJ44048 protein	Fsip2	IPI00767813	762	0	0	0	0	2	0	2	1.6	0.5000	1.0000	
Isoform 1 of Protein transport protein Sec31A	Sec31a	IPI00210147	135	0	0	0	0	2	0	2	1.6	0.5000	1.0000	
Integrin alpha-1	Iga1	IPI00324586	131	2	0	0	0	2	0	2	1.6	0.5000	1.0000	
Chloride intracellular channel protein 1	Clic1	IPI00421995	27	0	10	1	19	15	11	34	1.5	0.0008	0.0111	
similar to aldehyde dehydrogenase 8 family, member A1 isoform 2	LOC683474	IPI00359623	63	0	3	9	20	16	12	36	1.5	0.0007	0.0097	
Heat shock protein HSP 90-beta	Hsp90ab1	IPI00471584	83	0	7	12	36	16	19	52	1.4	0.0001	0.0019	
14-3-3 protein zeta/delta	Ywhaz	IPI00324893	28	0	14	4	34	14	18	48	1.3	0.0003	0.0043	

Protein	Gene	IPI	MW	TMD	SpC				ΣSpC		Rsc	p	BY _p
					BBMV _{CTX1}	BBMV _{CTX2}	BBMV _{PCT1}	BBMV _{PCT2}	BBMV _{CTX}	BBMV _{PCT}			
Fructose-bisphosphate aldolase	Aldob	IPI00876620	40	0	38	92	164	163	130	327	1.3	0.0000	0.0000
Sulfotransferase 1C2	Sult1c2	IPI00204467	35	0	22	6	41	31	28	72	1.3	0.0000	0.0003
Cytoplasmic dynein 1 heavy chain 1	Dync1h1	IPI00327830	532	0	3	4	11	8	7	19	1.3	0.0291	0.2972
Voltage-dependent anion-selective channel protein 2	Vdac2	IPI00198327	32	0	0	5	0	14	5	14	1.3	0.0837	0.5771
Cytosolic non-specific dipeptidase	Cndp2	IPI00421899	53	0	1	0	3	1	1	4	1.3	0.3751	1.0000
UPF0404 protein C11orf59 homolog	MGC72560	IPI00207707	18	0	1	5	14	2	6	16	1.3	0.0527	0.4927
Isoform 1 of Mucin and cadherin-like protein	Mucdh1	IPI00200640	91	1	19	29	72	43	48	115	1.2	0.0000	0.0000
glutathione S-transferase, theta 3	Gstt3	IPI00915569	23	0	1	1	5	1	2	6	1.2	0.2892	1.0000
Na(+)/H(+) exchange regulatory cofactor NHE-RF1	Slc9a3r1	IPI00200898	39	0	25	44	66	95	69	161	1.2	0.0000	0.0000
Histone H2A	H2A	IPI00188888	14	0	0	8	9	10	8	19	1.1	0.0525	0.4927
Sulfotransferase 1C2A	Sult1c2a	IPI00204469	35	0	18	6	27	25	24	52	1.1	0.0018	0.0226
Membrane-bound carbonic anhydrase 12	Car12	IPI00366865	40	1	6	3	13	7	9	20	1.0	0.0617	0.5646
60S acidic ribosomal protein P2	Rplp2	IPI00188804	12	0	3	4	8	7	7	15	1.0	0.1341	1.0000
Ras-related protein Rab-7a	Rab7a	IPI00215564	24	0	5	29	51	15	34	66	0.9	0.0019	0.0230
Peroxiredoxin-1	Prdx1	IPI00211779	22	0	36	24	32	76	60	108	0.8	0.0004	0.0051
Glutamate dehydrogenase 1	Glud1	IPI00324633	61	0	2	10	0	22	12	22	0.8	0.1219	1.0000
Alpha-2-macroglobulin receptor-associated protein	Lrpap1	IPI00364124	42	0	1	2	6	0	3	6	0.8	0.5079	1.0000
similar to Heterogeneous nuclear ribonucleoprotein A1	Hdp1	IPI00567346	35	0	2	1	3	3	3	6	0.8	0.5079	1.0000
Heat shock protein HSP 90-alpha	Hsp90aa1	IPI00210566	85	0	10	16	32	13	26	45	0.7	0.0323	0.3206
Chloride intracellular channel protein 4	Clc4	IPI00208249	29	0	29	32	36	68	61	104	0.7	0.0013	0.0169
4F2 cell-surface antigen heavy chain	Slc3a2	IPI00211616	58	1	57	57	105	86	114	191	0.7	0.0000	0.0004
Ubc protein	Ubc	IPI00476033	48	0	11	16	28	16	27	44	0.7	0.0574	0.5314
Isoform p82 of Disabled homolog 2	Dab2	IPI00212608	82	0	17	40	44	47	57	91	0.6	0.0082	0.0929
Tumor-associated calcium signal transducer 1	Epcam	IPI00324920	35	1	9	9	16	13	18	29	0.6	0.1445	1.0000
Sodium- and chloride-dependent creatine transporter 1	Slc6a8	IPI00325655	71	12	0	6	4	6	6	10	0.6	0.4547	1.0000
ATPase, H transporting, lysosomal V1 subunit G1	Atp6v1g1	IPI00199600	14	0	20	22	39	26	42	65	0.6	0.0415	0.4041
Actin-related protein 3	Actr3	IPI00363828	48	0	2	5	6	5	7	11	0.6	0.4810	1.0000
Glutamate carboxypeptidase 2	Folh1	IPI00190555	85	1	24	24	47	23	48	70	0.5	0.0647	0.5824
PDZK1-interacting protein 1	Pdzk1ip1	IPI00203992	12	1	20	25	28	37	45	65	0.5	0.0851	0.7544
14-3-3 protein epsilon	Ywhae	IPI00325135	29	0	7	0	7	3	7	10	0.4	0.6293	1.0000
ATPase, H+ transporting, lysosomal V1 subunit H	Atp6v1h	IPI00364780	51	0	18	30	29	37	48	66	0.4	0.1330	1.0000
V-type proton ATPase subunit B, brain isoform	Atp6v1b2	IPI00199305	57	0	117	115	144	163	232	307	0.4	0.0027	0.0327
30 kDa protein, Protein fem-1 homolog C	Fem1c	IPI00781207	30	0	1	2	3	1	3	4	0.3	1.0000	1.0000
Tubulin alpha-4A chain	Tuba4a	IPI00362927	50	0	17	31	28	32	48	60	0.3	0.3351	1.0000

Protein	Gene	IPI	MW	TMD	SpC				ΣSpC		Rsc	p	BY _p
					BBMV _{CTX1}	BBMV _{CTX2}	BBMV _{PCT1}	BBMV _{PCT2}	BBMV _{CTX}	BBMV _{PCT}			
Na ⁺ /K ⁺ -ATPase α-1	Atp1a1	IPI00326305	113	10	357	371	480	415	728	895	0.3	0.0001	0.0021
Protein NDRG1	Ndrg1	IPI00421389	43	0	7	11	12	10	18	22	0.2	0.6363	1.0000
Sodium/potassium-transporting ATPase subunit α-3	Atp1a3	IPI00231451	112	8	142	139	202	135	281	337	0.2	0.0465	0.4448
Voltage-dependent anion-selective channel protein 1	Vdac1	IPI00421874	31	0	8	38	15	40	46	55	0.2	0.4856	1.0000
EH domain-containing protein 1	Ehd1	IPI00360340	61	0	18	25	25	26	43	51	0.2	0.4719	1.0000
Macrophage migration inhibitory factor	Mif	IPI00230907	12	0	5	0	5	1	5	6	0.2	1.0000	1.0000
Mitogen-activated protein kinase scaffold protein 1	Map2k1ip1	IPI00373435	14	0	1	4	4	2	5	6	0.2	1.0000	1.0000
Sodium/potassium-transporting ATPase subunit β-1	Atp1b1	IPI00339124	35	1	107	127	147	125	234	272	0.2	0.1515	1.0000
Isoform 1 of Tubulin β-5 chain	Tubb5	IPI00197579	50	0	26	41	40	38	67	78	0.2	0.4542	1.0000
V-type proton ATPase subunit E 1	Atp6v1e1	IPI00400615	26	0	48	61	55	65	109	120	0.1	0.5959	1.0000
Actin, α skeletal muscle	Acta1	IPI00193813	42	0	194	218	207	238	412	443	0.1	0.4458	1.0000
Protein FAM151A	Fam151a	IPI00471686	67	1	24	18	20	25	42	45	0.1	0.8309	1.0000
Cadherin 16	Cdh16	IPI00471800	90	1	19	25	23	24	44	47	0.1	0.8346	1.0000
Ezrin	Ezr	IPI00470254	69	0	144	184	158	185	328	343	0.0	0.7551	1.0000
Actin, cytoplasmic 1	Actb	IPI00193819	42	0	356	478	385	474	834	859	0.0	0.8417	1.0000
Vanin 1	Vnn1	IPI00371710	57	0	0	2	2	0	2	2	0.0	1.0000	1.0000
Potential RabGAP	Tbc1d10a	IPI00190657	57	0	1	3	0	4	4	4	0.0	1.0000	1.0000
Glutathione S-transferase α-1	Gsta2	IPI00231638	26	0	3	2	3	2	5	5	0.0	1.0000	1.0000
40S ribosomal protein S7	Rps7	IPI00214582	22	0	6	4	4	6	10	10	0.0	1.0000	1.0000
NHE3 regulatory cofactor NHE-RF3	Pdzk1	IPI00200998	57	0	187	444	270	353	631	623	0.0	0.5646	1.0000
Maltase-glucoamylase	Mgam	IPI00193894	198	1	153	217	159	202	370	361	-0.1	0.5496	1.0000
V-type proton ATPase subunit F	Atp6v1f	IPI00198291	13	0	1	12	3	9	13	12	-0.1	0.8436	1.0000
64 Kda Protein, Similar to Maltase-Glucoamylase	Acly	IPI00191437	64	0	58	125	66	104	183	170	-0.1	0.3920	1.0000
Sushi Domain containing protein	Susd2	IPI00191919	91	0	125	136	112	128	261	240	-0.2	0.2421	1.0000
60S ribosomal protein L4	Rpl4	IPI00202512	47	0	16	17	14	16	33	30	-0.2	0.7058	1.0000
Transient receptor potential cation channel V member 4	Trpv4	IPI00191593	98	6	2	7	2	6	9	8	-0.2	0.8128	1.0000
Cytochrome P450 4A2	Cyp4a2	IPI00203317	58	1	8	1	1	7	9	8	-0.2	0.8128	1.0000
Alkaline phosphatase, tissue-nonspecific isozyme	Alpl	IPI00327143	58	0	10	9	12	5	19	17	-0.2	0.7406	1.0000
ATPase, H ⁺ -transporting, lysosomal V1 subunit A	Atp6v1a	IPI00373076	68	0	126	96	111	85	222	196	-0.2	0.1399	1.0000
Sodium/glucose cotransporter 2	Slc5a2	IPI00212934	73	14	137	152	143	111	289	254	-0.2	0.0834	0.7431
actin, β-like 2	Actb2	IPI00360356	42	0	77	91	69	77	168	146	-0.2	0.1566	1.0000
Tubulin α-1B chain	Tuba1b	IPI00339167	50	0	38	50	35	41	88	76	-0.2	0.3090	1.0000
amionless homolog	Amn	IPI00870509	49	1	3	3	2	3	6	5	-0.3	0.7722	1.0000
Radixin	Rdx	IPI00369635	69	0	73	64	54	61	137	115	-0.3	0.1291	1.0000

Protein	Gene	IPI	MW	TMD	SpC				ΣSpC		Rsc	p	BY _p
					BBMV _{CTX1}	BBMV _{CTX2}	BBMV _{PCT1}	BBMV _{PCT2}	BBMV _{CTX}	BBMV _{PCT}			
Ras homolog gene family, member C	Rhoc	IPI00191114	22	0	21	20	18	16	41	34	-0.3	0.4187	1.0000
similar to Na ⁺ dependent glucose transporter 1	RGD1310495	IPI00361210	55	11	13	14	12	10	27	22	-0.3	0.4762	1.0000
Pls1 protein	Pls1	IPI00370944	70	0	23	43	25	29	66	54	-0.3	0.2355	1.0000
10-formyltetrahydrofolate dehydrogenase	Aldh1f1	IPI00196725	99	0	4	0	3	0	4	3	-0.4	0.7239	1.0000
Syntaxin-binding protein 2	Stbp2	IPI00208188	67	0	9	15	6	13	24	19	-0.4	0.4475	1.0000
Cytochrome c, somatic	Cycc	IPI00231864	12	0	14	19	12	14	33	26	-0.4	0.3625	1.0000
Vil1 protein	Vil1	IPI00362757	93	0	138	221	132	148	359	280	-0.4	0.0007	0.0090
Dipeptidyl peptidase 4	Dpp4	IPI00209422	88	1	313	219	244	165	532	409	-0.4	0.0000	0.0002
Aminopeptidase N	Arpep	IPI00230862	109	1	322	505	331	304	827	635	-0.4	0.0000	0.0000
4 kDa protein, Putative glycine-rich cell wall structural protein		IPI00782004	4	0	0	7	3	2	7	5	-0.4	0.5773	1.0000
Lysosome-associated membrane glycoprotein 1	Lamp1	IPI00206336	44	1	39	41	32	26	80	58	-0.5	0.0497	0.4701
Myosin-9	Myh9	IPI00209113	226	0	24	91	20	63	115	83	-0.5	0.0184	0.1941
Collectrin	Tmem27	IPI00191929	25	1	63	57	41	44	120	85	-0.5	0.0095	0.1064
Low-density lipoprotein receptor-related protein 2	Lrp2	IPI00205325	519	1	368	318	289	198	686	487	-0.5	0.0000	0.0000
Moesein	Msn	IPI00212314	68	0	141	162	81	132	303	213	-0.5	0.0000	0.0004
Ectonucleotide pyrophosphatase/phosphodiesterase member 6	Erpp6	IPI00358524	51	0	19	0	10	3	19	13	-0.5	0.2919	1.0000
Membrane-bound aminopeptidase P	Xrpep2	IPI00197884	76	0	86	59	66	32	145	98	-0.6	0.0016	0.0198
similar to myosin XVIIIa	LOC360570	IPI00568245	233	0	0	2	0	1	2	1	-0.6	0.6213	1.0000
Sodium/hydrogen exchanger 3	Slc9a3	IPI00193371	93	12	0	2	0	1	2	1	-0.6	0.6213	1.0000
Homogentisate 1, 2-dioxygenase	Hgd	IPI00556987	50	0	13	9	7	7	22	14	-0.6	0.1839	1.0000
Tripeptidyl-peptidase 1	Tpp1	IPI00190499	61	0	5	8	3	5	13	8	-0.7	0.2818	1.0000
Lysozyme C-1	Lyz2	IPI00211927	17	0	41	45	38	17	86	55	-0.7	0.0068	0.0800
Electroneutral sodium monocarboxylate cotransporter	Slc5a12	IPI00769286	68	13	33	29	18	21	62	39	-0.7	0.0214	0.2215
Sodium-dependent phosphate transport protein 2C	Slc34a3	IPI00203529	64	11	15	23	14	9	38	23	-0.7	0.0540	0.5022
Ras-related protein Rap-1A	Rap1a	IPI00187747	21	0	16	24	14	10	40	24	-0.7	0.0447	0.4299
Isoform 1 of Glutamyl aminopeptidase	Erpep	IPI00327398	108	1	144	90	81	54	234	135	-0.8	0.0000	0.0000
Cubilin	Cubn	IPI00196620	399	0	8	12	9	2	20	11	-0.8	0.1070	0.9434
ATPase, H ⁺ transporting, lysosomal V1 subunit D	Atp6v1d	IPI00365851	28	0	17	17	7	12	34	19	-0.8	0.0386	0.3781
Ras-related C3 botulinum toxin substrate 1	Rac1	IPI00422092	21	0	20	18	9	12	38	21	-0.9	0.0261	0.2684
Myosin light polypeptide 6	Myf6l	IPI00365944	17	0	17	14	7	10	31	17	-0.9	0.0426	0.4126
ATP-binding cassette protein C4	Abcc4	IPI00421457	149	9	15	24	10	11	39	21	-0.9	0.0194	0.2033
Calmodulin	Calm3	IPI00231955	17	0	15	26	7	15	41	22	-0.9	0.0160	0.1697
Guanine nucleotide-binding protein G(I)/G(S)/G(T) subunit beta-2	Gnb2	IPI00212658	37	0	34	54	27	20	88	47	-0.9	0.0003	0.0041
Dipeptidase 1	Dpep1	IPI00327897	46	0	73	58	45	25	131	70	-0.9	0.0000	0.0002

Protein	Gene	IPI	MW	TMD	SpC				ΣSpC		Rsc	p	BY _p
					BBMV _{CTX1}	BBMV _{CTX2}	BBMV _{PCT1}	BBMV _{PCT2}	BBMV _{CTX}	BBMV _{PCT}			
Retinal dehydrogenase 1	Aldh1a1	IPI00332042	54	0	3	0	1	0	3	1	-1.0	0.3701	1.0000
prominin 1 isoform 1	Prom1	IPI00326312	97	5	5	0	1	1	5	2	-1.0	0.2843	1.0000
V-type proton ATPase subunit C 1	Atp6v1c1	IPI00213457	44	0	4	9	4	2	13	6	-1.0	0.1119	0.9816
Folate binding protein	Folr1	IPI00202950	29	0	14	11	9	3	25	12	-1.0	0.0320	0.3193
Lysosome-associated membrane glycoprotein 2	Lamp2	IPI00212730	45	1	16	18	13	3	34	16	-1.1	0.0103	0.1145
Isoform 1 of Cell division control protein 42 homolog	Cdc42	IPI00285606	21	0	13	19	8	7	32	15	-1.1	0.0125	0.1380
Aquaporin-1	Aqp1	IPI00327202	29	6	24	34	14	12	58	26	-1.2	0.0004	0.0058
similar to Villin-like protein	Vill	IPI00373579	97	0	7	23	4	9	30	13	-1.2	0.0090	0.1007
napsin A aspartic peptidase	Napsa	IPI00212697	46	0	15	41	1	23	56	24	-1.2	0.0003	0.0042
Ras-related GTP binding C	Rragc	IPI00188288	44	0	3	3	2	0	6	2	-1.3	0.1754	1.0000
Ras-related protein Rab-9A	Rab9a	IPI00196789	24	0	0	6	2	0	6	2	-1.3	0.1754	1.0000
Epoxyde hydrolase 1	Ephx1	IPI00209690	53	0	1	5	0	2	6	2	-1.3	0.1754	1.0000
Lysosomal acid phosphatase	Acp2	IPI00201276	48	2	7	6	5	0	13	5	-1.3	0.0611	0.5625
Cystathionine gamma-lyase	Cth	IPI00194650	44	0	3	8	4	0	11	4	-1.3	0.0740	0.6632
Myosin-10	Myh10	IPI00211813	233	0	1	15	2	4	16	6	-1.3	0.0330	0.3256
Elongation factor 2	Eef2	IPI00203214	95	0	1	3	0	1	4	1	-1.4	0.2141	1.0000
Kidney-specific Na-K-Cl symporter	Slc12a1	IPI00213335	120	12	62	61	29	18	123	47	-1.4	0.0000	0.0000
Adaptor protein complex AP-2, alpha 2 subunit	Ap2a2	IPI00471901	104	0	7	5	1	3	12	4	-1.4	0.0469	0.4467
Guanine nucleotide-binding protein G(i) subunit alpha	Gnai3	IPI00231726	41	0	5	18	2	6	23	8	-1.4	0.0065	0.0773
Neutral and basic amino acid transport protein rBAT	Slc3a1	IPI00211648	79	1	393	415	104	190	808	294	-1.5	0.0000	0.0000
Gamma-glutamyltranspeptidase 1	Ggt1	IPI00206254	62	1	166	149	41	67	315	108	-1.6	0.0000	0.0000
Myosin-Id	Myo1d	IPI00207989	116	0	1	4	1	0	5	1	-1.6	0.1213	1.0000
ATPase, H⁺ transporting, lysosomal V0 subunit A4	Atp6v0a4	IPI00193777	95	6	85	96	33	24	181	57	-1.7	0.0000	0.0000
ATP-binding cassette sub-family G member 2	Abcg2	IPI00327093	73	6	69	76	21	23	145	44	-1.7	0.0000	0.0000
ATPase, H⁺ transporting, lysosomal V0 subunit D1	Atp6v0d1	IPI00476086	40	0	49	53	14	16	102	30	-1.8	0.0000	0.0000
High-affinity sodium-dependent carnitine cotransporter	Slc22a5	IPI00199585	63	11	15	28	4	7	43	11	-1.9	0.0000	0.0002
Guanine nucleotide-binding protein subunit alpha-11	Gna11	IPI00200437	42	0	10	8	2	2	18	4	-2.0	0.0024	0.0290
System B(0) neutral amino acid transporter(B(0)AT1)	Slc6a19	IPI00391783	57	10	34	53	19	3	87	22	-2.0	0.0000	0.0000
Clastrin heavy chain 1	Ctic	IPI00193983	192	0	145	59	26	26	204	52	-2.0	0.0000	0.0000
Sodium-dependent phosphate transport protein 2A	Slc34a1	IPI00193397	69	11	26	20	7	4	46	11	-2.0	0.0000	0.0000
Pincher	Ehd4	IPI00200271	61	0	1	2	0	0	3	0	-2.0	0.1213	1.0000
Isoform B of AP-1 complex subunit beta-1	Ap1b1	IPI00201713	104	0	26	14	6	3	40	9	-2.1	0.0000	0.0001
ADP-ribosylation factor-like protein 8B	Arl8b	IPI00191587	22	0	9	28	8	0	37	8	-2.1	0.0000	0.0002
similar to Myosin-6	Myo6	IPI00764111	148	0	54	92	6	28	146	34	-2.1	0.0000	0.0000

Protein	Gene	IPI	MW	TMD	SpC				ΣSpC		Rsc	p	BY _p
					BBMV _{CTX1}	BBMV _{CTX2}	BBMV _{PCT1}	BBMV _{PCT2}	BBMV _{CTX}	BBMV _{PCT}			
G(I)G(S)G(T) subunit beta-1	Gnb1	IPI00212655	37	0	10	11	2	2	21	4	-2.2	0.0005	0.0066
six transmembrane epithelial antigen of the prostate 2	Steap2	IPI00372913	56	6	6	2	1	0	8	1	-2.2	0.0203	0.2111
G(I), alpha-2 subunit	Gnai2	IPI00231925	41	0	8	17	0	4	25	4	-2.4	0.0001	0.0009
G(s) subunit alpha isoforms XLas	Gnas	IPI00464920	123	0	19	21	4	2	40	6	-2.6	0.0000	0.0000
Glutamine synthetase	Glu1	IPI00324020	42	0	40	47	2	11	87	13	-2.7	0.0000	0.0000
Multidrug and toxin extrusion protein 1	Slc47a1	IPI00372692	61	13	16	3	2	0	19	2	-2.8	0.0001	0.0017
Isoform 2 of AP-2 complex subunit beta-1	Ap2b1	IPI00231502	106	0	24	9	3	1	33	4	-2.8	0.0000	0.0000
Fetub protein	Fetub	IPI00212708	43	0	5	1	0	0	6	0	-2.8	0.0147	0.1600
Sodium-independent sulfate anion transporter	Slc26a11	IPI00372997	39	4	2	4	0	0	6	0	-2.8	0.0147	0.1600
myosin IC	Myo1c	IPI00393867	120	0	10	11	1	1	21	2	-2.9	0.0000	0.0005
similar to Harmonin isoform 1	Ush1c	IPI00209014	102	0	9	6	0	1	15	1	-3.0	0.0002	0.0037
hemoglobin alpha 2 chain	LOC360504	IPI00205036	15	0	46	53	4	7	99	11	-3.1	0.0000	0.0000
similar to myosin VIIb	Myo7b	IPI00208315	241	0	28	47	3	3	75	6	-3.5	0.0000	0.0000
guanine nucleotide binding protein, alpha q polypeptide	Gnaq	IPI00230868	42	0	14	8	1	0	22	1	-3.6	0.0000	0.0001
Isoform 7 of Solute carrier organic anion transporter 1A3	Slc21a4	IPI00231181	63	7	7	4	0	0	11	0	-3.6	0.0004	0.0061
DnaJ homolog subfamily C member 5	Dnajc5	IPI00210881	22	0	6	5	0	0	11	0	-3.6	0.0004	0.0061
Serum albumin	Alb	IPI00191737	69	0	9	5	0	0	14	0	-3.9	0.0001	0.0009
Band 3 anion transport protein	Slc4a1	IPI00231379	103	10	4	10	0	0	14	0	-3.9	0.0001	0.0009
Multidrug resistance protein 1a	Abcb1a	IPI00470287	140	11	10	5	0	0	15	0	-4.0	0.0000	0.0005
23 kDa protein	Chp	IPI00207794	23	0	7	11	0	0	18	0	-4.3	0.0000	0.0001
Podocalyxin	Podxl	IPI00325860	52	1	4	14	0	0	18	0	-4.3	0.0000	0.0001
ATPase, class VI, type 11A	Atp11a	IPI00869709	136	7	11	8	0	0	19	0	-4.4	0.0000	0.0000
V-H+ATPase subunit a1-IV	Atp6v0a1	IPI00202120	97	6	14	8	0	0	22	0	-4.6	0.0000	0.0000
Sodium glucose cotransporter 1	Slc5a1	IPI00212933	73	14	15	7	0	0	22	0	-4.6	0.0000	0.0000
Thiazide-sensitive sodium-chloride cotransporter	Slc12a3	IPI00231043	111	11	16	29	1	0	45	1	-4.6	0.0000	0.0000
Meprin A subunit alpha	Mep1a	IPI00210872	85	1	62	38	0	3	100	3	-4.7	0.0000	0.0000
Monoglyceride lipase	Mgll	IPI00197344	33	0	16	10	0	0	26	0	-4.8	0.0000	0.0000
Neprilysin	Mme	IPI00231789	86	1	128	90	1	6	218	7	-4.8	0.0000	0.0000
Sodium- and chloride-dependent transporter XTRP2	Slc6a18	IPI00207180	70	12	14	13	0	0	27	0	-4.8	0.0000	0.0000
Organic anion transporting polypeptide A	Slco1a1	IPI00214674	74	10	16	11	0	0	27	0	-4.8	0.0000	0.0000
Hemoglobin subunit beta-1	Hbb	IPI00230887	16	0	24	46	1	0	70	1	-5.2	0.0000	0.0000
Sodium-independent aspartate/glutamate transporter 1	Slc7a13	IPI00388452	54	9	24	17	0	0	41	0	-5.4	0.0000	0.0000
Na(+)-glucose cotransporter 5	Slc5a10	IPI00369551	65	14	31	18	0	0	49	0	-5.7	0.0000	0.0000
Urate anion exchanger 1	Slc22a12	IPI00554326	60	10	17	32	0	0	49	0	-5.7	0.0000	0.0000

Protein	Gene	IPI	MW	TMD	SpC				ΣSpC		Rsc	p	BY _p
					BBMV _{CTX1}	BBMV _{CTX2}	BBMV _{PCT1}	BBMV _{PCT2}	BBMV _{CTX}	BBMV _{PCT}			
Peptide transporter 2	Slc15a2	IPI00326990	83	11	30	21	0	0	51	0	-5.7	0.0000	0.0000
Sodium-dependent vitamin C transporter 1	Slc23a1	IPI00203446	65	10	36	27	0	0	63	0	-6.0	0.0000	0.0000
Meprin A subunit beta	Mep1b	IPI00204808	79	1	89	87	0	1	176	1	-6.5	0.0000	0.0000

CHAPTER 4

Proteomic Analysis of the Effect of Metabolic Acidosis on the Apical Membrane of the Renal Proximal Convoluted Tubule

This chapter will be submitted to *Molecular and Cellular Proteomics* for publication

Scott J. Walmsley and Norman P. Curthoys

4.1 Abstract

The physiological response to the onset of metabolic acidosis requires pronounced changes in renal gene expression. Adaptations within the proximal convoluted tubule support the increased extraction of plasma glutamine and the increased synthesis and transport of NH_4^+ and HCO_3^- ions and glucose. Many of these adaptations involve proteins associated with the apical membrane. To quantify the temporal changes in these proteins, proteomic analyses were performed using brush border membrane vesicles isolated from proximal convoluted tubules (BBMV_{PCT}) that were purified from normal and acidotic rats. This preparation is essentially free of contaminating apical membranes from other renal cortical cells. The analysis identified 298 proteins, 26% of which contained one or more transmembrane domains. Spectral counts were used to assess changes in protein abundance. The onset of acidosis produced a pronounced, but

transient, increase in the Na⁺-dependent glucose transporter and a more gradual increase in the Na⁺-dependent lactate transporter. These changes were associated with a pronounced decrease in the levels of glycolytic and gluconeogenic enzymes contained in the isolated BBMV_{PCT}. In addition, the levels of γ -glutamyltranspeptidase increased significantly, while aminopeptidase N and transporters that participate in the uptake of neutral amino acids, including glutamine, were decreased. These changes could facilitate the deamidation of glutamine within the tubular lumen. Finally, pronounced changes were also observed in the levels of NHERF3, DAB2, and myosin 6, proteins that participate in endocytosis of apical membrane proteins.

4.2 Introduction

The kidney is a very complex organ that contains multiple nephron segments, each of which is composed of one or more unique cell types. Thus, the coordinate regulation of multiple types of cells is required to accomplish the various physiological functions of the kidney. Similarly, to mediate the appropriate adaptive response to a physiological or pathological stress, such as metabolic acidosis, requires coordinate changes in protein expression in multiple cell types [71]. The renal response to metabolic acidosis is characterized by an increased extraction and catabolism of plasma glutamine, an increased reabsorption and *de novo* synthesis of bicarbonate ions, and an increased synthesis and excretion of ammonium ions that facilitates the excretion of titratable acids [147]. This process is initiated in the proximal convoluted tubule which is the primary site of glutamine extraction and catabolism [23]. The adaptive responses within the proximal convoluted tubule are sustained, in part, by increased expression of the genes

that encode the mitochondrial glutamine transporter [148], glutaminase [121, 149] and glutamate dehydrogenase [150], the cytoplasmic phosphoenolpyruvate carboxykinase (PEPCK1) [19, 151], the apical Na^+/H^+ exchanger [152], and the basolateral glutamine transporter [37] and $\text{Na}^+-3\text{HCO}_3^-$ co-transporter [152]. The resulting increases in the corresponding proteins facilitate the basolateral uptake of glutamine, the increased reabsorption of bicarbonate ions, the increased synthesis of ammonium and bicarbonate ions, and their vectoral transport across the apical and basolateral membranes, respectively. However, the ultimate excretion of ammonium ions also requires the increased expression of the $\text{Na}^+\text{K}^+2\text{Cl}^-$ co-transporter in the thick ascending limb [66]. This adaptation facilitates the removal ammonium ions from the tubular fluid and the creation of a cortical to medullary gradient. The ammonium ion gradient provides the driving force for the transport of the appropriate amount of ammonium ions across the α -intercalated cells of the medullary and inner medullary collecting duct [153]. The latter process is facilitated by the increased expression of the ammonia channels, RhBG and RhCG [154, 155].

While the primary renal adaptations to metabolic acidosis are well characterized, many questions remain regarding the cellular and molecular mechanisms that mediate this response. Genomic and proteomic approaches offer great potential for directing research to answer these questions. For example, microarray analysis [71] compared the mRNAs isolated from whole kidneys of control mice and of mice that were made acidotic for 2 d and 7 d. This analysis detected 13,000 mRNAs or ~ 40% of the genes on the mouse genomic array. The levels of 333 mRNAs were up-regulated and another 342 were down-regulated during both acute and chronic acidosis. An even greater number were

transiently increased or decreased during onset of acidosis. Cluster analysis indicated that a large proportion of the regulated genes encode solute transporters and proteins involved in cell growth, proliferation, apoptosis, ammoniogenesis, water homeostasis, and energy metabolism. Without prior fractionation, it remains uncertain which of the observed changes occur within a specific cell type or within multiple segments of the nephron. However, this analysis clearly established that the expression of a very large number of genes is altered in the kidney in response to acidosis.

By contrast, mass spectrometry has been used to profile the proteome of individual nephron segments including the proximal convoluted tubule [33], the thick ascending limb [156], and the inner medullary collecting duct [157, 158]. Additional proteomic analyses have been performed with isolated intercalated cells [159] and with various established kidney cell lines [160, 161]. This approach has also been employed to discover many of the molecular details of the mechanism by which vasopressin activates water [158, 162] and urea transport [163] in the inner medullary collecting duct. An initial proteomic analysis of the temporal changes that occur in isolated proximal convoluted tubules during onset of acidosis was performed using Difference Gel Electrophoresis [33]. This analysis identified 21 proteins which are increased and 16 proteins that are decreased. The observed changes indicate that amino acid catabolism, an ER-stress response, and Ca^{++} -signaling are activated, while conversion of glycine to creatine, oxidation of pyruvate, and fatty acid catabolism are decreased in the proximal convoluted tubule during chronic metabolic acidosis. The temporal analysis also indicated that selective mRNA stabilization may be the primary mechanism by which protein expression is increased or sustained in response to acidosis.

Isolation of subcellular fractions from purified nephron segments offers the potential to characterize the remodeling of the proteome that occurs within specific sites in the cell. Previous studies have established that brush border membrane vesicles isolated from purified proximal convoluted tubules (BBMV_{PCT}) are a highly enriched membrane fraction that is essentially free of contaminating apical membranes from other cells within the renal cortex [33, 164]. In the current study, this isolation protocol was used to perform a proteomic analysis of the temporal changes that occur in the brush border membrane of the proximal convoluted tubule during onset of acidosis. This analysis identified 298 proteins and characterized novel adaptations in proteins that participate in carbohydrate and amino acid transport and metabolism and in the recycling of proteins to and from the brush border membrane.

4.3 Materials and Methods

4.3a Animals.

Male Sprague-Dawley rats weighing ~200 g (8-10 weeks old) were obtained from Charles River Laboratories (Kingston, NY). The rats were allowed free access to a rodent chow (Harlan-Teklad, Madison, WI) and the control group (n = 3) was given tap water to drink. To induce acidosis, rats were gavaged with 20 mmol NH₄Cl/kg body weight and then provided with 0.28 M NH₄Cl *ab libitum* as the sole drinking source. The acidotic groups (n = 3 per group) were treated for 1 d, 3 d, or 7 d before the kidneys were excised and processed. Animals were observed daily to ensure consumption of 0.28 M NH₄Cl. All of the acidotic rats consumed a volume of the NH₄Cl solution that was greater than the amount of water consumed by the control rats. All four groups of rats

exhibited similar behavior. All procedures were approved by the Institutional Animal Care and Use Committee at Colorado State University.

4.3b Purification of Proximal Convoluted Tubules

Rat renal proximal convoluted tubules were isolated by Percoll density gradient centrifugation [164-166]. Briefly, approximately 1 mm³ pieces of dissected kidney cortex were incubated in phosphate-buffered saline (PBS) containing 5 mM glucose, 1 mg/ml bovine serum albumin, 0.1 mg/ml DNase, 2 mg/ml collagenase B (Roche Diagnostics, Mannheim), 1 mM heptanoic acid, 1 mM phenylmethylsulfonyl fluoride, and 1 mM sodium orthovanadate. The resulting nephron segments were washed twice in PBS containing 5 mM glucose to remove collagenase and then resuspended in an osmotically and pH balanced PBS solution containing 5 mM glucose, 45% Percoll (Sigma Life Sciences), and 10 mM Hepes, pH 7.4. After centrifugation, the tubules were recovered from a band that formed near the bottom of the gradient and were washed twice with PBS containing 5 mM glucose to remove the Percoll.

4.3c Isolation of Brush Border Membrane Vesicles.

Brush border membranes vesicles were prepared from isolated proximal convoluted tubules (BBMV_{PCT}) using the standard method of MgCl₂ precipitation [80, 81]. Purified tubules were resuspended in 10 volumes/wet wt. of a solution containing 300 mM mannitol, 5 mM EGTA, 1 mM phenylmethylsulfonyl fluoride, 1 mM sodium orthovanadate and 12 mM Hepes, pH 7.1. After Polytron homogenization (90 sec, setting 5), the homogenate was diluted 2-fold with H₂O and then MgCl₂ was added to

yield a final concentration of 12 mM. The mixture was then incubated on ice for 15 min with intermittent and gentle mixing. Following centrifugation at 3,000 x g for 10 min at 4°C to remove mitochondria and cellular debris, the resultant supernatant was centrifuged at 30,000 x g for 40 min at 4°C to pellet the BBMV. The pellet was then resuspended in 1 volume of 150 mM mannitol, 2.5 mM EGTA, and 6 mM HEPES, pH 7.1 and homogenized with 15 passes of a glass Teflon homogenizer. The BBMV_{PCT} were again precipitated by addition of 12 mM MgCl₂ and repetition of the incubation and centrifugation steps. The final pellet was resuspended in the previous mannitol buffer and the BBMV_{PCT} were stored at -80°C.

4.3d γ -Glutamyltranspeptidase Assay.

Aliquots of the cortical homogenates and the isolated BBMV_{PCT} were assayed for protein [123] and γ -glutamyltranspeptidase activity [124]. The specific activity ($\mu\text{mol}\cdot\text{min}^{-1}\cdot\text{mg}^{-1}$) was determined by quantifying the liberation of p-nitroaniline from 2.5 mM γ -glutamyl-p-nitroaniline (Sigma-Aldrich) with 20 mM glycylglycine (Sigma-Aldrich) as the acceptor.

4.3e Sample Preparation and Mass Spectrometric Analysis.

Aliquots of BBMV_{PCT} containing 100 μg of protein were denatured by heating at 95°C for 5 min. After cooling to room temperature, the samples were dried and reconstituted to 3 mg/ml in 7 M urea/2M thiourea. The ultra-sonicated samples were reduced (14 mM dithiothreitol, 30 min, 37°C), alkylated (7 mM iodoacetamide, 1 h, 37°C), and then diluted 5-fold with 100 mM ammonium bicarbonate, pH 8.0. Sequencing

grade modified trypsin (Promega) was added (1:30, enzyme:protein) and the samples were incubated for 16 h at 37°C. The peptides were dried (SpeedVac) and reconstituted in 30 µl of 0.1% formic acid/3% acetonitrile. Each sample was analyzed in triplicate by injecting 1.5 µl aliquots onto an Agilent C-18 reverse phase HPLC Chip (15 µm ID x 1.5 cm) with a nanospray tip. Peptides were eluted directly into an Agilent 6520 QTOF mass spectrometer using a 22 min linear gradient of 15%-45% acetonitrile in 0.1% formic acid at a flow rate of 300 nl/min. MS spectra were collected over an m/z range of 200-2400 Da. MS/MS spectra were collected from the triplicate injections using a different data dependent acquisition mode for each injection: (1) the 8 most abundant ions in each MS scan were selected for MS/MS analysis with no dynamic exclusion limit, (2) the 5 most abundant ions in each MS scan were selected using a dynamic exclusion of 3 MS/MS spectra of a given mass within an exclusion duration of 20 sec, and (3) the same conditions as (2) but including an exclusion list of the ten most abundant proteins and their respective peptides identified in the first two injections. Compound lists of the resulting spectra were generated using Mass Hunter Acquisition 3.2 software (Agilent) with an intensity threshold of 1000 and 1 scan/group.

4.3f Bioinformatic analysis.

The resulting mass spectra were searched against the Uniprot-KB *Rattus norvegicus* database using SEQUEST and X!Tandem (v.2009.10.01) search engines [90, 125, 126]. Each search was performed with a mass tolerance of 50 ppm for MS and 0.1 Da for MS/MS spectra and with settings for tryptic peptides with up to 2 missed cleavages, with carbamidomethylation of cysteine as a fixed modification, and with oxidation of

methionine as a variable modification. Peptide false discovery rates (FDR) were determined by a target decoy approach using a reversed database concatenated to the parent forward database [127, 128]. The results of the searches were combined and the identifications were validated using Scaffold v.3.06 (Proteome Software). Peptide and protein identifications were validated with settings of 95% Peptide Prophet [167], 80% Protein Prophet [168], and a minimum precursor mass error of 15 ppm. The use of these settings produced a peptide FDR of $\leq 0.1\%$. Lists of protein identifications were assembled separately for each sample group (Control, 1-d, 3-d, or 7-d acidotic). An additional requirement for protein identification was a minimum of 2 identified peptides per protein or the manual verification of a protein identified from a single peptide. Only proteins that were identified in a minimum of 2 biological replicates were included in the final list of identified proteins.

4.3g Spectral counting.

Spectral counting was used to assess the relative abundance of a protein in each sample group [135, 169]. Similarity of sampling across injections and biological samples were tested by comparing the spectral counts (SpC) for each injection and each biological sample. Spectral counts for each protein were computed by summing the spectra identified using SEQUEST and X!Tandem from each of the three data acquisition modes per biological sample. Principal components analysis and Pearson's test for correlation were performed using both the R statistics package (v.2.11.1) (<http://www.r-project.org>) and the Dante v.1.2 software package (<http://omics.pnl.gov/software/DAnTE.php>) [170] to assess and visualize similarity across all the samples, between injections and among

each of the biological samples. Spectral data were compared for variance by analyzing the number of proteins identified per sample group, the percent of the total spectra identified, and the percent of the total peptides identified. Once the similarity and variance between the biological samples were determined, the significance of the differences in SpC was calculated

4.3h Cluster analysis and heat maps.

SpC data were normalized to the total spectra in each sample and then filtered to display proteins which were identified in a minimum of 3 injections per sample group. To prevent calculating logarithms of zero, a pseudocount of 1 was added to each SpC of the filtered data [103, 132]. The resultant normalized data were then analyzed using the Hierarchical clustering function in Dante using an average agglomerative method with a Spearman distance matrix.

4.3i Statistical Analysis.

Significant changes between the sample groups were calculated using the filtered SpC data produced for the cluster analysis. Student's t test was used to infer significance of differentially expressed proteins. A p value < 0.05 and a minimum of two identified peptides per protein were used as the criteria for a significant change in protein abundance between the control and each of the acidotic groups. For each protein, the \log_2 ratio of the spectral counts (R_{SC}) for the 1-d, 3-d, or 7-d acidotic samples versus the control samples was calculated using Eq. 1 [103, 132], where $n_{control}$ and $n_{acidotic}$ are the

total spectral counts in the control and acidotic samples, respectively, and t is the total spectral counts for all of the identified proteins in each of the two samples.

$$(Eq. 1) \quad R_{SC} = \log_2 \left[\frac{(n_{acidosis} + 1.0)}{(n_{control} + 1.0)} \right] + \log_2 \left[\frac{(t_{control} - n_{control} + 1.0)}{(t_{acidosis} - n_{acidosis} + 1.0)} \right]$$

Once significant differences were determined, the R_{SC} values were plotted versus the total spectral counts for each protein in the combined control and acidotic samples. The corrected p values were then used to visualize the distribution of the proteins that were significantly different in the 1-d, 3-d and 7-d acidotic BBMV sample groups versus the control group.

4.3j Enrichment of Functional Annotations.

Scaffold files were created separately for each of the control or acidotic groups. Lists of total proteins per sample were tested for enrichment of functional annotations using the manually curated Gene Ontology [171] terms within the Scaffold software. Functional annotations were selected based on known inferences of cell function (*ie.*, brush border membrane, proximal tubule function, glycolysis, etc.). Lists of interest were assembled based on these inferences and then expanded by manually evaluating proteins whose functional annotations were incomplete.

4.4 Results

4.4a Purification of Proximal Convoluted Tubules and BBMV.

By microscopic inspection, the isolated tubules are > 90% proximal convoluted tubules (S1 and S2 segments) with very few proximal straight tubules (S3 segments).

The isolated tubules were homogenized and used to isolate BBMV_{PCT} by MgCl_2 precipitation. Prior to proteomic analysis by liquid chromatography/tandem mass spectrometry, the BBMV_{PCT} were assayed for protein and γ -glutamyltranspeptidase (γ GT) activity, which is expressed primarily in the apical membrane of the S3 segment [172]. Similar to our previous study [164, 173], the specific activity of γ GT is increased only 2-fold in the BBMV_{PCT} compared to the cortical homogenate. However, the specific activity of γ GT measured in isolated BBMV_{PCT} gradually increases during onset of chronic acidosis (Figure 4.1). The observed 3.2-fold increase in BBMV_{PCT} isolated from 7-d acidotic rats is greater than the previous increases reported in whole cortical homogenates [174].

4.4b Proteomic analysis of BBMV_{PCT} from control, 1-d, 3-d and 7-d acidotic rats.

BBMV_{PCT} were subjected to in-solution digestion and proteomic analysis using a QTOF mass spectrometry equipped with a C_{18} -reverse phase HPLC-chip as outlined in Figure 4.2A. To increase peptide identifications, precursor ions from triplicate injections were selected for collision induced dissociation using three different dynamic acquisition methods [175]. The incorporation of an exclusion list in the third dynamic acquisition mode increased the number of unique peptides and proteins identified. Excluding peptides from highly abundant proteins, such as megalin (LRP2) and the α -subunit of Na^+/K^+ ATPase (Na^+/K^+ ATPase subunit alpha 1), also had the effect of increasing spectral counts for the lower abundance proteins (Figure 4.2B). Spectra were identified using both SEQUEST and X!Tandem spectral matching algorithms which further increased the spectral assignments per protein. The false discovery rate (FDR) for the

Figure 4.1 Onset of acidosis causes an increase in γ -glutamyltranspeptidase activity in isolated BBMV_{PCT} . BBMV_{PCT} were isolated from proximal convoluted tubules that were purified from control and acidotic rats and assayed for γ -glutamyltranspeptidase activity (γ -glutamyltranspeptidase) activity and for protein. The fold increase in specific activity was calculated relative to the specific activity of the control rats. The data are plotted as mean \pm S.E. of triplicate samples. Significance was determined by Student's t test: * $p < 0.05$, ** $p < 0.01$.

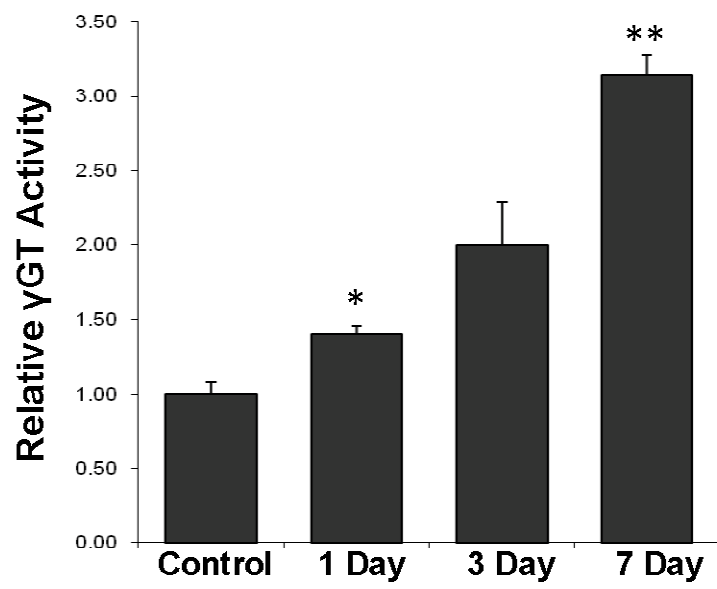


Figure 4.1

Figure 4.2. Work flow for analysis of peptides using a QTOF mass spectrometer. Panel A. Proteins were solubilized in 7M urea/2M thiourea, treated to block disulfide formation, and subsequently digested with trypsin. Three data dependent acquisition modes (DA mode) were utilized to increase peptide identifications. The third DA mode used an exclusion list of the peptides identified from the ten most abundant proteins as determined from the spectral counts acquired in the first two DA modes. The Venn Diagrams illustrate the protein and peptide identifications obtained from each DA mode. Panel B. The highly abundant proteins (LRP2 and Na⁺/K⁺ ATPase subunit alpha 1) yield fewer spectral counts in DA mode 3, while less abundant proteins produce greater spectral counts. Data are shown for only the control group.

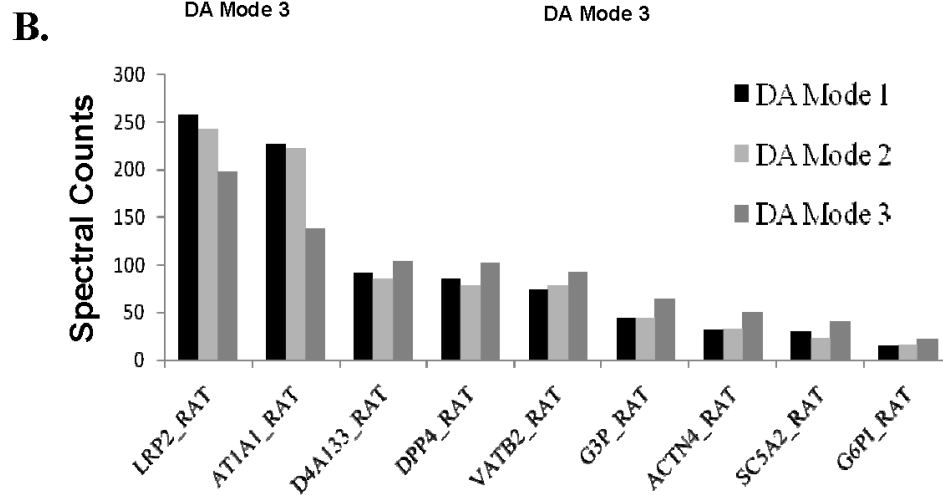
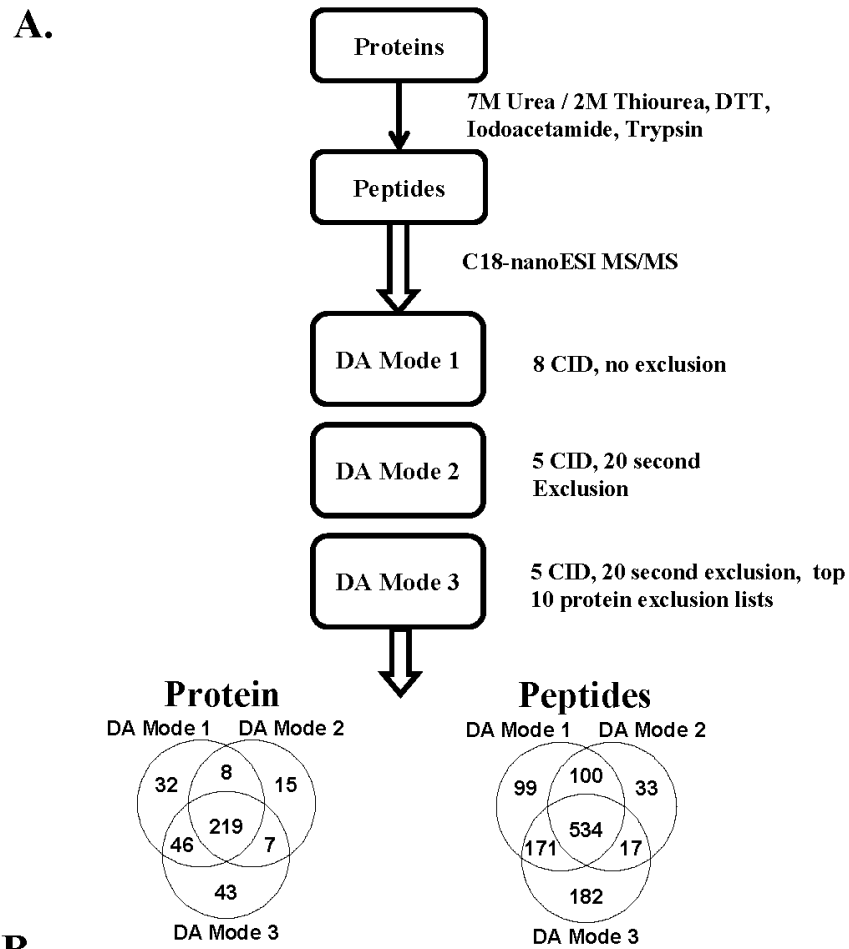


Figure 4.2

spectral assignments was determined by searching a reverse sequence database concatenated to the forward database. The search parameters used in this study produced both a peptide and a protein FDR < 0.1%. The total number of peptides and proteins identified in all four sample groups were 1087 and 298, respectively. Gene Ontology annotations, as edited in Scaffold, were used to identify the functional categories represented in the four sample groups (Figure 4.3). The total number of proteins identified per category was similar for each of the sample groups. The largest categories of identified proteins included membrane proteins, enzymes of metabolic processes, hydrolases and transporters. These annotations are consistent with the physiological function of the brush border membrane of the proximal convoluted tubule.

Topology predictions (<http://www.cbs.dtu.dk/services/TMHMM/>) indicated that 80 proteins, or 26% of the total identified, have a predicted transmembrane domain (TMD). Functional categories for the TMD proteins included receptors, peptidases and transporters. In total, 27 transporters with 6 or more TMDs were identified. The functional classification of molecular transport also includes several proteins that participate in translocation and membrane insertion of transporters. The search also identified a novel membrane protein, D3ZTX4, which has 1 TMD and is not a transporter. A search for conserved domains using the protein families database (<http://www.pfam.sanger.ac.uk>) indicated D3ZTX4 contained 2 trefoil domains (PF00088) that are important for exocellular protection and 2 glycosyl hydrolases domains (PF01055) that are functional motifs used to hydrolyze carbohydrate bonds. Based upon this sequence homology, the protein was assigned a functional annotation of

Figure 4.3. Functional classification of proteins identified in control and acidotic BBMV_{PCT} samples. The proteins identified in the control, 1-d, 3-d, and 7-d acidotic sample groups were classified into selected Gene Ontology annotations using Scaffold software. To better visualize the data, the protein counts were plotted on a log scale.

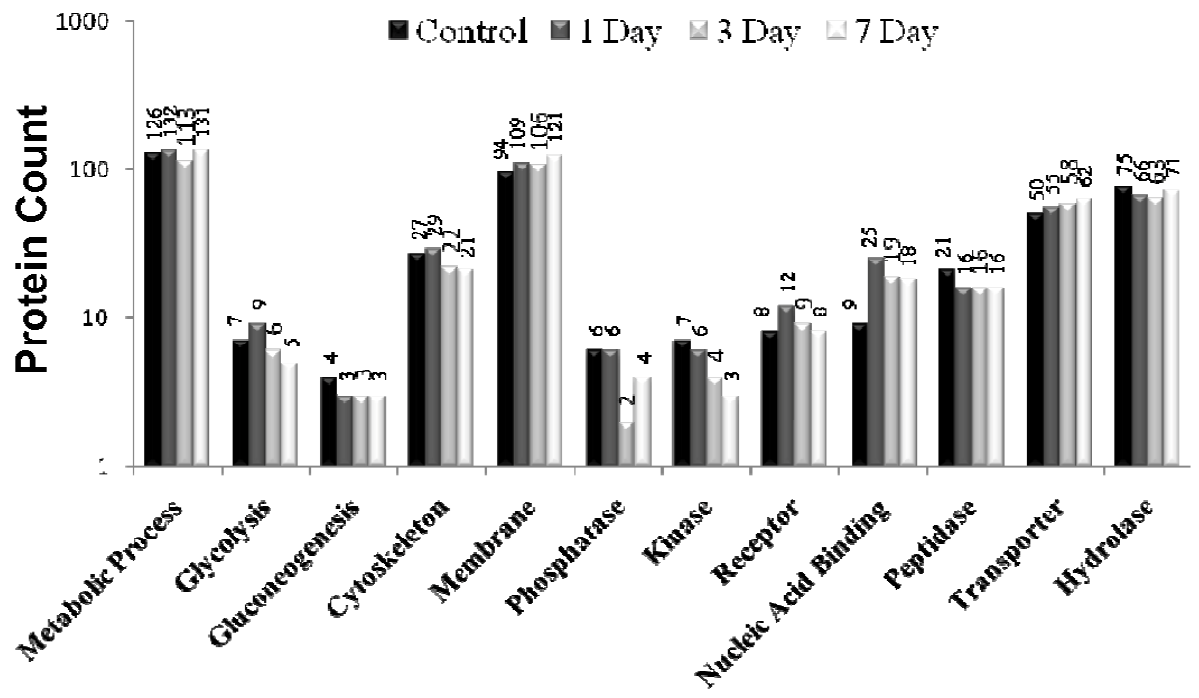


Figure 4.3

a O-glycosyl hydrolase (GO:0004553). Thus, the novel protein may participate in the cleavage of di- or trisaccharides prior to transport across the plasma membrane[176].

The number of proteins identified per sample group, the percent of the total spectra identified, and the percent of the total peptides identified were calculated to assess the variance between the four sample groups. The variances, expressed as percent of the mean, for all of the assessments were between 5.3% and 22.4%, with the greatest deviation occurring in the percent of total peptides identified in the control group. However, a heat map illustrating the correlation between spectral counts indicated highly correlated biological replicates with an average r value equal to 0.95 (Figure 4.4). The samples from the 1-d and 3-d acidotic rats exhibit the greatest correlation ($r \geq 0.98$). The two sets of samples differ from the 7-d acidotic samples ($r \sim 0.85$) and the control samples ($r < 0.70$).

4.4c Quantitative analysis of changes in protein abundance in $BBMV_{PCT}$ during onset of acidosis.

Since the spectral counts (SpC) for each sample group produced highly correlated data sets, spectral counting could be used to assess changes in relative protein abundance [104, 177]. Principal components analysis of the data set was performed to compare the 3 biological replicates within the 4 sample groups (Control, 1-d, 3-d and 7-d acidotic) (Supplemental Figure 1A). The biological replicates grouped in three primary regions of the plot. The 1-d and 3-d samples were found to be most similar to each other, with slight overlap. By contrast, the control and 7-d acidotic samples were significantly different from each other and from the 1-d and 3-day acidotic samples. Further analysis of the

Figure 4.4 Correlation of overall proteomic data obtained from control, 1-d, 3-d and 7-d acidotic rats. Heat map of Pearson's correlation data among the 12 biological samples (3 per group). Colors indicate low correlation ($r \sim 0.65$, blue) to highest correlation ($r \sim 0.99$, red).

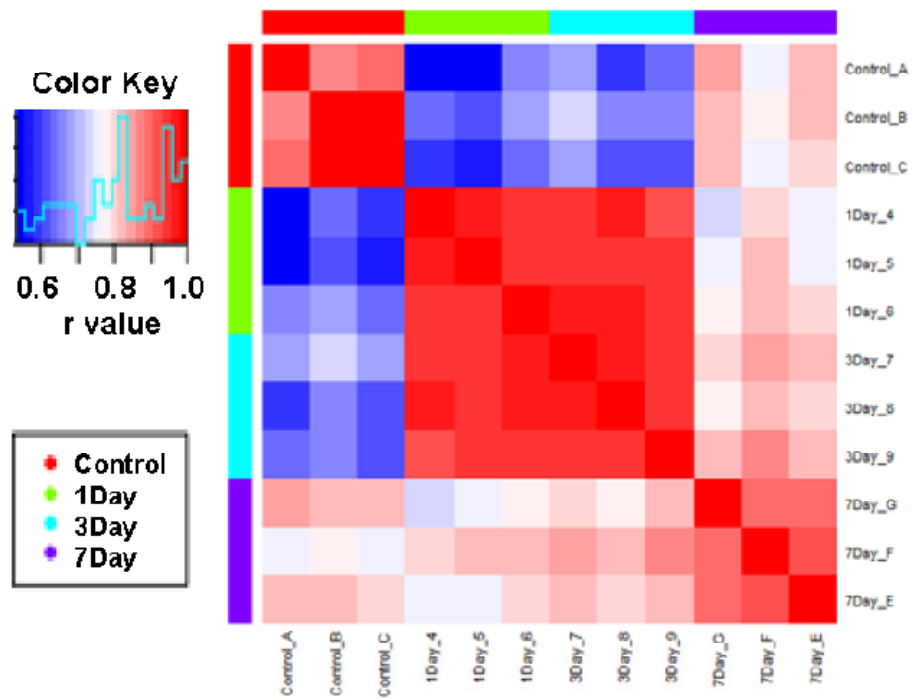


Figure 4.4

SpC data by hierarchical clustering indicated similar trends in the data (Figure 4.5). Several proteins clustered into a group which exhibited a transient decrease in abundance during 1 d and 3 d of acidosis, while others decreased rapidly and remained decreased even after 7 d. Fewer proteins exhibited a transient increase during 1 d and 3 d of acidosis or increased rapidly and remained increased for 7 d.

ANOVA was used to determine the statistical significance of the changes in SpC for each protein after 1 d, 3 d and 7 d of acidosis compared to the control group. The data were plotted as the log adjusted and normalized ratio of spectral counts (Rsc) versus total SpC and color-coded to indicate significant differences (Figure 4.6B). The plot illustrates that it is difficult to validate significant changes in low abundance proteins (< 10 SpC). However, significant differences become more evident with increasing abundance. Frequently, an arbitrary cutoff of a 2-fold change is used to establish significance for proteomic analyses. However, using this approach it was possible to determine significant differences ($p < 0.05$), which may be less than 2-fold, for each protein between each of the acidotic groups and the control samples. To further illustrate the significant differences, the fold change for each protein in each of the acidotic groups was calculated relative to the control group and then plotted versus the calculated p value (Figure 4.7). After 1 d of acidosis, 62 of the 298 identified proteins (20.8%) were significantly ($p \leq 0.05$) increased or decreased (± 1.5 -fold). Most of these proteins remain altered in the 3-d acidotic animals. However, by 7 d of acidosis, nearly half of the initially affected proteins have returned to control levels, while a new set of proteins are now significantly increased or decreased. Each of these analyses indicates that the

Figure 4.5. Cluster analysis of the spectral count data. To illustrate trends in the data, all 298 proteins were clustered using the Dante software as described in the text. The spectral counts for each protein in the separate samples were expressed relative to the mean of the spectral counts for that protein in all the samples. The results were color coded green (below the mean) or red (above the mean) on a \log_2 scale.

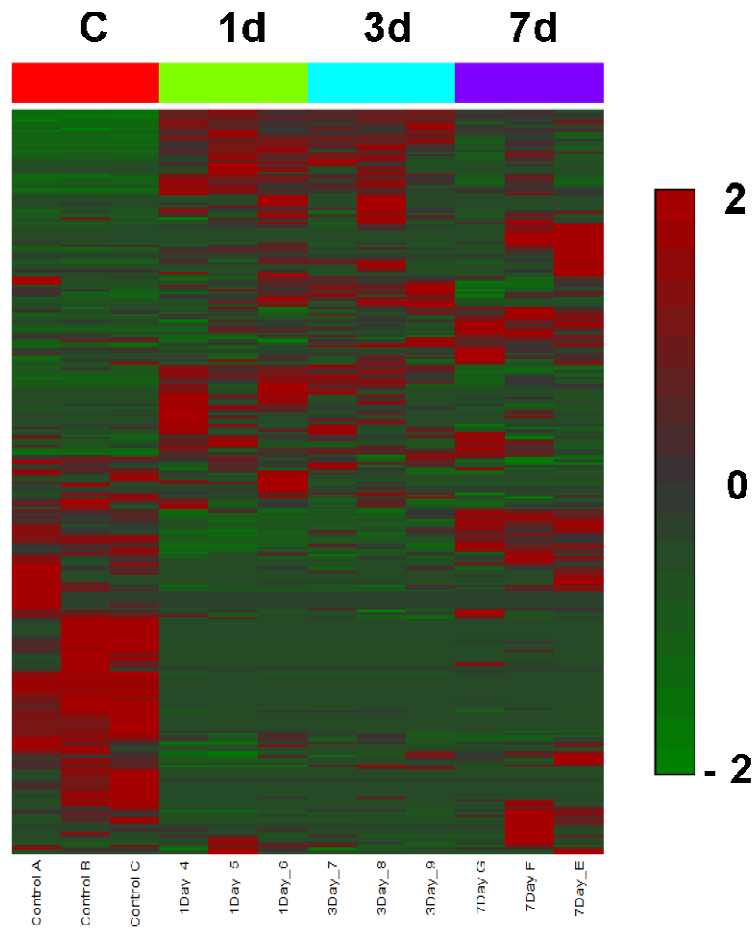


Figure 4.5

Figure 4.6. Statistical analysis of spectral count data. Panel A. Principal component analysis. A plot of the \log_2 values of the principle components indicate that the greatest differences were observed between the control and the 7-d acidotic groups, whereas the 1-d and 3-d acidotic samples were the most similar. Panel B. Significance analysis. Spectral counts were summed for each protein and then plotted versus the Rsc values. Colored data points indicate those proteins that were significantly increased (red) or decreased (green) versus the control group. To account for the variance among samples, the statistical analysis was calculated using a Student's t test ($p \leq 0.05$) prior to summing the spectral counts.

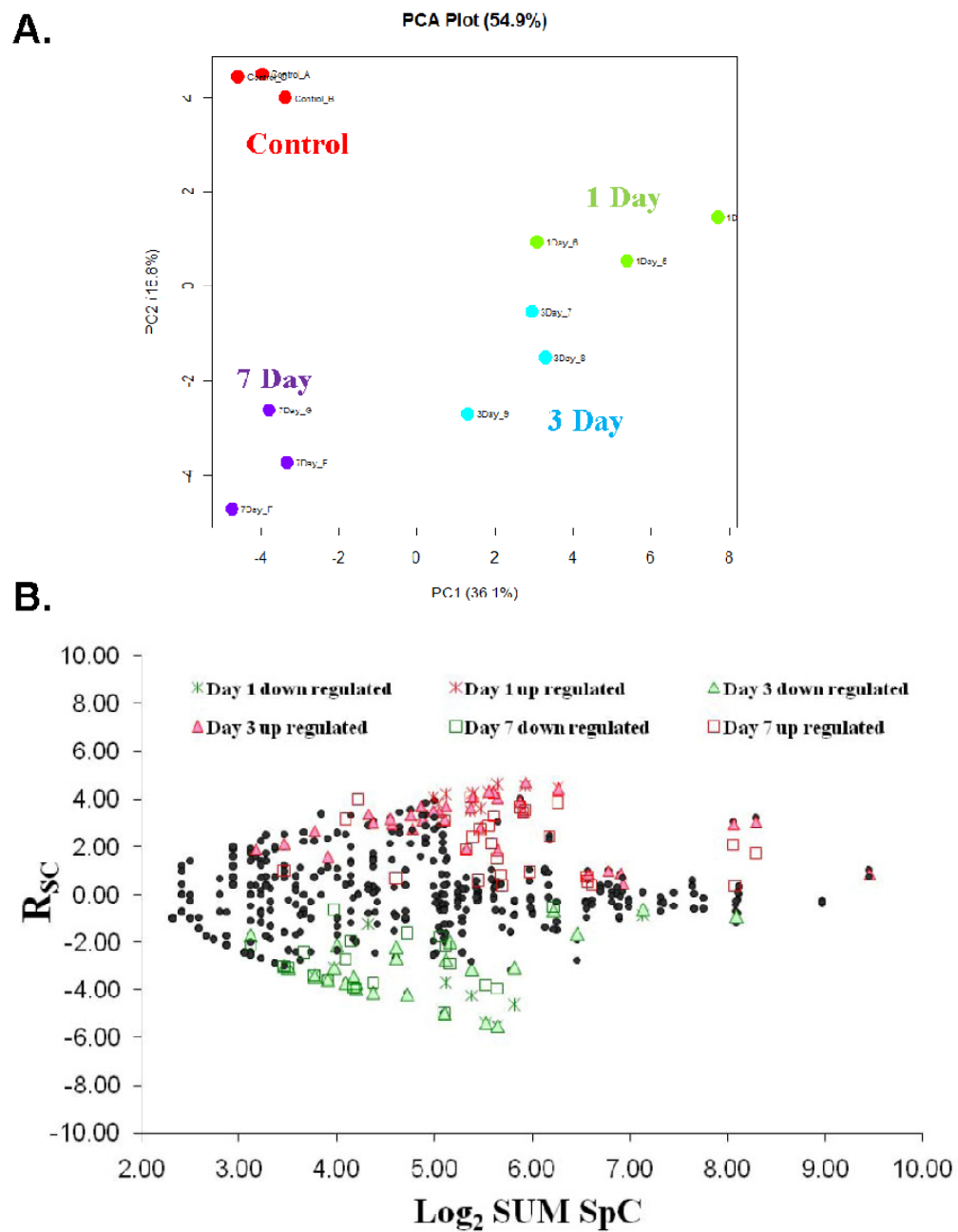


Figure 4.6

Figure 4.7. Global analysis of significant changes in protein abundance. The fold change for each protein in each of the 3 acidotic groups was calculated relative to its level in the control group and then plotted versus the associated p value. The proteins that were significantly ($p \leq 0.05$) increased or decreased (± 1.5 -fold) after 1 day of acidosis were colored blue (upper panel). The levels of most of these proteins remain significantly altered after 3 d of acidosis (middle panel). By 7 d of acidosis, most of these proteins are no longer significantly different from control values (lower panel). However, a new set of proteins now become significantly increased or decreased compared to the control levels.

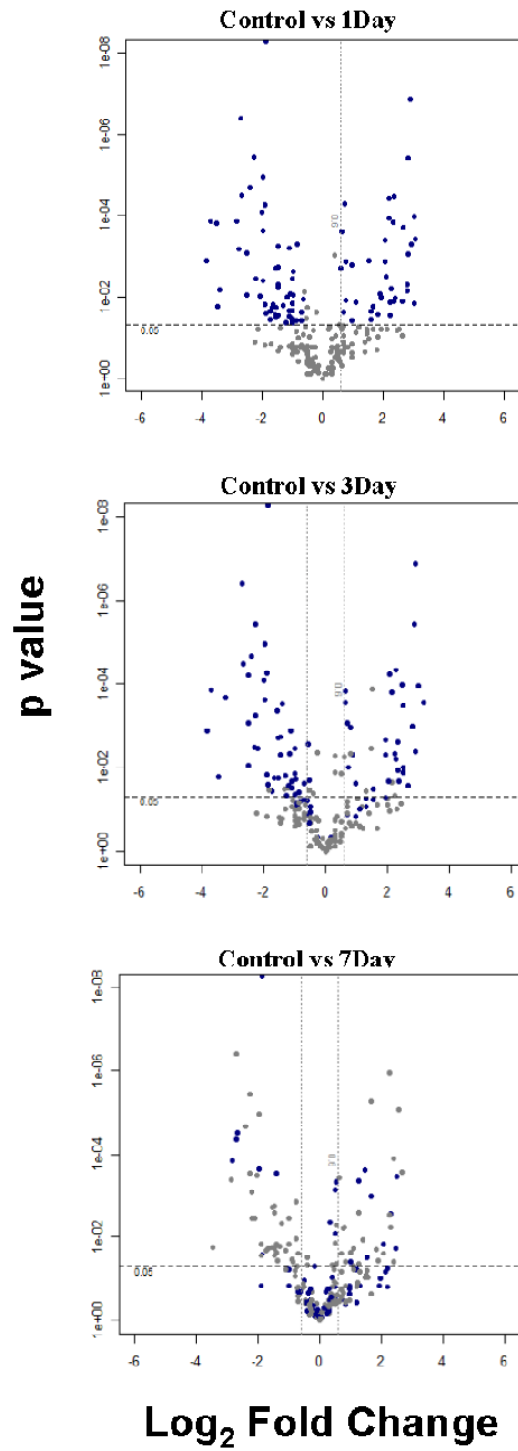


Figure 4.7

proteome of the brush border membrane of the proximal convoluted tubule undergoes a rapid and pronounced remodeling during onset of acidosis. In addition, each of the affected proteins follows one of the limited subsets of temporal patterns.

Using the Gene Ontology annotations and spectral count data, several transporters and other membrane proteins were analyzed for changes in protein abundance (Table 1A). Two members of the Na⁺-dependent glucose transporter family, SLC5A2 and SLC5A8 were significantly increased in abundance during onset of acidosis. The apical Na⁺-dependent glucose transporter, SLC5A2 (aka SGLT2), is increased nearly 2-fold within 1-d and 3-d of onset of acidosis, but returns to normal by 7-d of acidosis. SGLT2 is the primary glucose transporter in the apical membrane of the early proximal convoluted tubule [178]. By contrast, the apical Na⁺-dependent lactate transporter, SLC5A8 (aka SGLT5) [179], is increased more gradually and remains elevated (3-fold) even after 7 d of acidosis. Additional transporters that exhibit less pronounced but significant increases include the apical Na⁺-dependent phosphate transporter, SLC34A3 (aka NaPi2C), and the very abundant basolateral Na⁺/3HCO₃⁻ co-transporter, SLC4A4 (aka NBC-1). By contrast, the Na⁺-dependent phosphate transporter, SLC34A1 (aka NaPi2A) is rapidly decreased during onset of acidosis, but returns to normal levels by 3-d of acidosis. The Na⁺/K⁺ ATPase alpha (Na⁺/K⁺ ATPase subunit alpha 1) and beta (AT1B1) subunits are primarily localized to the basolateral membrane. The levels of the two Na⁺/K⁺ ATPase subunits associated with the BBMV_{PCT} samples were unchanged during onset of acidosis (data not shown). The B, C, E, F and L subunits of the V-type H⁺-ATPase (VAT), a known apical marker, were also identified (Table 1A). Of these,

the C and E subunits increased significantly (> 2-fold) by 3 d of acidosis. By contrast, the levels of the B and L subunits were decreased slightly.

Proteins identified as having peptidase activity were also quantified (Table 1B). Based upon total SpC, dipeptidyl peptidase IV, aminopeptidase N, X-prolyl aminopeptidase and γ -glutamyltranspeptidase were the most abundant peptidases. Based upon SpC data, γ -glutamyltranspeptidase and glutamyl aminopeptidase were increased significantly only after 7 d of acidosis. However, the dipeptidase, collectrin (TMM27), was increased significantly in all of the acidotic samples, but was maximally increased (1.9-fold) at 3 d of acidosis. By contrast, aminopeptidase N decreased significantly in the 1-d and 3-d acidotic groups and a soluble dipeptidase (CNDP2) was detected only in the control sample.

Our previous analysis established that BBMV_{PCT} contain significant levels of many of the enzymes of glycolysis and gluconeogenesis [164]. Most of these proteins are significantly decreased in BBMV_{PCT} isolated from 1-d, 3-d and 7-d acidotic animals (Table 2A). These include fructose-1,6-bisphosphatase and phosphoenolpyruvate carboxykinase (PCK1), two enzymes that are unique to gluconeogenesis, and five enzymes that catalyze reversible reactions of the glycolytic pathway. Additional enzymes of carbohydrate metabolism that are decreased include transketolase and cytoplasmic isoforms of malate dehydrogenase and isocitrate dehydrogenase. Of this group, only Aldolase decreases transiently during 1-d and 3-d of acidosis and then returns to control levels.

Proteins involved in cytoskeleton structure, membrane scaffolding, vesicle trafficking and signal transduction were also analyzed (Table 2B). NHERF1, NHERF3 and

PDZKIP1 are known apical markers of the proximal tubule [180]. This group of proteins contain PDZ, PDZ interacting, Src homology, or plekstrin homology domains which function to target proteins to the apical plasma membrane via their scaffolding interactions. These results, combined with the identification of ezrin, radixin, moesin and proteins of the actin filament complex, are consistent with enrichment of BBMV_{PCT} [181]. Of these proteins, only myosin 9 was greatly increased (10-fold), while NHERF3 and PDZK1IP were significantly decreased (2-fold), during early onset of acidosis. Identified proteins involved in vesicle trafficking included various isoforms of Rab, Ras and Rho, all of which are important for vesicle trafficking and endosomal recycling. Two guanine nucleotide-binding proteins, the alpha-2 subunit of G_i and the beta-2 subunit of $G_i/G_s/G_t$ were also observed. Both are membrane-associated proteins that are GTP-dependent modulators of signal transduction. Sequence annotation from uniprot.org suggests that G_i alpha-2 subunit may function as a MAP-Kinase-Kinase activator. Of these proteins, only Rab1A and Rab7A exhibit transient decreases during onset of acidosis.

4.5 Discussion

4.5a Proteins involved in carbohydrate transport and metabolism.

During metabolic acidosis, the kidney becomes an important gluconeogenic organ. The initial conversion of glutamine to α -ketoglutarate generates 2 NH_4^+ ions. In rats [182, 183] and humans [145], the α -ketoglutarate generated from the renal catabolism of glutamine is primarily converted to glucose. This process requires the cataplerotic activity of phosphoenolpyruvate carboxykinase to convert intermediates of the

tricarboxylic acid cycle to phosphoenolpyruvate. This pathway generates 2 H⁺ and 2 HCO₃⁻ ions per α-ketoglutarate. The 2 H⁺ ions are subsequently consumed during the conversion of phosphoenolpyruvate to glucose. Therefore, the combined pathways of ammoniogenesis and gluconeogenesis result in a net production of 2 HCO₃⁻ per glutamine, which are transported into the renal venous blood. As a result, the combined adaptations create a net renal release of HCO₃⁻ ions that partially restore acid-base balance. This process is activated, in part, by the rapid and pronounced (7-fold) increase in phosphoenolpyruvate carboxykinase that occurs within the proximal convoluted tubule [33, 151].

Previous proteomic analysis established that enzymes of glycolysis and gluconeogenesis are enriched in BBM_V_{PCT} compared to BBM_V isolated from renal cortex [164]. The latter preparation contains apical membranes from multiple cortical cells in addition to the proximal convoluted tubule. The observed enrichment suggests that during normal acid-base balance enzymes of glucose metabolism may form a complex that is sequestered near or associated with the brush border membrane of the proximal convoluted tubule. Previous immunofluorescence studies have clearly established that aldolase [140] and fructose 1,6-bisphosphatase [143] are normally localized to the apical membrane of the proximal convoluted tubule [142]. Similar observations in erythrocytes [184] suggested that the association of the enzymes of glycolysis with the membrane may generate a higher localized concentration of ATP that is used to support active transport processes [184]. The finding that several proteins involved in the reversible steps of glycolysis and in gluconeogenesis are significantly decreased or no longer detectable in BBM_V_{PCT} isolated from acidotic rats suggests that

the sequestered complex may dissociate from the apical membrane during acidosis. The release of enzymes, including fructose-1,6-bisphosphatase and phosphoenolpyruvate carboxykinase, may support the rapid increase in glucose synthesis [145]. The selective return of aldolase to the brush border membrane following 7 d of acidosis may be due to its functional association with the A, B, and E subunits of the V-type H⁺-ATPase [140]. Previous studies have clearly established that aldolase co-localizes with the H⁺-ATPase and that this interaction is essential for the membrane insertion and correct assembly of the H⁺-ATPase [141]. Thus, the transient decrease in aldolase may contribute to the altered ratios of H⁺-ATPase subunits that are observed during onset of acidosis.

The observed transient increase in the Na⁺-dependent glucose transporter (SGLT2) was confirmed by western blot analysis. This finding suggests that a greater proportion of the filtered glucose may be reabsorbed within the early proximal convoluted tubule during onset of acidosis. The reabsorbed glucose could provide energy to support the pronounced remodeling of the cellular proteome that occurs during early onset of acidosis. However, given the rapid and pronounced shift towards gluconeogenesis, it is more likely that the reabsorbed glucose undergoes transepithelial transport and is returned to the blood. Finally, the gradual increase in the Na⁺-dependent lactate transporter (SGLT5) suggests lactate may become a more important metabolic fuel or gluconeogenic precursor in the proximal convoluted tubule during prolonged metabolic acidosis.

4.5b Cytoskeletal, scaffolding and trafficking proteins.

Scaffolding proteins within the apical projections of the proximal convoluted tubule play an important role in the insertion and recycling of brush border membrane proteins [181]. The PDZ domain containing proteins, NHERF1 and NHERF3, were quantified in our analysis (Table 2B). NHERF1 was originally identified as a protein kinase A dependent modulator of the apical Na⁺/H⁺-exchanger (NHE3) activity [185]. However, it is now known that NHERF1 interacts with multiple membrane proteins including CLC3, SLC34A1, Gi/Gs/Gt Guanine nucleotide binding protein complex and H⁺-ATPase [181]. NHERF1 also interacts with the ezrin-radixin-moesin complex that binds to actin. These interactions contribute to the targeting of vesicles and the insertion of proteins into the apical membrane. Therefore, changes in this class of proteins could contribute to the pronounced remodeling of the brush border membrane that occurs during onset of acidosis. Several of these proteins were identified in our analysis. However, total SpC detected for many of these proteins were not as pronounced as other classes of proteins. As a result, the observed increase in NHERF1 was not statistically significant. However, the transient decreases observed for the more abundant NHERF3 and the adapter protein, DAB2, were significant. The most significant change was the pronounced increase (10-fold) in myosin 6. This isoform of myosin functions to move proteins along actin filaments from the body to the base of the microvilli of the proximal tubule [186]. Recent experiments using TIRF microscopy and a dominant negative form of myosin 6 in opossum kidney cells demonstrated that this isoform participates in the parathyroid hormone-stimulated removal of NaPi2 from the apical membrane [187]. Therefore, the observed increase in myosin 6 levels in BBMV_{PCT} isolated from acidotic rats suggests

that it may also contribute the pronounced remodeling of the apical membrane during onset of acidosis.

Rab proteins also participate in the recycling of membrane proteins. We identified two isoforms, Rab5c and Rab7, that are known regulators of endocytosis from apical clathrin coated pits [188, 189]. Clathrin levels were significantly increased, while Rab5c and Rab7 were either not detected or transiently decreased, respectively, during 1-d and 3-d of acidosis. Many of the additional Rab proteins have low SpC compared to the proteins that are specific to the apical membrane. These proteins are probably associated with endosomes that are trapped in the vesicles during homogenization.

4.5c Amino acid transport and metabolism.

The observed increase in γ -glutamyltranspeptidase (γ GT) was confirmed by enzymatic assay. This enzyme also catalyzes a phosphate-independent glutaminase activity [122]. In normal rats, γ GT is expressed primarily on the luminal surface of the proximal straight tubule [54, 172], which contains little glutamine [23]. However, the observed increase in γ GT in BBMV_{PCT} suggests that during acidosis, it may facilitate the deamidation of filtered glutamine within the lumen of the proximal convoluted tubule. This process would be enhanced by the observed transient decreases in rBAT and B^oAT1, which are apical neutral amino acid transporters that facilitate glutamine uptake [24].

4.5d Relevance to brush border membrane physiology.

Proteomic analyses are typically completed for two purposes, the identification of proteins in a particular sample and the quantification of changes in protein abundance. In

this study, the inclusion of multiple dynamic acquisition modes increased the number of proteins that were confidently identified in the BBMV_{PCT} samples. In addition, statistical analyses of spectral counts were used to provide an initial assessment of the changes in protein abundance that occur during onset of metabolic acidosis. A large proportion of the identified proteins exhibit transient increases or decreases, while a smaller number of proteins exhibit changes that are sustained even after 7 d of acidosis. Some of the observed changes were confirmed by western blot analysis and shown to involve even greater changes than assessed by spectral counting. Not all of the observed changes were discussed in this manuscript. Thus, researchers are encouraged to peruse the complete data set given in Supplemental Table 1 to determine if their protein of interest may respond to metabolic acidosis. In the future, targeted proteomic analyses will be performed to further validate the observed changes and to develop testable hypotheses for biochemical and immunofluorescence studies.

4.6 Acknowledgements

This research was supported in part by National Institute of Diabetes and Digestive and Kidney Diseases Grants DK-37124 and DK-75517 awarded to N. P. Curthoys. All mass spectrometry was performed at the Genomics and Proteomics Core facility of the Rocky Mountain Regional Center of Excellence for Biodefense and Emerging Infectious Diseases Research (<http://www.rmrc.colostate.edu>). The authors wish to thank Brian Cranmer, for his assistance in the operation and maintenance of the mass spectrometer and Dr. Ann Hess, from the Department of Statistics, for her help with the statistical analysis of the spectral counts.

Table 1

A. Transporters, phosphatase, peptidase Protein	Gene_Symbol (Uniprot)	Mass (kDa)	TMD (TMHMM)	SpC								Functional Category Subclass	Apical?
				C	±SE	1 Day	±SE	3 Day	±SE	7 Day	±SE		
Excitatory amino acid transporter 3 GN=Slc1a1	EAA3_RAT	57	9	5.7	1.3	3.7	2.2	4.7	2.0	10.3	1.2	dicarboxylic acid	Y
Neutral and basic amino acid transport protein rBAT GN=Slc3a1	SLC31_RAT	79	1	28.7	6.2	11.3	3.2	13.0	5.3	25.3	3.2	amino acid	Y
4F2 cell-surface antigen heavy chain GN=Slc3a2	4F2_RAT	58	1	43.3	4.1	22.3	6.1	24.7	2.9	34.0	7.9	neutral amino acid	Y
Electrogenic sodium bicarbonate cotransporter 1 GN=Slc4a4	S4A4_RAT	121	9	23.0	2.5	24.7	6.9	33.0	1.5	39.0	4.6	bicarbonate ion	-
Sodium/glucose cotransporter 1 GN=Slc5a1	SC5A1_RAT	73	14	2.7	1.2	1.0	0.0	1.3	0.3	1.7	0.7	carbohydrate	Y
Sodium/glucose cotransporter 2 GN=Slc5a2	SC5A2_RAT	73	14	21.0	0.6	38.7	1.2	38.3	4.1	20.3	0.9	carbohydrate	Y
Putative uncharacterized protein Slc5a8 GN=Slc5a8	D3Z9E5_RAT	66	13	5.3	0.9	8.7	1.5	20.3	0.3	16.7	1.9	neurotransmitter	Y
Slc5a10 protein GN=Slc5a10	B1WBS5_RAT	59	13	3.3	1.9	1.0	0.0	1.0	0.0	8.3	1.5	transmembrane	Y
Sodium- and chloride-dependent creatine transporter 1 GN=Slc6a8	SC6A8_RAT	71	12	3.7	1.5	1.0	0.0	1.0	0.0	1.0	0.0	creatine	Y
Transporter GN=Slc6a18	S6A18_RAT	66	12	3.0	1.0	3.7	0.9	9.7	0.7	1.0	0.0	neurotransmitter	Y
Transporter GN=Slc6a19	S6A19_RAT	57	12	13.0	1.5	15.7	4.2	15.7	3.8	6.3	0.9	neutral amino acid	Y
Monocarboxylate transporter 1 GN=Slc16a1	MOT1_RAT	53	11	1.3	0.3	1.3	0.3	1.0	0.0	1.0	0.0	monocarboxylate	Y
Putative uncharacterized protein Slc22a1 GN=Slc22a1	S22A1_RAT	62	12	2.0	0.0	1.0	0.0	1.0	0.0	1.7	0.7	organic cation	-
Putative uncharacterized protein Slc22a6 GN=Slc22a6	S22A6_RAT	60	8	11.0	1.0	8.3	0.9	11.7	1.2	11.3	0.3	organic anion	-
Solute carrier family 22 member 8 GN=Slc22a8	S22A8_RAT	59	9	3.3	1.9	1.0	0.0	1.3	0.3	4.3	2.0	quaternary ammonium	-
Solute carrier family 22 member 12 GN=Slc22a12	S22AC_RAT	60	10	1.0	0.0	1.0	0.0	1.0	0.0	1.7	0.7	urate	Y
Mitochondrial dicarboxylate carrier GN=SLC25a10	O89035_RAT	31	0	1.0	0.0	4.7	2.3	5.0	1.0	2.7	1.7	malate	-
Sodium-dependent phosphate transport protein 2A GN=Slc34a1	NPT2A_RAT	69	11	11.0	6.5	4.3	0.3	8.0	2.1	9.0	0.6	phosphate	Y
Sodium-dependent phosphate transport protein 2C GN=Slc34a3	NPT2C_RAT	64	11	3.3	0.9	5.7	0.7	7.7	1.9	4.7	1.9	phosphate	Y
Aquaporin-1 GN=Aqp1	AQP1_RAT	29	6	9.3	0.3	8.0	3.1	8.7	0.9	14.0	1.2	Glycerol, water	Y
ATP-binding cassette sub-family G member 2 GN=Abcg2	ABCG2_RAT	73	6	1.3	0.3	1.7	0.7	1.3	0.3	4.0	1.0	drug transmembrane activity	Y

Solute carrier family 22 member 12 GN=Slc22a12	S22AC_RAT	60	10	1.0	0.0	1.0	0.0	1.0	0.0	1.7	0.7	urate	Y
Mitochondrial dicarboxylate carrier GN=SLC25a10	O89035_RAT	31	0	1.0	0.0	4.7	2.3	5.0	1.0	2.7	1.7	malate	-
Sodium-dependent phosphate transport protein 2A GN=Slc34a1	NPT2A_RAT	69	11	11.0	6.5	4.3	0.3	8.0	2.1	9.0	0.6	phosphate	Y
Sodium-dependent phosphate transport protein 2C GN=Slc34a3	NPT2C_RAT	64	11	3.3	0.9	5.7	0.7	7.7	1.9	4.7	1.9	phosphate	Y
Aquaporin-1 GN=Aqp1	AQP1_RAT	29	6	9.3	0.3	8.0	3.1	8.7	0.9	14.0	1.2	Glycerol, water	Y
ATP-binding cassette sub-family G member 2 GN=Abcg2	ABCG2_RAT	73	6	1.3	0.3	1.7	0.7	1.3	0.3	4.0	1.0	drug transmembrane activity	Y
Collectrin GN=Tmem27	TMM27_RAT	25	1	14.7	1.8	26.3	1.7	28.3	3.0	23.3	0.3	phosphatidyl-di-peptidase activi	Y
V-type proton ATPase subunit B, brain isoform GN=Atp6v1b2	VATB2_RAT	57	-	50.7	1.3	40.3	2.4	34.7	4.5	47.7	7.8	ATPase	Y
V-type proton ATPase subunit C 1 GN=Atp6v1c1	VATC1_RAT	44	-	11.7	2.7	23.7	3.2	26.7	0.7	5.3	1.3	ATPase	Y
V-type proton ATPase subunit E 1 GN=Atp6v1e1	VATE1_RAT	26	-	15.3	0.9	32.3	2.0	33.3	4.5	22.7	2.3	ATPase	Y

Table 1

B. Peptidase, phosphatase Protein	Gene_Symbol (Uniprot)	Mass (kDa)	TMD (TMHMM)	SpC									
				C	±SE	1 Day	±SE	3 Day	±SE	7 Day	±SE		
Alkaline phosphatase, tissue-nonspecific isozyme GN=Alpl	PPBT_RAT	58	-	8.7	0.9	9.7	0.9	8.0	3.2	11.0	3.2	Protein Phosphatase	Y
Protein phosphatase 2 (Formerly 2A), regulatory subunit A (PR 65), alpha isoform,	Q5XI34_RAT	65	-	1.3	0.3	1.3	0.3	1.0	0.0	1.0	0.0	Protein Phosphatase	-
Aminopeptidase N GN=Anpep	AMPN_RAT	109	1	94.0	5.5	41.7	4.3	53.3	6.9	87.3	8.2	Serine-type peptidase	Y
Dipeptidyl peptidase 4 GN=Dpp4	DPP4_RAT	88	1	59.3	2.8	35.0	8.5	35.0	6.4	64.7	4.7	Aminopeptidase	Y
Membrane-bound aminopeptidase P GN=Xpnpep2	Q99MA2_RAT	76	-	47.0	2.6	26.3	3.0	38.0	6.0	45.3	4.1	Metallo exopeptidase	Y
Gamma-glutamyltranspeptidase 1 GN=Ggt1	GGT1_RAT	62	1	26.0	2.0	14.3	2.7	15.7	2.4	44.0	2.6	Acyltransferase	Y
Glutamyl aminopeptidase GN=Enpep	AMPE_RAT	108	1	24.0	5.6	13.3	1.3	13.0	2.9	14.7	3.8	Aminopeptidase	Y
Dipeptidase 1 GN=Dpep1	DPEP1_RAT	46	-	7.0	1.5	7.0	3.5	14.7	9.1	5.3	0.7	Dipeptidase	Y
Cytosolic non-specific dipeptidase GN=Cndp2	CNDP2_RAT	53	-	8.0	1.0	1.0	0.0	1.0	0.0	1.0	0.0	Carboxypeptidase	-
Retinoid-inducible serine carboxypeptidase GN=Scpep1	RISC_RAT	51	1	5.3	2.3	1.0	0.0	1.0	0.0	1.0	0.0	Serine type carboxypeptidase	-
Xaa-Pro dipeptidase GN=Pepd	PEPD_RAT	55	-	2.7	1.2	1.0	0.0	1.0	0.0	1.0	0.0	Metallo exopeptidase	Y
Glutamate carboxypeptidase 2 GN=Folh1	FOLH1_RAT	85	1	4.7	1.2	2.7	0.7	7.0	3.5	13.3	3.0	Metalloprotease	-
Xaa-Pro aminopeptidase 1 GN=Xpnpep1	XPP1_RAT	70	-	2.0	0.0	1.0	0.0	1.0	0.0	1.0	0.0	Metalloamino peptidase	Y
Dipeptidyl peptidase 2 GN=Dpp7	DPP2_RAT	55	-	1.7	0.3	1.0	0.0	1.0	0.0	1.0	0.0	Serine-type peptidase	-
Low-density lipoprotein receptor-related protein 2 GN=Lrp2	LRP2_RAT	519	1	147.0	7.0	122.3	6.4	112.7	4.3	126.3	6.6	Receptor, SH3 domain binding	Y

Table 2

A. Carbohydrate Metabolic Process

Protein	Gene_Symbol (Uniprot)	Mass (kDa)	SpC								Functional Category	KEGG ID	
			Control	±SE	1 Day	±SE	3 Day	±SE	7 Day	±SE			
Phosphoenolpyruvate carboxykinase, cytosolic [GTP] GN=Pck1	PCKGC_RAT	69	8.0	3.6	1.3	0.3	1.0	0.0	5.0	1.2	gluconeogenesis	rno00010	Glycolysis/ gluconeogenesis
L-lactate dehydrogenase B chain GN=Ldhb	LDHB_RAT	37	30.7	3.3	7.0	1.0	6.5	1.2	3.3	1.2	glycolysis	rno00010	Glycolysis/ gluconeogenesis
Malate dehydrogenase, cytoplasmic GN=Mdh1	MDHC_RAT	36	22.7	3.9	1.0	0.0	1.0	0.0	1.0	0.0	glycolysis	rno00620	Pyruvate metabolism
Enolase GN=Eno1	Q5EB49_RAT	47	50.3	4.2	1.7	0.3	2.0	0.8	4.3	2.3	glycolysis	rno00010	Glycolysis/ gluconeogenesis
Glyceraldehyde-3-phosphate dehydrogenase GN=Gapdh	Glyceraldehyde-3-phosphate dehydrogenase_RAT	36	51.3	3.7	1.7	0.3	4.0	0.0	20.3	1.7	gluconeogenesis / glycolysis	rno00010	Glycolysis/ gluconeogenesis
Fructose-bisphosphate aldolase GN=Aldob	Q66HT1_RAT	40	71.0	4.0	24.0	4.2	27.5	1.2	60.0	8.2	glycolysis	rno00010	Glycolysis/ gluconeogenesis
Fructose-1,6-bisphosphatase 1 GN=Fbp1	F16P1_RAT	40	80.7	1.9	14.0	3.6	23.0	4.1	12.3	6.6	gluconeogenesis	rno00010	Glycolysis/ gluconeogenesis
Glucose-6-phosphate isomerase GN=Gpi	G6PI_RAT	63	15.0	3.1	1.0	0.0	1.5	0.4	2.3	0.3	gluconeogenesis / glycolysis	rno00010	Glycolysis/ gluconeogenesis
Transketolase GN=Tkt	TKT_RAT	68	24.7	5.0	1.0	0.0	1.0	0.0	4.3	2.8	pentose- phosphate shunt	rno00030	Pentose phosphate pathway
Triosephosphate isomerase GN=LOC500959	Q6SA19_RAT	27	9.3	0.3	1.0	0.0	1.0	0.0	1.0	0.0	glycolysis	rno00010	Glycolysis/ gluconeogenesis
Isocitrate dehydrogenase [NADP] cytoplasmic GN=Idh1	IDHC_RAT	47	14.7	3.5	1.0	0.0	1.0	0.0	1.0	0.0	glyoxylate cycle	rno00480	Glutathione metabolism
Putative uncharacterized protein Ogdh GN=Ogdh	D3ZFA6_RAT	118	1.0	0.0	8.0	1.2	4.5	2.0	2.0	0.6	carbohydrate metabolic process	-	-
Putative uncharacterized protein ENSRNOP00000016912	D3ZTX4_RAT	197	18.7	0.7	12.3	2.0	19.0	0.0	17.7	7.9	carbohydrate metabolic process	-	-

Table 2

B. Signal transduction, Trafficking, Cytoskeleton

Protein	Gene_Symbol	(kDa)	SpC								Functional Category	Domain or famil	PFAM ID
			Control	±SE	1 Day	±SE	3 Day	±SE	7 Day	±SE			
Ras-related protein Rab-1A GN=Rab1A	RAB1A_RAT	23	8.0	0.6	1.7	0.3	9.3	1.9	6.7	1.5	protein transport, small GTPase mediated signal	Ras	PF00071
Ras-related protein Rab-1B GN=Rab1b	RAB1B_RAT	22	1.0	0.0	1.0	0.0	1.0	0.0	1.7	0.7	protein transport, small GTPase mediated signal	Ras	PF00071
RCG32615, isoform CRA_a GN=Rab5c	B0BNK1_RAT	23	3.0	1.2	1.0	0.0	1.0	0.0	4.3	2.0	protein transport, small GTPase mediated signal	Ras	PF00071
Ras-related protein Rab-7a GN=Rab7a	RAB7A_RAT	24	10.7	0.9	3.0	1.0	6.7	1.3	15.0	4.4	protein transport, small GTPase mediated signal	Ras	PF00071
Putative uncharacterized protein Rab8a GN=Rab8a	D3Z848_RAT	24		0.3	1.7	0.3	1.3	0.3	1.3	0.3	protein transport, small GTPase mediated signal	Ras	PF00071
RAB10, member RAS oncogene family GN=Rab10	Q5RKJ9_RAT	23	2.7	0.7	3.0	1.0	2.0	1.0	5.0	2.3	protein transport, small GTPase mediated signal	Ras	PF00071
Ras-related protein Rap-1A GN=Rap1a	RAP1A_RAT	21	9.7	0.3	13.7	2.8	11.3	1.9	8.3	1.7	protein transport, small GTPase mediated signal	Ras	PF00071
RCG40097 OS=Rattus norvegicus GN=Rras2	Q5BJU0_RAT	23	2.0	0.6	2.3	0.9	1.7	0.7	1.7	0.3	protein transport, small GTPase mediated signal	Ras	PF00071
Guanine nucleotide-binding protein G(i) subunit alpha-2 GN=Gnai2	GNAI2_RAT	41	1.0	0.0	1.0	0.0	1.0	0.0	2.3	0.7	signal transducer activity	WD40	PF00400
Guanine nucleotide-binding protein G(I)/G(S)/G(T) subunit beta-2 GN=Gnb2	GBB2_RAT	37	1.3	0.3	1.7	0.3	1.0	0.0	2.7	1.7	signal transducer activity	G-alpha	PF00503
Na(+)/H(+) exchange regulatory cofactor NHERF1 GN=Slc9a3r1	NHRF1_RAT	39	8.7	2.7	5.7	1.2	9.7	1.5	14.7	6.1	PDZ Domain containing	PDZ	PF00595
Na(+)/H(+) exchange regulatory cofactor NHERF3 GN=Pdzk1	NHRF3_RAT	57	47.7	14.8	32.3	11.0	49.7	6.2	35.0	9.5	PDZ Domain containing	PDZ	PF00595
Putative uncharacterized protein ENSRNOP0000048147 DAB2 similar	D3ZGX5_RAT	49	15.7	1.8	6.0	1.5	10.0	2.1	22.7	2.4	PDZ Interacting	PTB/PIC	PF00640
PDZK1-interacting protein 1 GN=Pdzk1ip1	PDZ1I_RAT	12	4.7	3.2	6.0	2.9	14.0	1.5	8.7	2.6	Protein binding	-	-
Alpha II spectrin GN=Spna2	C9EH87_RAT	288	3.3	0.9	11.7	3.9	13.3	3.3	12.3	5.5	protein complex binding	SH3_1	PF00018
Non-erythroid spectrin beta GN=Sptbn1	Q6XD99_RAT	274	1.3	0.3	5.0	0.6	4.0	1.7	11.7	5.8	actin binding	CH , PH	PF00307, PF00169
Mitogen-activated protein kinase scaffold protein 1 GN=Mapksp1	MPKS1_RAT	14	4.3	1.3	1.7	0.3	2.0	0.6	5.7	0.9	Protein binding	MAPKK1_Int	PF08923
Actin, cytoplasmic 1 GN=Actb	ACTB_RAT	42	56.7	10.2	74.0	4.5	75.7	7.8	68.0	12.8	actin cytoskeletal	Actin	PF00022
Actin-related protein 3 GN=Actr3	ARP3_RAT	47	3.7	0.9	2.0	1.0	1.0	0.0	2.0	1.0	actin binding	Rob1_LC7	PF03259
Alpha-actinin-4 GN=Actn4	ACTN4_RAT	105	23.7	5.0	28.7	3.7	25.7	1.5	23.7	9.2	actin cytoskeletal	CH,efhand	PF00307,PF00036
Programmed cell death 6-interacting protein GN=Pdc6ip	PDC6L_RAT	97	1.7	0.3	1.0	0.0	1.0	0.0	1.0	0.0	Protein Binding	Bro1	PF03097
Ezrin GN=Ezr	EZRI_RAT	69	52.7	6.3	32.3	3.0	52.7	4.7	63.7	6.9	actin filament	FERM_C.FERM_M.	PF09379
Radixin GN=Rdx	Q5PQK5_RAT	69	16.3	4.8	14.7	1.8	18.7	1.8	10.0	2.5	cytoskeletal protein binding	FERM_C.FERM_M.FER	PF09379
Moesin GN=Msn	MOES_RAT	68	8.3	3.5	1.7	0.7	2.3	0.7	5.3	4.3	actin binding	FERM_C.FERM_M.FER	PF09379
Myosin-9 GN=Myh9	MYH9_RAT	226	1.7	0.3	10.3	0.9	8.0	1.5	12.7	5.0	actin filament based movement	IQ	PF00612
My16 protein GN=My16	B2GV99_RAT	17	4.3	0.3	3.0	1.0	3.7	1.2	5.7	1.2	motor activity	efhand	PF00036

CHAPTER 5

Validation by AMT and LC-MS Mass Spectrometry

5.1 Introduction

Accurate mass and time tag (AMT) technology was originally developed for the identification and quantitation of peptides by LC-MS using high mass accuracy mass spectrometers[112, 190]. LC-MS identification of peptides are matched to a database of high quality peptide identifications based on their mass and reproducible normalized retention time as determined using C₁₈ reversed phase chromatography. Typically, this method utilized orbitrap or fourier transform ion cyclotron resonance (FTICR) mass spectrometers. Mass accuracy of these instruments are ± 0.1 ppm to 1 ppm mass error for both MS and CID spectra. The AMT matching of the LC-MS eluted and subsequently detected peptides to a database of “tags” was dependent on two primary parameters: 1) the mass accuracy of the instrument, and 2) the reproducibility of the retention time (RT) for the charged peptides that are detected with the mass spectrometer. The reproducibility of the RT for each peptide is dependent on its sequence [191].

Due to the complexity of a typical sample from whole cell lysate and due to the mass accuracy of the instrument, it is difficult to identify a precursor peak solely using mass or RT. Such an ability is dependent on the theoretical mass distribution of peptides produced in a typical trypsin treated sample. For a complex sample, in order to obtain

the statistical confidence of identification by AMT analysis, a very high mass accuracy mass spectrometer is required. Such instruments are beyond the fiscal capabilities of a typical laboratory.

The quadrupole time of flight (QTOF) mass spectrometer is an instrument more common in laboratories. The QTOF offers a mass accuracy of ± 5 ppm (or less) of the selected precursor ions. These parameters are ideal when combined with samples that have reduced complexity as produced by subcellular fractionation. This, together with predictable and specific trypsin activity can result in a robust platform for AMT based identification of LC-MS peptide features.

In this chapter, we describe an adaptation of the AMT methods based on our spectral counting data in Chapter 3 and Chapter 4 [173]. Using the SpC identifications from our previous two studies, selected markers of acidosis from PCT brush border membrane vesicles were identified by AMT and then the abundances were validated using the more accurate peak intensity measurements. The differential LC-MS analysis produced high quality abundance data. The peptide abundances were combined to produce protein level quantification. Selected markers of MA were profiled and positively correlated with the spectral count data ($R^2=0.71-0.88$). Of these, enolase A, fructose 1,6- bisphosphatase and glyceraldehyde-3,4-phosphate dehydrogenase were significantly reduced in BBMV during 1-d,3-d and 7-d MA. Additionally, the Na⁺-facilitated glucose transporter 2 (SGLT2) increased during 1-d and 3-d MA. The altered abundances of the enzymes of glucose metabolism together with altered abundance of SGLT2 indicated a remodeling of these proteins to aid in the PCT response to MA.

5.2 Materials and Methods

5.2a Materials

Aliquots of the same BBMV samples used in chapter 4 were set aside for analysis by LC-MS and AMT. The methods of sample preparation for mass spectrometry are outlined in the Methods in section 4.3 of chapter 4. Data files used for the AMT database preparation are from the same analysis produced in the spectral counting study.

5.2b AMT Database preparation

Using the spectra identified in chapter 4, the individual X!Tandem [125] result files were combined by group and then the AMT database was built. Individual databases grouped by condition were assembled using the msInspect v2.3 --createamt command with the default settings and using a minimum PeptideProphet score of 0.9[109, 167]. A curated protein fasta database containing every protein identified in our SpC analysis was used for building the AMT database. The individual AMT databases were then combined and then non linear aligned with the default settings.

5.2c LC-MS analysis

Each sample was analyzed in triplicate by injecting 0.25 µl aliquots onto an Agilent C-18 reverse phase HPLC Chip (15 µm ID x 1.5 cm) with a nanospray tip. Peptides were eluted directly into an Agilent 6520 QTOF mass spectrometer using a 22 min linear gradient of 15%-45% acetonitrile in 0.1% formic acid at a flow rate of 300 nl/min. MS spectra were collected over an m/z range of 200-3000 Da. Data was

collected in profile mode and then the raw data files converted to mzXML format using Trapper v4.3.1 with a custom Perl script.

5.2d LC-MS peptide feature finding and matching to the AMT database

LC-MS features from each replicate were identified separately using the *findpeptides* mode of msInspect v2.3 with the *walksmoothed* parameter. Features were filtered so that only MS peaks with two or more monoisotopic peaks were included in the analysis. The MS peaks in each separate LC-MS feature file were then matched to the AMT database. This was accomplished by using the LC-MS mzXML files for retention time information together with the *loosedeltamass=100ppm* and *loosedeltaelution=.30* parameters. After matching each file to the AMT database, individual match files were aligned using the *peptidearray* function with the *alignbytags=loose* parameter.

5.2e Quantitation of relative abundance changes

The peptide array containing the aligned and AMT matched features from the replicate datasets were analyzed for differential changes in abundance. The log₂ adjusted data were Loess normalized using DanteR v0.1.1[170]. To determine significance, the altered abundances were analyzed using ANOVA at both the level of the peptide and protein in separate analysis. PCA and volcano plots were created using DanteR.

5.2f Additional Statistical analysis

Peptide uniqueness statistics and normalized retention time (NRT) predictions were analyzed using the Sequence Specific Retention Time Calculator v3.0 (<http://hs2.proteome.ca/SSRCalc/SSRCalcHelp.htm>) (gradient delay time of 0.1 min, slope = 0.35) and the Protein Digestion Simulator v2.2 (<http://omics.pnl.gov/software/>) [113, 192]. Additional analysis was performed using R v2.12.1 (<http://www.r-project.org/>).

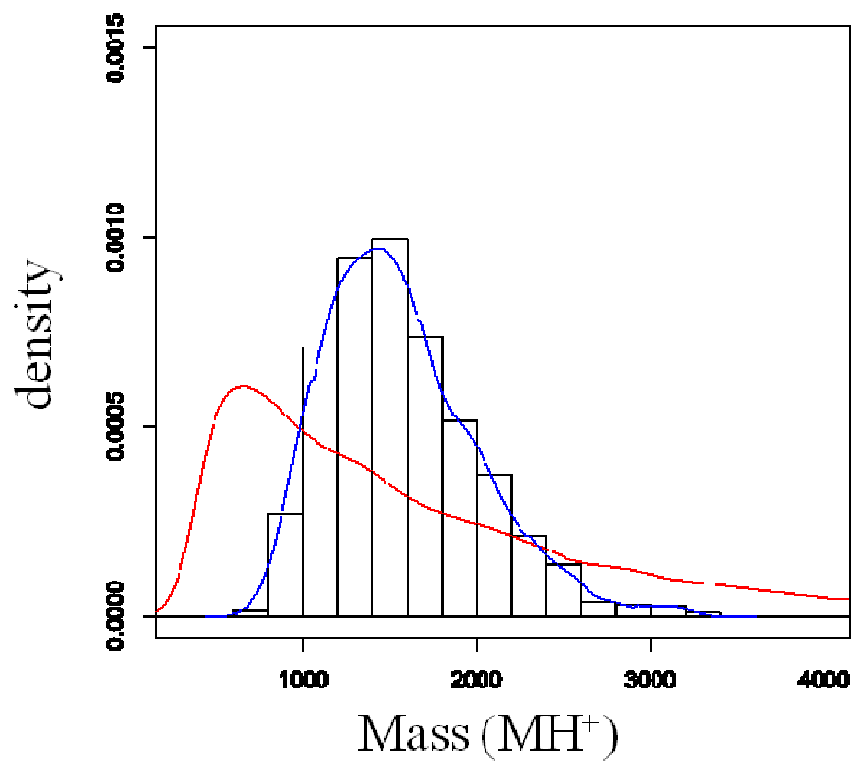
5.3 Results

5.3a Mass distribution of interpreted tandem mass spectra and uniqueness statistics

The frequency distribution of the masses for the previously identified peptides were analyzed (Figure 5.1). The frequency distribution of masses of the theoretical digests of the BBMV database produced peptides ranging from 400 Da to 6000 Da with a median mass of 1320 Da for a total of 40878 theoretical peptides produced from 298 proteins. For the observed peptides, the peptides ranged in mass from 723 Da to 3336 Da with a median mass of 1512 Da for a total of 1165 peptides from the same 298 proteins. The differences in the frequency distributions for the observed and theoretical peptides significantly altered the uniqueness statistics for the predictably produced and the experimentally detected peptides (Figure 5.2). For the theoretical database, using an NRT error of 5%, a < 5ppm error for the AMT matching was required to ensure the peptide match was 80% unique. For the observed peptides, the least unique measurement was ~85% for the median mass of 1512 Da when the constraints were 5% NRT and 20 ppm error. The distribution of mass errors of precursor ions were < ±10ppm error (not

Figure 5.1 Effect of tryptic peptide distribution on uniqueness statistics. **A)** Histogram of the density distribution for the peptides identified using tandem mass spectrometry. The frequency distribution of monoisotopic masses represent those mass ranges of peptides produced using the conditions for sample preparation and digestion as outlined in Chapter IV. The blue line represents the density of the identified peptides from the BBMV dataset. The red line indicates the distribution of masses for a theoretical digest of the BBMV subset protein database and every possible peptide between 400 - 6000 Da. **B)** Percent uniqueness statistics using the peptides plotted in A. Calculation of percent unique peptides for a given mass were calculated for every 100 Da between 400 and 6000 Da for both the real and theoretical datasets. Uniqueness scores are based on the SLiC score ($P > 0.95$) implemented in the Protein Digestion Parser from PNNL. Calculations were based on 5% normalized retention time (NRT) error and for 20, 10, and 5ppm mass error.

A.



B.

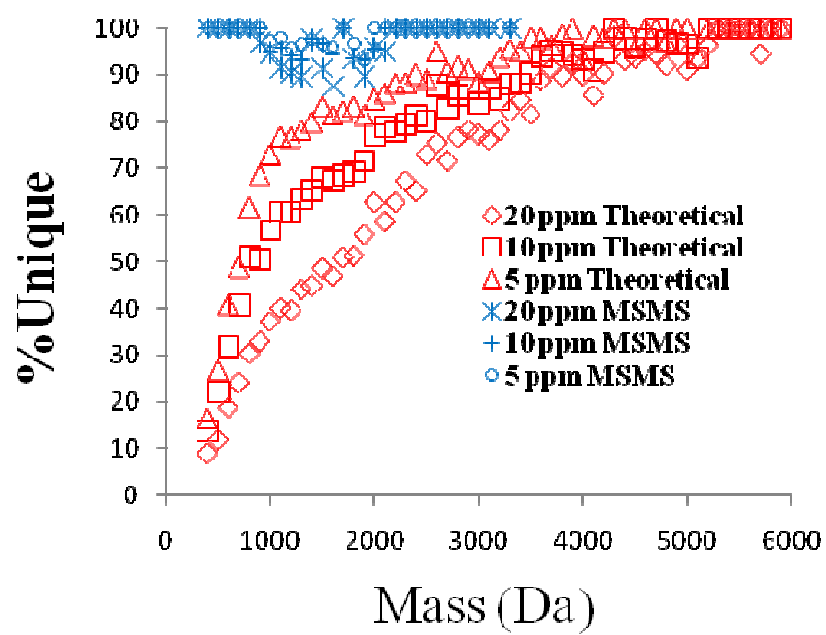


Figure 5.1

Figure 5.2 Mass versus retention time plots. A) Masses and predicted retention times for the theoretical digest of peptides from the proteins identified in Chapter IV were plotted. The results indicated a dense distribution of peptides that would be difficult to identify using the AMT approach. B) Distribution of experimentally produced peptides from Chapter IV. Since not all theoretical peptides for a sample are detected during a typical MS experiment, the identified peptides yield a set that are more amenable to AMT analysis.

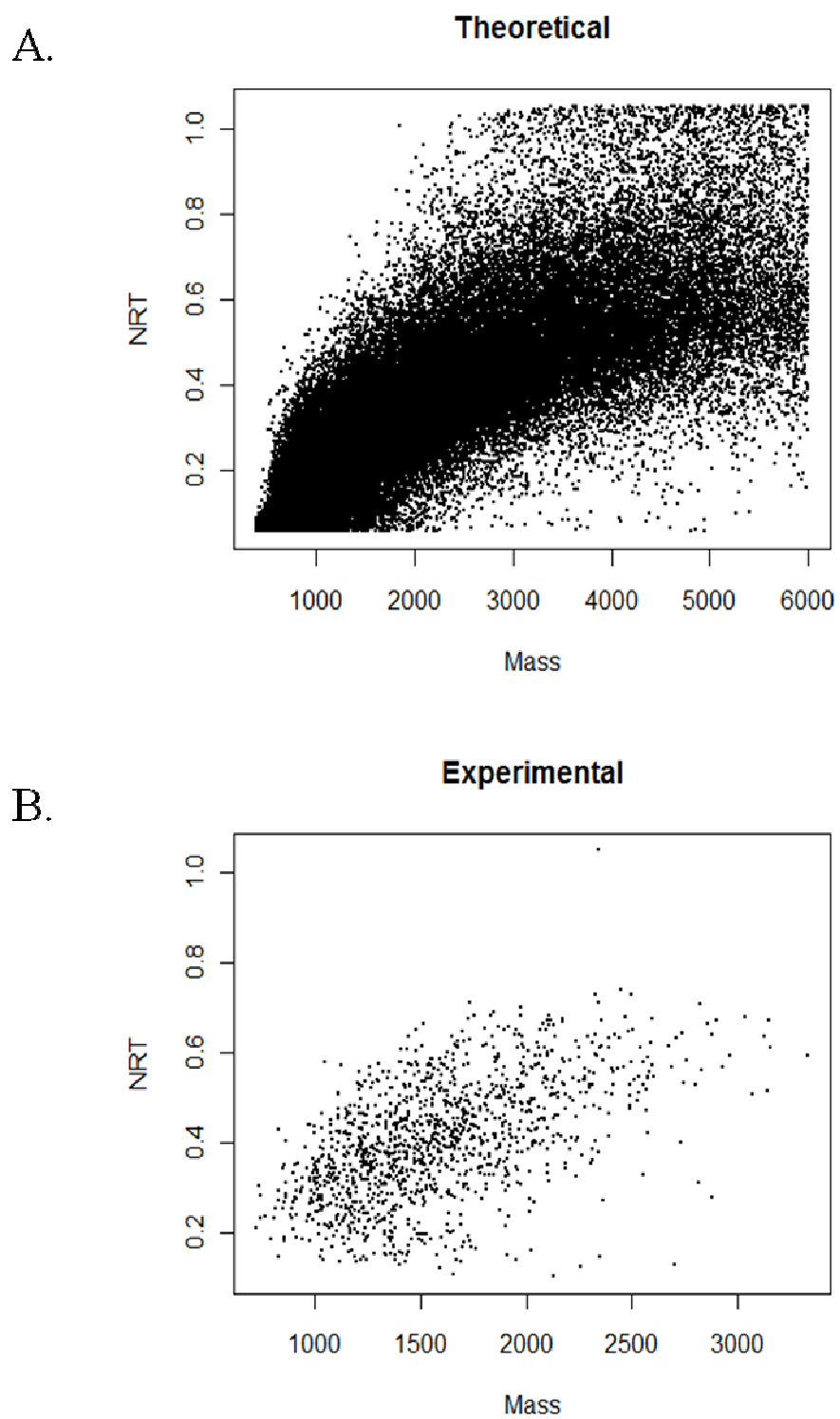


Figure 5.2

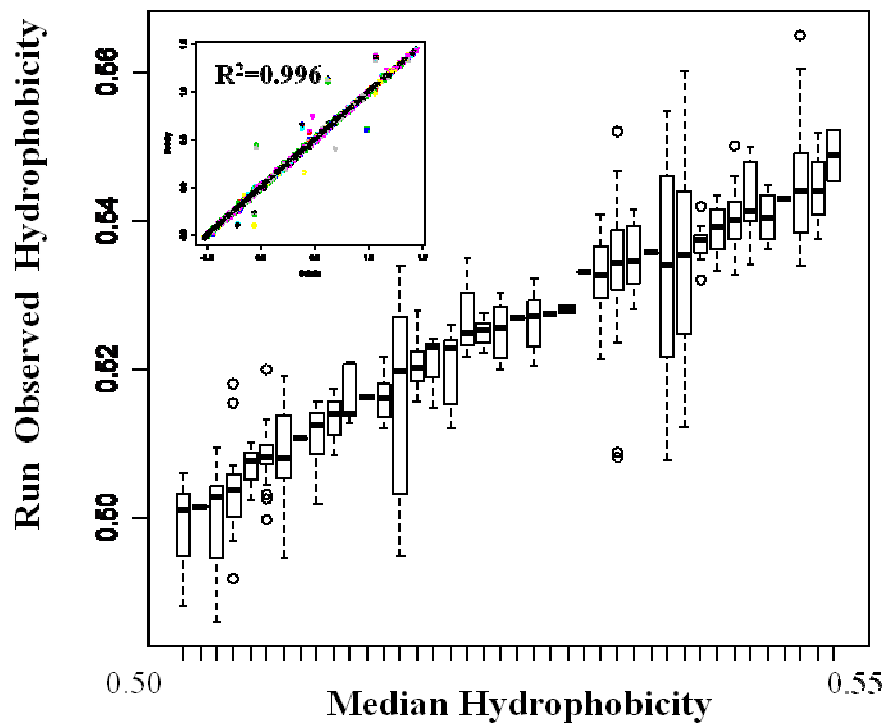
shown). Taken together, the results indicated that the mass error for assignment of precursor ions in the SpC study was sufficient for AMT identification of LC-MS peptide features.

5.3b Development of the AMT database and matching to LC-MS features

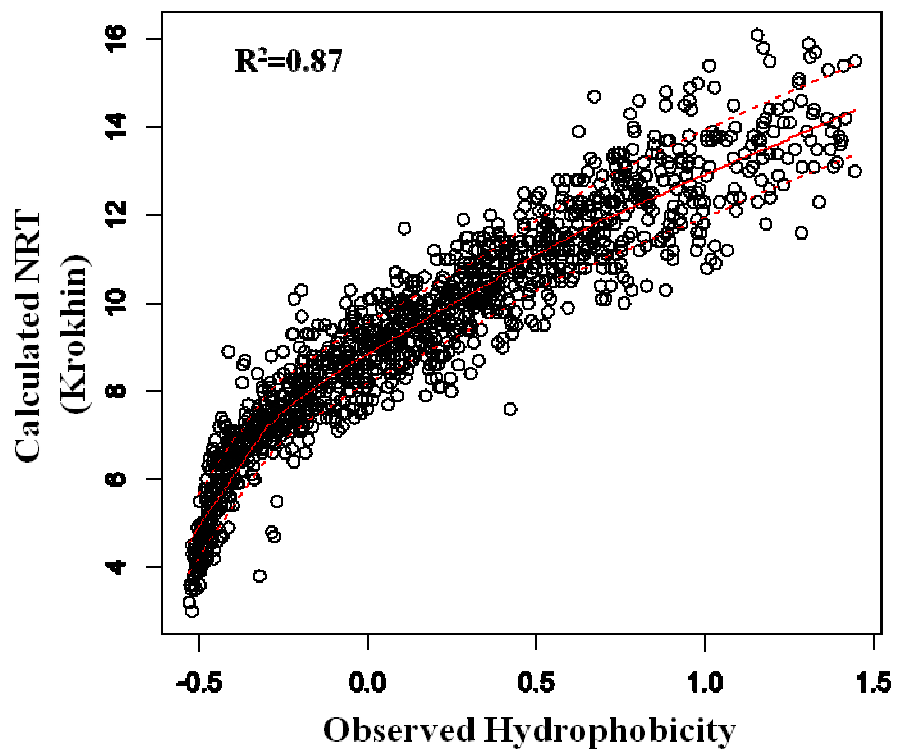
The assembled AMT database was filtered for the highest quality peptides identified during the SpC study. 1331 peptides from 298 proteins were successfully included in the AMT database. To ensure that the abundances could be measured between the sample categories, the aligned database contained peptides from each group which were subsequently filtered for a minimum of 50% of replicates per sample group. The LC-MS runs were subsequently matched to the database individually and then aligned into a peptide array. This array contained a total of 483 peptides from 183 proteins and contained the most reproducible LC-MS features matched to the AMT database. Reproducibility of retention time is a measure of peptide hydrophobicity and adds statistical confidence for a match to the AMT database[113]. To assess the reproducibility of elution times for each of the matched and aligned LC-MS runs, the calculated observed hydrophobicities for the aligned peptides were compared to the median observed hydrophobicities (Figure 5.3A). Visual inspection of the clustered peptides indicated that the observed hydrophobicities were highly reproducible and were within 3% error of the entire range of hydrophobicity (NRT) for each peptide identified. Additionally, the AMT matches were positively correlated ($R^2=0.87$) with the predicted NRT values that were calculated using the prediction utility (Figure 5.3B), an algorithm

Figure 5.3 Analysis by normalized elution times for the AMT identified and filtered peptide features **A)** Detail of boxplots of the median observed hydrophobicity versus the run observed hydrophobicities for each of the 482 filtered AMT peptides. The % observed hydrophobicity was less than 3% for all reported peptides as compared between samples. Inset that shows the alignment of each peptide to the median observed hydrophobicity, colored by injection, was highly correlated. **B)** Plot of calculated normalized retention times (NRT) versus the observed hydrophobicities of each peptide identified in the aligned AMT database. NRT values were calculated using the identified peptide sequences and the Sequence Specific Retention Calculator v3.1 (<http://hs2.proteome.ca/>). Observed hydrophobicities for the ~1200 AMT peptides were calculated using the msInspect v2.3 (<http://proteomics.fhcrc.org/>) Peptidearray method. Red lines indicate the 95% confidence interval. Linear regression analysis of the observed versus theoretical retention times showed a positive correlation ($R^2 = 0.87$).

A.



B.



used in msInspect[192]. While several peptides were outside the 95% confidence limits, these were not excluded as outliers since the AMT prediction is dependent on both observed hydrophobicity and monoisotopic mass.

5.3c Data normalization

In order to determine the true magnitude of the effect on the abundances due to MA, the dataset was log 2 adjusted and then normalized using the Lowess method in the DanteR software[193]. Diagnostic boxplots indicated that the data was normally distributed and normalized (Figure 5.4). Additional analysis indicated positive correlation between all samples (avg $R^2=0.82$). PCA analysis indicated that the samples within the categories were most similar (Figure 5.5). The Control and 7 Day MA samples were most dissimilar whereas the 1 and 3 Day MA samples were most similar. These results reproduced the general trends in the data observed for the SpC study.

5.3d Significance analysis for peptide level changes in abundance

The significance of the differential changes in abundances of peptides were determined. Analysis of variance (ANOVA) was performed using the Control group as the reference group (Figure 5.6). For the 1-d group, there were 108 peptides with an increase in abundance and 95 peptides with a decrease in abundance ($p<0.5$, Fold change > 1.5). For the 3-d group, the total peptides with a significant increase and decrease in abundance were 123 and 87, respectively. The total peptides with significant changes for the 7-d group were 107 and 78, respectively.

The overall trends in the dataset indicated that the significant changes in the 1-d, 3-d, and 7-d acidotic groups versus the controls were similar, but that there were also

Figure 5.4 Boxplots of the peptide abundances for each LC-MS injection replicate. The log₂ adjusted data was lowess normalized and then filtered for the most reproducible peptides across all categories. Black dots in the plot represent each datapoint (peptide) and are normally distributed and open circles represent outlier observations. Numbers indicate total number of peptides per category.

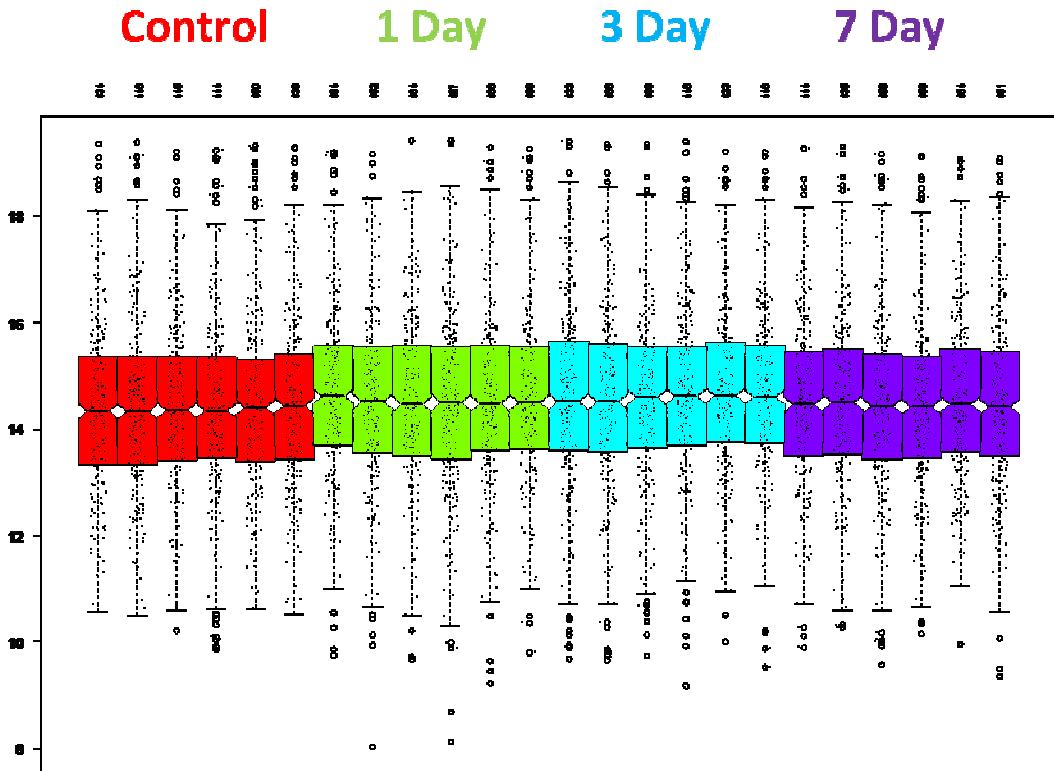


Figure 5.4

Figure 5.5. Principle components analysis of the peptides identified using AMT. The data grouped similar to the spectral count data in chapter 4. Each colored point represents one technical replicate. The Control and 7 day MA group groups were most unique and the 1 and 3 day MA samples were most similar.

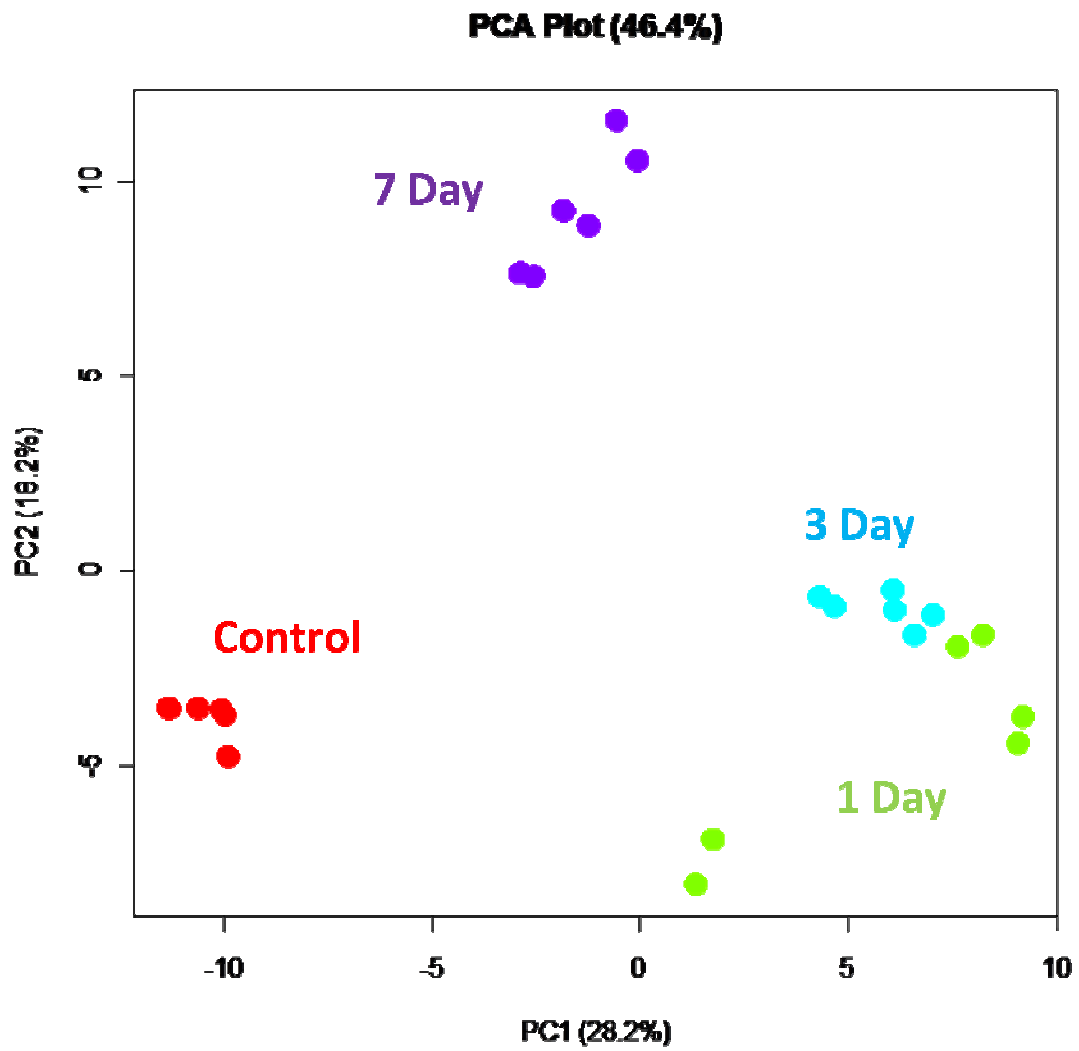


Figure 5.5

Figure 5.6 Peptide level volcano plots of log 2 fold change of abundance versus pvalue. The significance of peptide abundances for each condition as compared to the control group was determined and plotted versus the fold changes. Blue dots indicate data which was significant for the Control versus 1-d MA group (ANOVA, $p < 0.05$). Vertical dash lines indicate 1.5 fold change and horizontal dashed lines indicate the p value cutoff.

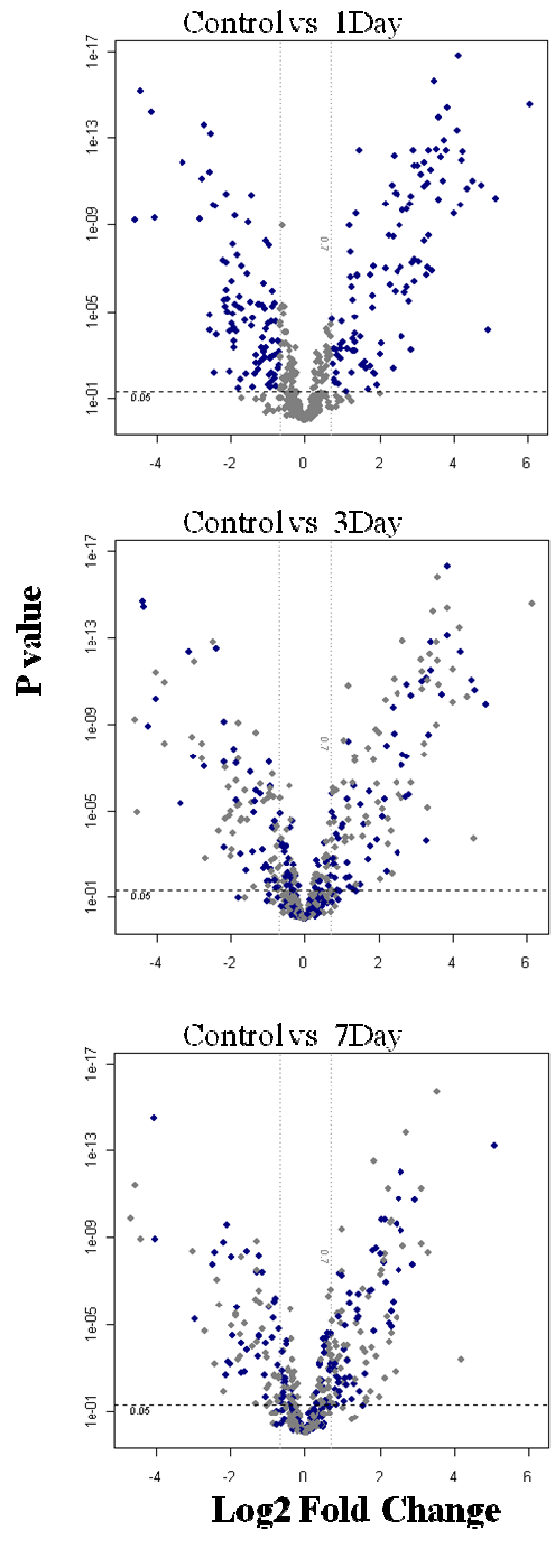


Figure 5.6

significant changes in the 3-d and 7-d groups that were not detected during the 1-d vs Control comparison. The individual trends for the peptides for a selected marker identified during the SpC study were analyzed (Figure 5.7). For FBP1, an important enzyme of gluconeogenesis and the response to MA, the individual trends for the 5 identified peptides were similarly decreased during MA. These analysis indicated changes at the peptide level that were similar to the protein level analysis using SpC.

5.3e Significance analysis for protein level changes in abundance

Since trends in the data were similar to those for select markers identified during the SpC analysis, significance of those changes at the protein level were determined. Again, using ANOVA ($p < 0.05$, Fold change > 1.5), several significant changes were noted (Table 1). For the 1-d group, there were 16 proteins whose abundances were increased and 17 proteins whose abundances were decreased. For the 3-d group, the total proteins with a significant increase and decrease in abundance were 22 and 15, respectively. The total concordant significant changes for the 7 Day group were 16 and 14, respectively. Of interest were those proteins identified during the SpC study that are known enzymes of glycolysis and gluconeogenesis in addition to other markers (Figure 5.8). Of these, FBP1 (F16P1), enolase (ENOA), and aldolase (Q66HT1) were significantly decreased during 1,3, and 7 days MA. In addition, the SGLT2 (SC5A2) transporter significantly increased during 3 Day chronic metabolic acidosis, although was not detected for a significant change during 1 day chronic metabolic acidosis as in the SpC study. The Na⁺ dependent phosphate transporter 2 was significantly increased during

Figure 5.7 . Peptide level abundance analysis of fructose-1,6- biphosphatase -1 (F16P1). Top panel shows the log 2 abundances for individual peptides identified by AMT decreasing through 7 Days acidosis. Bottom panels represent two of the peptides identified in the spectral counting study and which were used to build the AMT database.

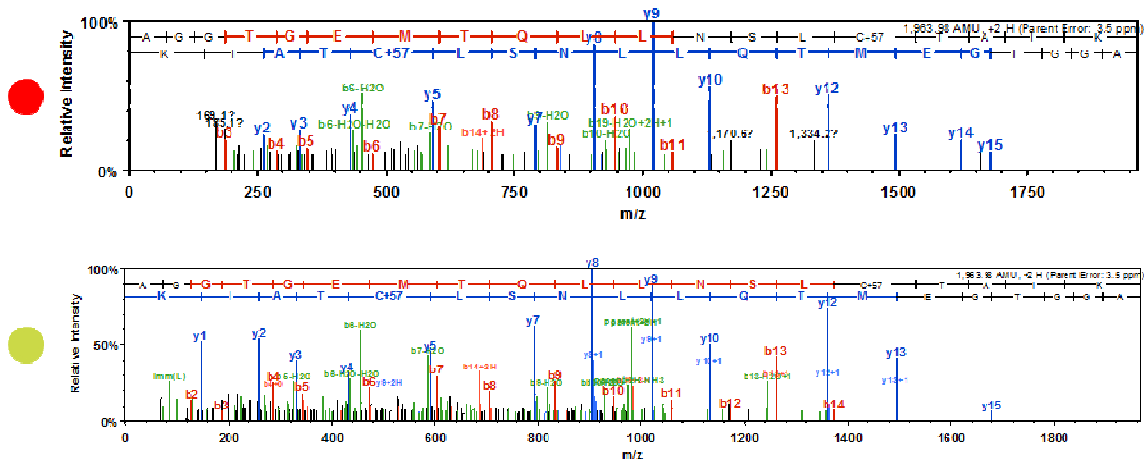
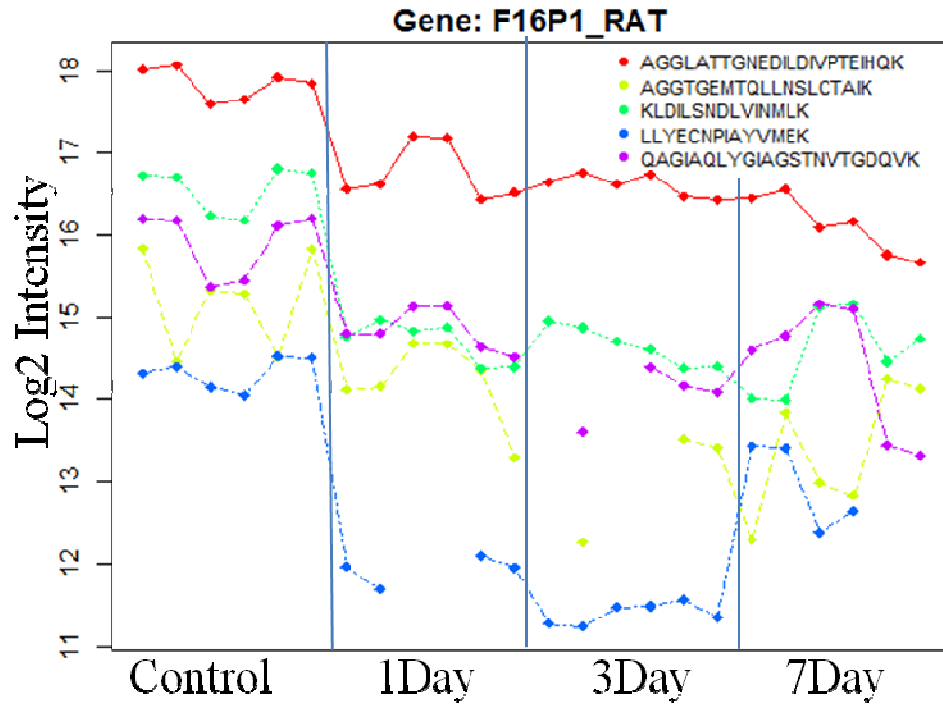


Figure 5.7

Figure 5.8 Log fold changes of selected markers identified using AMT. Aquaporin 1 (Aquaporin 1), Gamma glutamyl transpeptidase (GGT1), B⁰AT1 transporter (S6A19), Na⁺ facilitated glucose transporter SGLT2 (SC5A2), glyceraldehyde-3-phosphate dehydrogenase (Glyceraldehyde-3-phosphate dehydrogenase), enolase a (ENOA), fructose-1,6-bis-phosphatase 1 (F16P1), aldolase a (ALDO_A).

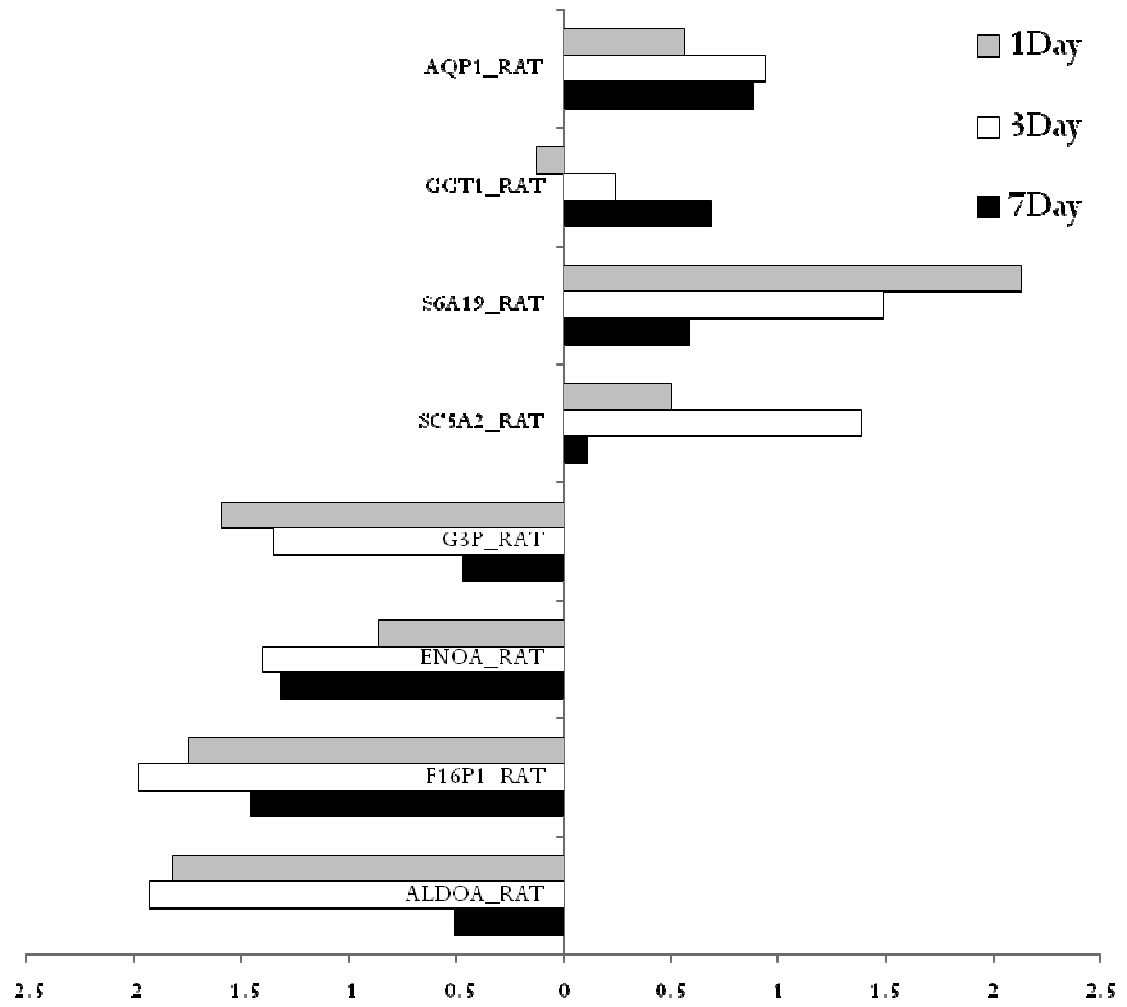


Figure 5.8

3 and 7 days MA. Additionally, the Na⁺ dependent neutral amino acid transporter B⁰AT1 (S6A19) was significantly increased during 1 and 3 days MA.

5.3f Comparison of measurements of abundance by LC-MS versus SpC of selected markers.

To show correlation between the LC-MS and SpC methods, selected markers were compared (Figure 5.9). These markers, including γ -glutamyltranspeptidase, SC5A2, TMM27, ENOA, Glyceraldehyde-3-phosphate dehydrogenase and F16P1, exhibited similar trends for their changes in abundance. The log 2 fold changes were overestimated for some of the changes that were determined using the SpC method. Generally, there were increases or decreases in abundance detected by both LC-MS and SpC.

5.3g Western blot data of SC5A2 and GLUT2 changes during MA.

SGLT2 is an apical specific marker of the PCT[43]. Likewise, the renal facilitated glucose transporter (GLUT2) is specific to the basolateral surface of the PCT[194, 195]. The detected changes by LC-MS during MA indicated that SGLT2 increased during 1-d MA, and then significantly increased during 3 Day MA. These results were similar to the SGLT2 data from the SpC study. Since SGLT2 is involved in glucose influx and GLUT2 is involved in glucose efflux from the PCT, we performed Glut2 and SGLT2 immunoblots on cortical homogenate (Figure 5.10). The results indicated an increase in the expression of SGLT2 during 1 and 3 days MA, similar to the

Figure 5.9. Correlation of log 2 fold changes for selected markers using SpC versus AMT. The log 2 fold change of LC-MS peak intensities for the selected markers from Table 5.1 were compared to the dataset produced in Chapter IV. Proteins with an increase in abundance are shown in red. Proteins with a decrease in abundance are shown in green. The data positively correlated SpC abundance measurements with those garnered from peak intensity dataset in Chapter IV. This indicated that there was correlation between abundance measurements using SpC with those using peak intensities.

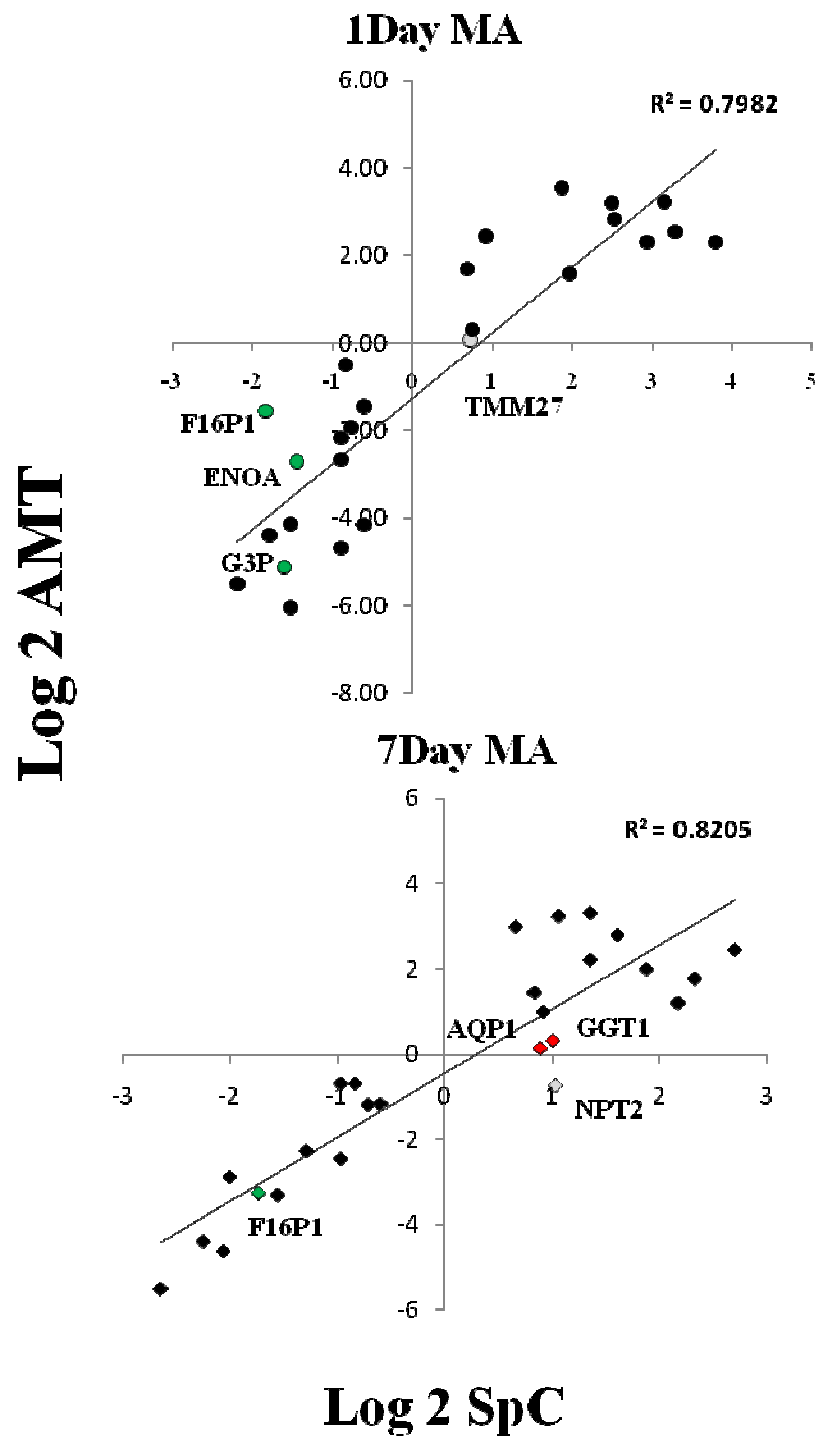


Figure 5.9

Figure 5.10 Immunoblot analysis of SGLT2 and Glut2 expression. 20ug of cortical homogenate was probed for PCT specific markers SGLT2 and GLUT2 expression. SGLT2 exhibited significant increases during 1-d and 3-d ($p < 0.01$, T test, $FC > 7.0$) and 7 day ($p < 0.05$ ($FC > 3.0$)) MA. Glut2, a basolateral marker only exhibited a slight increase during 7-d MA. Coomassie stained samples are shown to indicate equivalent loading.

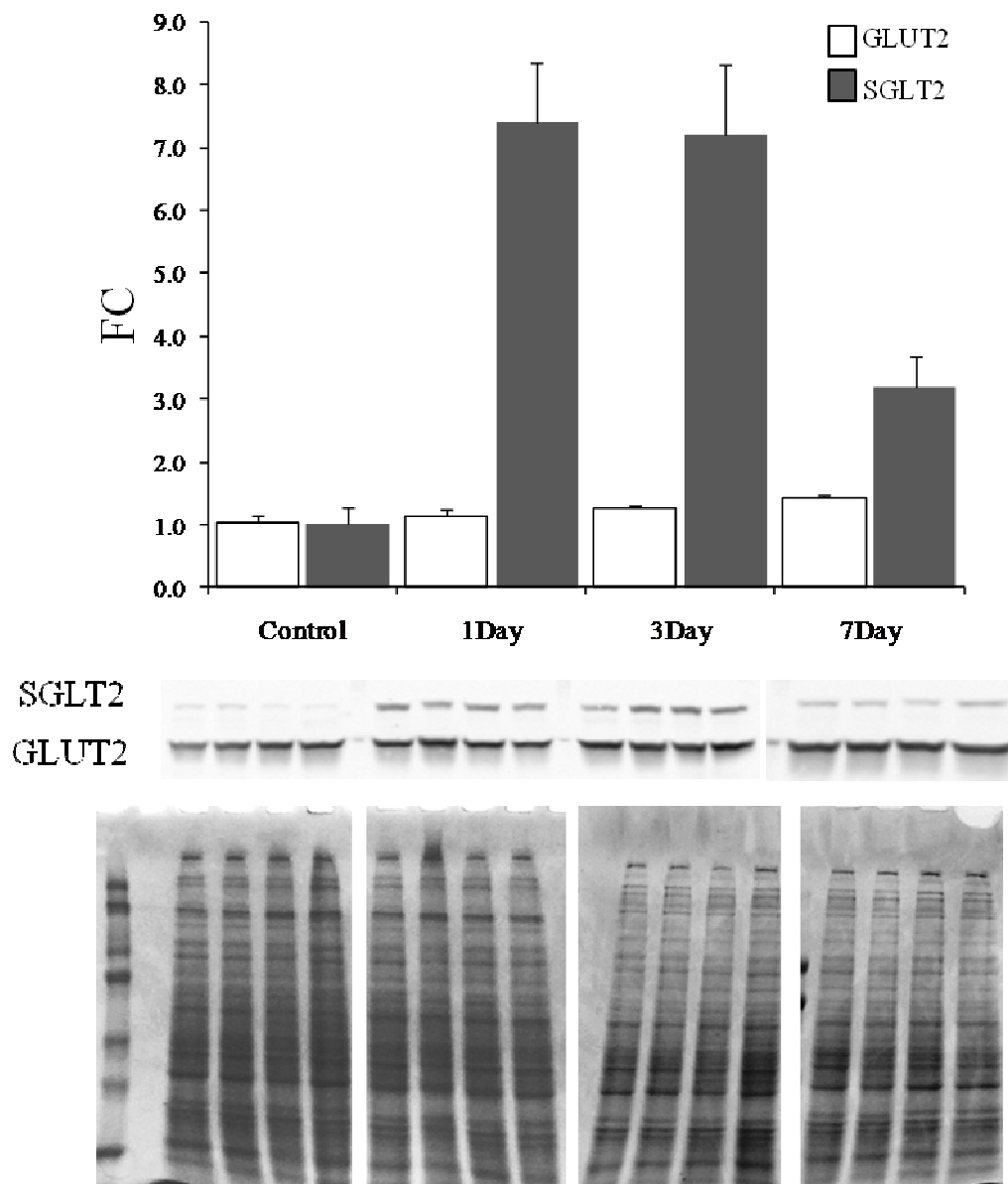


Figure 5.10

LC-MS and SpC results. Similarly, GLUT2 expression increased for the same timepoints, but maintained its increased expression during 7 day MA.

5.4 Discussion

Using AMT identification and the more accurate abundance profiling by LC-MS, our results positively correlate with those from the SpC study in chapter 4. In addition, the identification of peptides using AMT and data acquired on a QTOF instrument is a novel concept. While AMT with the QTOF is commonly used for metabolite and small molecule research, there have been few published reports using this approach for proteomics. Two previous studies using msInspect have been completed [196, 197]. However, both of these studies utilized a targeted MS/MS approach after identification of those peptide features with altered abundances. Due to our reduced sample complexity through enrichment of the BBMV, we have been able to take advantage of the short protein list and the predictable activity of trypsin. There could be potential unidentified peptides from the samples missed in AMT, but the similar protein lists from both the fractionated SpC (Chapter III) and the altered dynamic data acquisition mode SpC (Chapter IV) and AMT studies produced similar identifications. In addition, the main proteins of interest such as those involved in glucose metabolism, SGLT2, TMM27, among others were identified in the mixture by AMT.

TABLE 5.1

Proteins altered during 1 Day MA			Proteins altered during 3 Day MA			Proteins altered during 7 Day MA		
Protein Name	Fold Change	p Value	Protein Name	Fold Change	p Value	Protein Name	Fold Change	p Value
ATPB_RAT	13.80	3.537E-44	ATPB_RAT	13.16	1.879E-43	ATP5H_RAT	6.49	1.284E-12
NDUS1_RAT	9.73	3.968E-15	ATP5H_RAT	10.71	1.214E-15	ATPA_RAT	5.00	7.154E-21
ATP5H_RAT	8.88	1.453E-14	NDUS1_RAT	9.69	6.214E-15	ATPB_RAT	4.49	2.003E-24
ATPA_RAT	7.63	9.940E-28	ATPA_RAT	8.37	3.565E-29	NDUS1_RAT	3.67	4.923E-07
VDAC1_RAT	5.75	1.465E-09	ATPO_RAT	7.26	8.701E-10	VDAC1_RAT	3.04	3.161E-05
ATPO_RAT	5.59	2.366E-08	VDAC1_RAT	3.80	1.093E-06	ATPO_RAT	2.56	7.507E-04
S6A19_RAT	4.36	3.546E-05	Q8SEZ5_RAT	3.36	5.569E-04	Q8SEZ5_RAT	2.56	6.456E-03
D3ZE15_RAT	3.92	3.934E-08	D3ZE15_RAT	3.15	2.995E-06	Q6XD99_RAT	2.08	6.419E-07
Q8SEZ5_RAT	3.65	3.714E-04	S6A19_RAT	2.80	2.677E-03	NPT2A_RAT	2.04	2.363E-03
SPTA2_RAT	2.35	7.790E-08	SC5A2_RAT	2.60	2.105E-04	GGT1_RAT	2.00	6.890E-04
RAP1A_RAT	2.09	1.730E-04	SPTA2_RAT	2.26	7.918E-08	D3ZE15_RAT	1.88	5.550E-03
MYH9_RAT	1.89	4.775E-07	MYH9_RAT	2.22	4.822E-10	AQP1_RAT	1.85	1.209E-02
VATC1_RAT	1.68	2.170E-03	MYL6_RAT	2.21	2.109E-05	NDRG1_RAT	1.78	1.347E-03
MYL6_RAT	1.67	1.528E-03	NHRF3_RAT	2.19	7.415E-05	SPTA2_RAT	1.65	6.639E-04
TMM27_RAT	1.65	1.742E-04	PDZ11_RAT	1.94	1.474E-02	MYH9_RAT	1.58	1.470E-04
Q6XD99_RAT	1.60	1.185E-03	AQP1_RAT	1.92	1.419E-02	RAP1A_RAT	1.55	1.287E-02
PRDX1_RAT	0.66	6.366E-05	RAP1A_RAT	1.88	6.886E-04	D4A133_RAT	0.66	1.240E-06
EZRI_RAT	0.66	1.189E-03	VATC1_RAT	1.87	2.728E-04	A2IB2_RAT	0.65	8.694E-03
D3ZE15_RAT	0.62	1.060E-04	TMM27_RAT	1.66	3.225E-04	MOES_RAT	0.61	4.679E-06
AMPN_RAT	0.59	2.255E-04	Q6XD99_RAT	1.63	6.486E-04	TERA_RAT	0.56	1.002E-04
PPBT_RAT	0.56	6.051E-04	NPT2A_RAT	1.63	4.080E-02	HSP7C_RAT	0.51	1.118E-04
ENOA_RAT	0.55	1.604E-04	RAB1A_RAT	1.59	6.717E-03	VATB2_RAT	0.51	9.690E-16
ASSY_RAT	0.54	3.800E-04	PRDX1_RAT	0.65	2.025E-05	TKT_RAT	0.41	1.522E-04
DAB2_RAT	0.54	9.572E-09	D3ZTX4_RAT	0.57	4.727E-04	ENOA_RAT	0.40	6.167E-08
F151A_RAT	0.54	7.298E-09	HSP7C_RAT	0.57	7.824E-04	ASSY_RAT	0.34	1.074E-08
HSP7C_RAT	0.54	3.525E-04	F151A_RAT	0.56	2.172E-08	F16P1_RAT	0.30	1.448E-22
F16P1_RAT	0.37	4.994E-18	AMPN_RAT	0.53	1.174E-05	1433Z_RAT	0.25	4.567E-06
AK1A1_RAT	0.35	1.941E-07	ASSY_RAT	0.46	5.274E-06	AK1A1_RAT	0.24	1.504E-11
TKT_RAT	0.35	6.405E-05	DPP4_RAT	0.40	8.180E-07	NDKB_RAT	0.21	8.387E-11
G3P_RAT	0.33	8.935E-11	G3P_RAT	0.39	2.422E-08	MUP_RAT	0.16	5.121E-10
NDKB_RAT	0.29	1.639E-07	ENOA_RAT	0.38	5.942E-09			
Q66HT1_RAT	0.28	6.077E-23	NDKB_RAT	0.31	1.006E-07			
MUP_RAT	0.22	8.362E-08	Q66HT1_RAT	0.26	1.362E-24			
	2.73		TKT_RAT	0.26	1.781E-07			
			F16P1_RAT	0.25	1.619E-25			
			AK1A1_RAT	0.23	4.028E-11			
			MUP_RAT	0.17	3.707E-09			

CHAPTER 6

Conclusions and Future Directions

6.1 Overview

The nephron is a complex structure whose distribution of cell types impart distinct cellular and physiological functions. The earliest part of the nephron, the proximal convoluted tubule (PCT), is the primary location for solute and water reabsorption, active secretion, the maintenance of acid-base balance and the restoration of physiological pH during metabolic acidosis. At the apical brush border membrane the response during MA promotes the remodeling of proteins such as γ -glutamyltranspeptidase, NHE3, and B⁰AT-1 that are key to the cell's response to increased glutamine catabolism. Despite our current knowledge of this response, little is known about the concurrent changes which occur at the membrane following the onset of MA. To assess these changes, we performed three distinct proteomic analysis.

In chapter 3, we described the first characterization of brush border membrane vesicles (BBMV) specifically from the PCT (BBMV_{PCT}). A well established method by *Biber et. al*[80], has been suggested to specifically enrich BBMV from the PCT. Additionally, using this method, a previous proteomic analysis by *Cutillas et. al*[82] was completed that profiled the inventory of proteins for BBMV_{CTX}. However, our analysis by Western blot demonstrated that the method of Biber enriches not only BBMV_{PCT}, but

also apical membranes from the proximal straight tubule and other cells along the nephron. This demonstrated that the method used to enrich BBMV_{CTX} were subject to issues arising from sample heterogeneity. Due to this effect, we enriched BBMV from isolated PCT for our subsequent analysis. Using spectral counting as a measure of abundance, the comparative proteomic analysis for BBMV_{PCT} versus BBMV_{CTX} demonstrated several quantitative differences. These differences included enzymes of glucose metabolism that were enriched in the BBMV_{PCT} samples. The presence of this group of proteins were in agreement with the current knowledge PCT cell function. Because of this, it was hypothesized that due to the role of gluconeogenesis in glutamine catabolism together with the PCT role in glucose reabsorption, altered abundances of these proteins such as fructose-1,6-bisphosphatase 1 (FBP1) would occur during onset of acidosis.

For the second proteomic analysis, the effect of MA on the BBMV_{PCT} supported the hypothesis for the remodeling of the enzymes of glycolysis at the apical membrane. Again, using spectral counting, the relative changes in abundance during 1-d, 3-d, and 7-d MA were studied. Several proteins were found to be differentially altered in abundance, whereas others were found to increase or decrease during acute acidosis (1-d and 3-d) but return to control levels by 7-d of acidosis. It was determined that FBP1 and ENO1 both decreased during 1-d, 3-d, and 7-d acidosis, whereas aldolase decreased and then returned to basal levels at 7-d. Interestingly, SGLT2 increased during 1-d and 3-d of MA, then returned to near basal levels at 7-d MA. Spectral counting for the detection of changes in relative abundance has proven to be more accurate as the counts per protein increase. We noted several changes for proteins with larger spectral counts that were

significantly altered. These included SGLT2, the previous mentioned enzymes of glycolysis, as well as additional proteins involved in cytoskeletal transport (Myosin VI) and peptidase activity (MGAM). Since spectral counting is only a semi-quantitative estimate of abundance changes, more accurate LC-MS analysis was completed.

For this third proteomic analysis, a novel approach to accurate mass and time tag analysis was completed using the QTOF mass spectrometer. To accomplish this, we prepared a sample of reduced complexity from a distinct portion of the cell. For this study, it was important establish the reproducibility of the peptide lists from the previous spectral counting analysis together with the mass accuracy of the instrument. These two parameters combined with the micro scale HPLC C18 chip to serve as a robust platform for highly reproducible reversed phase HPLC - high mass accuracy mass spectrometry. The measured elution times for the eluted peptides for the 24 separate injections were highly reproducible. Clustering of these retention time values indicated an error of < 3.0% of the total retention time range. This, together with the < 5 ppm mass error produced during the spectral counting study on the same instrument enabled identification of the peptide sequences. Some of these identities were validated by testing for the concordant abundance changes between the SpC method and the LC-MS methods which used peak intensities as the abundance measurement. This AMT approach is promising for those with limited access to instrumentation if the sample complexity can be reduced, as is the case for subcellular proteomics. Additionally, if the reproducibility of obtaining the expected tryptic peptides can be established, then the robustness of the AMT approach will increase.

6.2 SGLT2, GLUT2, ENOA and FBPI altered abundances during metabolic acidosis

During acute (1-d) metabolic acidosis, SGLT2 expression increases, followed by a further increase during 3-d MA, then subsequently decreases to near basal levels during 7-d MA. Since SGLT2 is responsible for the recovery of glucose from the lumen[43], we tested expression of the basolateral glucose transporter 2 (GLUT2). GLUT2 expression remained relatively unchanged during MA, only increasing slightly at 7-d acidosis. It is possible that the high capacity GLUT2 transporter efficiently compensates for the increased recovery of glucose from the lumen. Glucose concentration in the urine is affected by the onset of MA, hence, the increased SGLT2 expression could account for increased renal extraction of glucose in the PCT during MA.

Fructose-1,6-bisphosphatase in the BBMV_{PCT} decreases significantly during 1-d, 3-d, and 7-d MA. In the nephron, FBPI is most abundant in the early parts of the PCT and is required for gluconeogenesis during MA[29]. During acidosis, the decrease in FBPI at the membrane may indicate a shift in localization of FBPI to aid in the increase of gluconeogenesis. Enolase 1 (ENOA), likewise is decreased at the apical surface. ENOA is responsible for the reversible catalysis of the conversion between 2-phosphoglycerate and phosphoenolpyruvate. As such, ENOA altered distribution may be supporting gluconeogenesis and the conversion of phosphoenolpyruvate from PEPCK to 2-phosphoglycerate to for subsequent steps in the gluconeogenic pathway during MA. These results suggest a model for enzyme translocation, suggest the movement of a glycolytic complex from the apical surface to the cytosol during MA (Figure 6.1).

Figure 6.1 Model for internalization of FBP1 and ENOA. During normal acid-base, many enzymes of glucose metabolism including FBP1 and ENOA are present at the apical surface. During MA, the enzymes decrease at the surface, and may aid in metabolism of GLN to produce glucose. SGLT2 increases probably to increase the reabsorption of glucose in the PCT, which GLUT2 facilitates its release to the blood. Red indicates an increase in the protein abundance or molecule concentration. Light red indicates a slight increase. Red arrow indicates an increased flux from GLN to glucose production. Green indicates a decrease during acidosis.

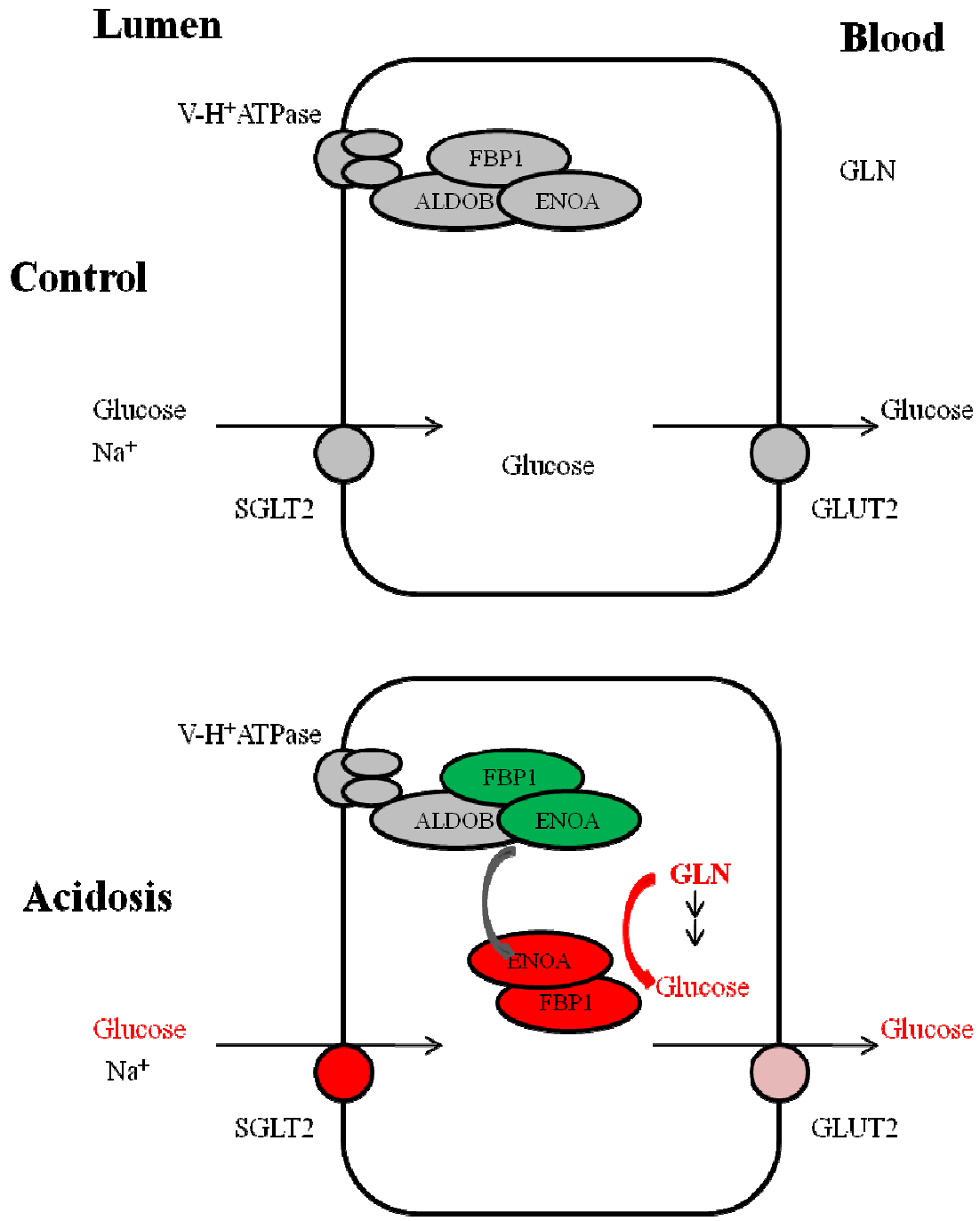


Figure 6.1

6.3 Future directions

Proteomic studies attempt to elucidate the global changes in proteins that occur during adaptations to physiological and pathological conditions. In other cases, they attempt to provide a 'snap-shot' inventory of the global complement of proteins. In our case, our snapshot inventory of a comparative analysis led to our testing and validation of our hypothesis using temporal and AMT studies. Subsequent analysis is required to validate the model. Multiple methods for validation exist and include traditional methods such as western blotting and immunofluorescence microscopy. The disadvantage to western blot is the lack of information about localization, therefore favoring the immuno-fluorescent technique. This approach would utilize kidney cortex slices and would enable the visualization of localization within the cell. Additionally, such an approach could help to visualize the distribution along the nephron and may indicate specific differences that occur between the proximal convoluted and the proximal straight tubule.

Another traditional approach could elucidate the specific interactions of the glycolytic complex during MA by affinity interaction studies. Fructose-1,6-bisphosphatase and aldolase are known to accumulate at the brush border. Therefore, this experimental route may help to elucidate the specific mechanisms by which protein-protein interactions are modulated within the PCT cell to meet its need to catabolize GLN. Specifically co-immunoprecipitation or pull-down experiments might reveal whether components of the glycolytic complex interact selectively with other enzymes. Selective sequence substitution or deletion constructs based on rigorous bioinformatic analysis could then be used to test these proposed interactions. A test for specificity to

the BBMV would include probing for interactions specific to the V-H⁺-ATPase and aldolase complex, a well documented interaction.

To more accurately validate the changes in abundance that occur for the chosen targets, a targeted MS approach could be utilized. For the work we presented in this thesis, we chose to match LC-MS features that contain intensity information using AMT technology. This approach is more robust than spectral counting and is advantageous due to the sensitivity of detection of the lower abundance of molecules in the mixture. However, one limitation for our approach was the sequence validation of the peptide molecule that was assayed. In addition, confirmation of the AMT matching could be completed by selective and multiple reaction monitoring of the peptides of interest. This approach commonly uses the triple quadrupole mass spectrometer (QQQ). This instrument combines more accurate quantitation of selected precursor ions followed by sequence verification of the same set of precursor ions during the same sample run. This technique increases the specificity for detection of the selected precursor ions. A limitation of this technique is the number of targeted transitions that can be acquired during a sample injection. These are limited due to instrument cycling times together with sample complexity. The study described in Chapter V revealed several proteins that were altered in abundance, and that were not part of the list of enzymes of glycolysis. As such, the shotgun approach for both spectral counting and LC-MS by AMT matching provided the best combination of identification together with robust quantification of abundance changes for a list of proteins that will be of interest to those in the field.

6.4 Conclusion

A thorough proteomic analysis of the changes that occur at the proximal convoluted tubule brush border during MA was completed. These experiments utilized a mixture of spectral counting and LC-MS to identify and quantify novel proteins which may be important to the tubular response to acidosis. These changes profiled at the brush border included those involved in glucose metabolism. Such findings are novel but not unexpected due to the central role of glucose synthesis that occurs during metabolic acidosis. Further validation of the localization of these events is required to more comprehensively understand these changes. Finally, the completed proteomic analysis still serves as a robust method for identification and measurement of the relative changes in abundance of these identified proteins in response to other physiological and pathological conditions.

REFERENCES

1. *Barcroft, J. and J.S. Haldane, A method of estimating the oxygen and carbonic acid in small quantities of blood. The Journal of Physiology, 1902. 28(3): p. 232-240.*
2. *La Mer, V.K. and T.R. Parsons, THE APPLICATION OF THE QUINHYDRONE ELECTRODE TO ELECTROMETRIC ACID-BASE TITRATIONS IN THE PRESENCE OF AIR, AND THE FACTORS LIMITING ITS USE IN ALKALINE SOLUTION. Journal of Biological Chemistry, 1923. 57(2): p. 613-631.*
3. *Nash, T.P. and S.R. Benedict, THE AMMONIA CONTENT OF THE BLOOD, AND ITS BEARING ON THE MECHANISM OF ACID NEUTRALIZATION IN THE ANIMAL ORGANISM. Journal of Biological Chemistry, 1921. 48(2): p. 463-488.*
4. *Van Slyke, D.D., et al., GLUTAMINE AS SOURCE MATERIAL OF URINARY AMMONIA. Journal of Biological Chemistry, 1943. 150(2): p. 481-482.*
5. *KENNAN, A.L., Glutamine Synthesis in Rats with Diabetic Acidosis. Endocrinology, 1962. 71(2): p. 203-208.*
6. *Pitts, R.F., L.A. Pilkington, and J.C.M. de Haas, N15 Tracer Studies on the Origin of Urinary Ammonia in the Acidotic Dog, with Notes on the Enzymatic Synthesis of Labeled Glutamic Acid and Glutamines*. The Journal of Clinical Investigation, 1965. 44(5): p. 731-745.*
7. *Fulgraff, G. and R.F. Pitts, Kinetics of ammonia production and excretion in the acidotic dog. Am J Physiol, 1965. 209(6): p. 1206-1212.*
8. *Pitts, R., Production and excretion of ammonia in relation to acid-base regulation., in Handbook of physiology, section 8: renal physiology, J. Orloff*

and R. Berliner, Editors. 1973, American Physiology Society: Washington, DC. p. 455-497.

9. Schrock, H., C.J. Cha, and L. Goldstein, *Glutamine release from hindlimb and uptake by kidney in the acutely acidotic rat. Biochem J*, 1980. 188(2): p. 557-60.
10. Addae, S. and W. Lotspeich, *Relation between glutamine utilization and production in metabolic acidosis. Am J Physiol*, 1968. 215(2): p. 269-277.
11. Fine, A., *The effects of chronic metabolic acidosis on liver and muscle glutamine metabolism in the dog in vivo. Biochem. J.*, 1982. 202(1): p. 271-273.
12. Feifel, E., et al., *p38 MAPK mediates acid-induced transcription of PEPCK in LLC-PK(1)-FBPase(+) cells. Am J Physiol Renal Physiol*, 2002. 283(4): p. F678-88.
13. Andratsch, M., et al., *TGF-beta signaling and its effect on glutaminase expression in LLC-PK1-FBPase+ cells. Am J Physiol Renal Physiol*, 2007. 293(3): p. F846-53.
14. Curthoys, N.P. and G. Gstraunthaler, *Mechanism of increased renal gene expression during metabolic acidosis. Am J Physiol Renal Physiol*, 2001. 281(3): p. F381-90.
15. Dhakras, P.S., et al., *cAMP-dependent stabilization of phosphoenolpyruvate carboxykinase mRNA in LLC-PK1-F+ kidney cells. Am J Physiol Renal Physiol*, 2006. 290(2): p. F313-8.
16. Drenowska, K., et al., *PEPCK mRNA localization in proximal tubule and gene regulation during metabolic acidosis. J. Physiol. Phram.*, 2002. 53: p. 3-20.
17. Gstraunthaler, G., et al., *Differential expression and acid-base regulation of glutaminase mRNAs in gluconeogenic LLC-PK(1)-FBPase(+) cells. Am J Physiol Renal Physiol*, 2000. 278(2): p. F227-37.
18. Ibrahim, H., Y.J. Lee, and N.P. Curthoys, *Renal response to metabolic acidosis: role of mRNA stabilization. Kidney Int*, 2008. 73(1): p. 11-8.

19. *Curthoys, N.P., Renal ammonium ion production and excretion. The Kidney: Physiology and Pathophysiology, 2007. 4th Edition(Chapter 56): p. 1601-1619.*
20. *Almond, M.K., et al., Substrate and pH effects on glutamine synthesis in rat liver. Consequences for acid-base regulation. Biochem J, 1991. 278 (Pt 3): p. 709-14.*
21. *Squires, E.J., D.E. Hall, and J.T. Brosnan, Arteriovenous differences for amino acids and lactate across kidneys of normal and acidotic rats. Biochem J, 1976. 160(1): p. 125-8.*
22. *Iqbal, K. and J.H. Ottaway, Glutamine synthetase in muscle and kidney.*
23. *Silbernagl, S., Tubular reabsorption of L-glutamine studied by free-flow micropuncture and microperfusion of rat kidney. Int J Biochem, 1980. 12(1-2): p. 9-16.*
24. *Bode, B.P., Recent molecular advances in mammalian glutamine transport. J Nutr, 2001. 131(9 Suppl): p. 2475S-85S; discussion 2486S-7S.*
25. *Yáñez, A.J., et al., Broad expression of fructose-1,6-bisphosphatase and phosphoenolpyruvate carboxykinase provide evidence for gluconeogenesis in human tissues other than liver and kidney. Journal of Cellular Physiology, 2003. 197(2): p. 189-197.*
26. *Gstraunthaler, G., W. Pfaller, and P. Kotanko, Lack of fructose-1,6-bisphosphatase activity in LLC-PK1 cells. Am J Physiol, 1985. 248(1 Pt 1): p. C181-3.*
27. *Gstraunthaler, G. and J.S. Handler, Isolation, growth, and characterization of a gluconeogenic strain of renal cells. Am J Physiol, 1987. 252(2 Pt 1): p. C232-8.*
28. *Burch, H.B., et al., Gluconeogenic enzymes in defined structures of developing rat nephron. Curr Probl Clin Biochem, 1977. 8: p. 290-8.*
29. *Burch, H.B., et al., Distribution along the rat nephron of three enzymes of gluconeogenesis in acidosis and starvation. Am J Physiol, 1978. 235(3): p. F246-53.*

30. Schoolwerth, A.C., et al., *Effect of aminooxyacetate and [alpha]-ketoglutarate on glutamate deamination by rat kidney mitochondria. International Journal of Biochemistry*, 1980. 12(1-2): p. 145-149.
31. Shapiro, R.A. and N.P. Curthoys, *Characterization of the apparent rates of glutamine transport in rat renal mitochondria. FEBS Lett*, 1978. 91(1): p. 49-52.
32. Weiner, I.D. and L.L. Hamm, *Molecular mechanisms of renal ammonia transport. Annu Rev Physiol*, 2007. 69: p. 317-40.
33. Curthoys, N.P., et al., *Proteomic analysis of the adaptive response of rat renal proximal tubules to metabolic acidosis. Am J Physiol Renal Physiol*, 2007. 292(1): p. F140-7.
34. Schroeder, J.M., et al., *Role of deadenylation and AUF1 binding in the pH-responsive stabilization of glutaminase mRNA. Am J Physiol Renal Physiol*, 2006. 290(3): p. F733-40.
35. Schroeder, J.M., W. Liu, and N.P. Curthoys, *pH-responsive stabilization of glutamate dehydrogenase mRNA in LLC-PK1-F+ cells. Am J Physiol Renal Physiol*, 2003. 285(2): p. F258-65. Epub 2003 Apr 08.
36. Tang, A. and N.P. Curthoys, *Identification of zeta-crystallin/NADPH:quinone reductase as a renal glutaminase mRNA pH response element-binding protein. J Biol Chem*, 2001. 276(24): p. 21375-80. Epub 2001 Apr 09.
37. Karinch, A.M., et al., *Regulation of expression of the SN1 transporter during renal adaptation to chronic metabolic acidosis in rats. Am J Physiol Renal Physiol*, 2002. 283(5): p. F1011-9.
38. Solbu, T.T., et al., *Induction and targeting of the glutamine transporter SN1 to the basolateral membranes of cortical kidney tubule cells during chronic metabolic acidosis suggest a role in pH regulation. J Am Soc Nephrol*, 2005. 16(4): p. 869-77.
39. Kwon, T.H., et al., *Chronic metabolic acidosis upregulates rat kidney Na-HCO cotransporters NBCn1 and NBC3 but not NBC1. Am J Physiol Renal Physiol*, 2002. 282(2): p. F341-51.

40. *Moret, C., et al., Regulation of renal amino acid transporters during metabolic acidosis. Am J Physiol Renal Physiol, 2007. 292(2): p. F555-66.*
41. *Seshadri, R.M., et al., Renal expression of the ammonia transporters, Rhbg and Rhcg, in response to chronic metabolic acidosis. Am J Physiol Renal Physiol, 2006. 290(2): p. F397-408.*
42. *Lee, Y.J. and H.J. Han, Regulatory mechanisms of Na(+)/glucose cotransporters in renal proximal tubule cells. Kidney Int Suppl, 2007(106): p. S27-35.*
43. *Vallon, V., et al., SGLT2 Mediates Glucose Reabsorption in the Early Proximal Tubule. Journal of the American Society of Nephrology.*
44. *Danilczyk, U., et al., Essential role for collectrin in renal amino acid transport. Nature, 2006. 444(7122): p. 1088-1091.*
45. *Seow, H.F., et al., Hartnup disorder is caused by mutations in the gene encoding the neutral amino acid transporter SLC6A19. Nat Genet, 2004. 36(9): p. 1003-7.*
46. *Chou, C.L., et al., Non-muscle myosin II and myosin light chain kinase are downstream targets for vasopressin signaling in the renal collecting duct. J Biol Chem, 2004. 279(47): p. 49026-35.*
47. *Gburek, J., et al., Renal uptake of myoglobin is mediated by the endocytic receptors megalin and cubilin. American Journal of Physiology - Renal Physiology, 2003. 285(3): p. F451-F458.*
48. *Kozyraki, R., et al., Megalin-dependent cubilin-mediated endocytosis is a major pathway for the apical uptake of transferrin in polarized epithelia. Proceedings of the National Academy of Sciences of the United States of America, 2001. 98(22): p. 12491-12496.*
49. *Katsuno, K., et al., Sertigliflozin, a Novel Selective Inhibitor of Low-Affinity Sodium Glucose Cotransporter (SGLT2), Validates the Critical Role of SGLT2 in Renal Glucose Reabsorption and Modulates Plasma Glucose Level. Journal of Pharmacology and Experimental Therapeutics, 2007. 320(1): p. 323-330.*

50. *Fujimori, Y., et al., Remogliflozin Etabonate, in a Novel Category of Selective Low-Affinity Sodium Glucose Cotransporter (SGLT2) Inhibitors, Exhibits Antidiabetic Efficacy in Rodent Models. Journal of Pharmacology and Experimental Therapeutics, 2008. 327(1): p. 268-276.*
51. *Pan, Y.X., H. Chen, and M.S. Kilberg, Interaction of RNA-binding proteins HuR and AUF1 with the human ATF3 mRNA 3'-untranslated region regulates its amino acid limitation-induced stabilization. J Biol Chem, 2005. 280(41): p. 34609-16.*
52. *Helbert, M.J., et al., Immunodissection of the human proximal nephron: flow sorting of SIS2S3, SIS2 and S3 proximal tubular cells. Kidney Int, 1997. 52(2): p. 414-28.*
53. *Pfaller, W., et al., Immunocytochemical localization of gamma-glutamyl-transferase on isolated renal cortical tubular fragments. Histochemistry, 1984. 80(3): p. 289-93.*
54. *Shimada, H., H. Endou, and F. Sakai, Distribution of gamma-glutamyl transpeptidase and glutaminase isoenzymes in the rabbit single nephron. Jpn J Pharmacol, 1982. 32(1): p. 121-9.*
55. *Curthoys, N.P. and R.P. Hughey, Characterization and physiological function of rat renal gamma-glutamyltranspeptidase. Enzyme, 1979. 24(6): p. 383-403.*
56. *Hosaka, K., et al., Megalin and nonmuscle myosin heavy chain IIA interact with the adaptor protein Disabled-2 in proximal tubule cells. Kidney Int, 2009. 75(12): p. 1308-1315.*
57. *Brandes, A., et al., Adaptive redistribution of NBCe1-A and NBCe1-B in rat kidney proximal tubule and striated ducts of salivary glands during acid-base disturbances. Am J Physiol Regul Integr Comp Physiol, 2007. 293(6): p. R2400-11.*
58. *Foreman, J.W., et al., Effect of acidosis on glutamine transport by isolated rat renal brush-border and basolateral-membrane vesicles. Biochem J, 1983. 212(3): p. 713-20.*

59. *Laghmani, K., et al., Endothelin-1/endothelin-B receptor-mediated increases in NHE3 activity in chronic metabolic acidosis. J Clin Invest, 2001. 107(12): p. 1563-9.*
60. *Laghmani, K., P.A. Preisig, and R.J. Alpern, The role of endothelin in proximal tubule proton secretion and the adaptation to a chronic metabolic acidosis. J Nephrol, 2002. 15 Suppl 5: p. S75-87.*
61. *Bezerra, C.N., et al., Mechanisms underlying the long-term regulation of NHE3 by parathyroid hormone. Am J Physiol Renal Physiol, 2008. 294(5): p. F1232-7.*
62. *Azarani, A., D. Goltzman, and J. Orlowski, Parathyroid hormone and parathyroid hormone-related peptide inhibit the apical Na⁺/H⁺ exchanger NHE-3 isoform in renal cells (OK) via a dual signaling cascade involving protein kinase A and C. J Biol Chem, 1995. 270(34): p. 20004-10.*
63. *Donowitz, M. and X. Li, Regulatory binding partners and complexes of NHE3. Physiol Rev, 2007. 87(3): p. 825-72.*
64. *Murtazina, R., et al., Tissue-specific regulation of sodium/proton exchanger isoform 3 activity in Na⁽⁺⁾/H⁽⁺⁾ exchanger regulatory factor 1 (NHERF1) null mice. cAMP inhibition is differentially dependent on NHERF1 and exchange protein directly activated by cAMP in ileum versus proximal tubule. J Biol Chem, 2007. 282(34): p. 25141-51.*
65. *Tsuganezawa, H., et al., Role of c-SRC and ERK in acid-induced activation of NHE3. Kidney Int, 2002. 62(1): p. 41-50.*
66. *Karim, Z., et al., Renal handling of NH₃/NH₄⁺: recent concepts. Nephron Physiol, 2005. 101(4): p. p77-81.*
67. *Bobulescu, I.A. and O.W. Moe, Na⁺/H⁺ exchangers in renal regulation of acid-base balance. Semin Nephrol, 2006. 26(5): p. 334-44.*
68. *Igarashi, T., [Renal tubular acidosis]. Ryoikibetsu Shokogun Shirizu, 1998(19 Pt 2): p. 578-82.*

69. *Aronson, P.S., Ion exchangers mediating Na⁺, HCO₃⁻ and Cl⁻ transport in the renal proximal tubule. J Nephrol, 2006. 19 Suppl 9: p. S3-S10.*
70. *Nowik, M., et al., Renal phosphaturia during metabolic acidosis revisited: molecular mechanisms for decreased renal phosphate reabsorption. Pflugers Arch, 2008. 457(2): p. 539-49.*
71. *Nowik, M., et al., Genome-wide gene expression profiling reveals renal genes regulated during metabolic acidosis. Physiol Genomics, 2008. 32(3): p. 322-34.*
72. *Wagner, C.A., Metabolic acidosis: new insights from mouse models. Current Opinion in Nephrology and Hypertension, 2007: p. 471-476.*
73. *Cheung, P.Y., et al., Acute and chronic effect of dietary phosphorus restriction on protein expression in young rat renal proximal tubules. 2002, WILEY-VCH Verlag. p. 1211-1219.*
74. *Bandara, L.R., et al., A Correlation between a Proteomic Evaluation and Conventional Measurements in the Assessment of Renal Proximal Tubular Toxicity. Toxicological Sciences, 2003. 73(1): p. 195-206.*
75. *Cutillas, P.R., et al., The urinary proteome in Fanconi syndrome implies specificity in the reabsorption of proteins by renal proximal tubule cells. Am J Physiol Renal Physiol, 2004. 287(3): p. F353-364.*
76. *Leong, P.K.K., et al., Effects of ACE inhibition on proximal tubule sodium transport. Am J Physiol Renal Physiol, 2006. 290(4): p. F854-863.*
77. *Zhang, D., et al., Proteomics analysis reveals diabetic kidney as a ketogenic organ in type 2 diabetes. Am J Physiol Endocrinol Metab: p. aipendo.00308.2010.*
78. *Puigmullá, M., et al., Differential proteomic analysis of cyclosporine A-induced toxicity in renal proximal tubule cells. Nephrology Dialysis Transplantation, 2009. 24(9): p. 2672-2686.*
79. *de Graauw, M., et al., Proteomic Analysis of Alternative Protein Tyrosine Phosphorylation in 1,2-Dichlorovinyl-cysteine-Induced Cytotoxicity in*

- Primary Cultured Rat Renal Proximal Tubular Cells. Journal of Pharmacology and Experimental Therapeutics, 2007. 322(1): p. 89-100.*
80. *Biber, J., et al., Isolation of renal proximal tubular brush-border membranes. Nat Protoc, 2007. 2(6): p. 1356-9.*
 81. *Biber, J., et al., A high yield preparation for rat kidney brush border membranes. Different behaviour of lysosomal markers. Biochim Biophys Acta, 1981. 647(2): p. 169-76.*
 82. *Cutillas, P.R., et al., Proteomic analysis of plasma membrane vesicles isolated from the rat renal cortex. Proteomics, 2005. 5(1): p. 101-12.*
 83. *Janech, M.G., J.R. Raymond, and J.M. Arthur, Proteomics in renal research. American Journal of Physiology - Renal Physiology, 2007. 292(2): p. F501-F512.*
 84. *JAMES, P., Protein identification in the post-genome era: the rapid rise of proteomics. Quarterly Reviews of Biophysics, 1997. 30(04): p. 279-331.*
 85. *Wilkins, M.R., et al., From Proteins to Proteomes: Large Scale Protein Identification by Two-Dimensional Electrophoresis and Amino Acid Analysis. Nat Biotech, 1996. 14(1): p. 61-65.*
 86. *Taylor, R.S., et al., Two-dimensional mapping of the endogenous proteins of the rat hepatocyte Golgi complex cleared of proteins in transit. Electrophoresis, 1997. 18(14): p. 2601-2612.*
 87. *Washburn, M.P., D. Wolters, and J.R. Yates, 3rd, Large-scale analysis of the yeast proteome by multidimensional protein identification technology. Nat Biotechnol, 2001. 19(3): p. 242-7.*
 88. *Hunt, D.F., et al., Protein sequencing by tandem mass spectrometry. Proceedings of the National Academy of Sciences of the United States of America, 1986. 83(17): p. 6233-6237.*
 89. *Eng, J.K., A.L. McCormack, and J.R. Yates Iii, An approach to correlate tandem mass spectral data of peptides with amino acid sequences in a protein*

- database. Journal of the American Society for Mass Spectrometry, 1994. 5(11): p. 976-989.*
90. *Yates, J.R., 3rd, et al., Method to correlate tandem mass spectra of modified peptides to amino acid sequences in the protein database. Anal Chem, 1995. 67(8): p. 1426-36.*
 91. *Yates, J.R., et al., Peptide Mass Maps: A Highly Informative Approach to Protein Identification. Analytical Biochemistry, 1993. 214(2): p. 397-408.*
 92. *Wolters, D.A., M.P. Washburn, and J.R. Yates, 3rd, An automated multidimensional protein identification technology for shotgun proteomics. Anal Chem, 2001. 73(23): p. 5683-90.*
 93. *Vatansever, B., et al., Comparison between a linear ion trap and a triple quadrupole MS in the sensitive detection of large peptides at femtomole amounts on column. Journal of Separation Science. 33(16): p. 2478-2488.*
 94. *Douglas, D.J., A.J. Frank, and D. Mao, Linear ion traps in mass spectrometry. Mass Spectrometry Reviews, 2005. 24(1): p. 1-29.*
 95. *Doroshenko, V.M. and R.J. Cotter, A quadrupole ion trap/time-of-flight mass spectrometer with a parabolic reflectron. Journal of Mass Spectrometry, 1998. 33(4): p. 305-318.*
 96. *Lund, T.C., et al., iTRAQ is a useful method to screen for membrane-bound proteins differentially expressed in human natural killer cell types. J Proteome Res, 2007. 6(2): p. 644-53.*
 97. *Armenta, J.M., I. Hoeschele, and I.M. Lazar, Differential Protein Expression Analysis Using Stable Isotope Labeling and PQD Linear Ion Trap MS Technology. Journal of the American Society for Mass Spectrometry, 2009. 20(7): p. 1287-1302.*
 98. *Borisov, O.V., et al., Low-Energy Collision-Induced Dissociation Fragmentation Analysis of cysteineteinyl-Modified Peptides. Analytical Chemistry, 2002. 74(10): p. 2284-2292.*

99. Ong, S.-E., et al., *Stable Isotope Labeling by Amino Acids in Cell Culture, SILAC, as a Simple and Accurate Approach to Expression Proteomics. Molecular & Cellular Proteomics*, 2002. 1(5): p. 376-386.
100. Wu, C.C., et al., *Metabolic Labeling of Mammalian Organisms with Stable Isotopes for Quantitative Proteomic Analysis. Analytical Chemistry*, 2004. 76(17): p. 4951-4959.
101. Molloy, M.P., et al., *Large-scale evaluation of quantitative reproducibility and proteome coverage using acid cleavable isotope coded affinity tag mass spectrometry for proteomic profiling. Proteomics*, 2005. 5(5): p. 1204-1208.
102. Gygi, S.P., et al., *Proteome Analysis of Low-Abundance Proteins Using Multidimensional Chromatography and Isotope-Coded Affinity Tags. Journal of Proteome Research*, 2002. 1(1): p. 47-54.
103. Old, W.M., et al., *Comparison of label-free methods for quantifying human proteins by shotgun proteomics. Mol Cell Proteomics*, 2005. 4(10): p. 1487-502.
104. Liu, H., R.G. Sadygov, and J.R. Yates, *A Model for Random Sampling and Estimation of Relative Protein Abundance in Shotgun Proteomics. Analytical Chemistry*, 2004. 76(14): p. 4193-4201.
105. Hendrickson, E.L., et al., *Comparison of spectral counting and metabolic stable isotope labeling for use with quantitative microbial proteomics. Analyst*, 2006. 131(12): p. 1335-1341.
106. Choi, H., D. Fermin, and A.I. Nesvizhskii, *Significance Analysis of Spectral Count Data in Label-free Shotgun Proteomics. Molecular & Cellular Proteomics*, 2008. 7(12): p. 2373-2385.
107. Reinert, K., et al., *OpenMS - A Framework for Quantitative HPLC/MS-Based Proteomics. Computational Proteomics, Dagstuhl Seminar Proceedings, Internationales Begegnungs- und Forschungszentrum für Informatik (IBFI), Schloss Dagstuhl, Germany, 2006.*
108. Sturm, M., et al., *OpenMS - An open-source software framework for mass spectrometry. BMC Bioinformatics*, 2008. 9(1): p. 163.

109. *May, D., et al., A Platform for Accurate Mass and Time Analyses of Mass Spectrometry Data. Journal of Proteome Research, 2007. 6(7): p. 2685-2694.*
110. *Smith, C., et al., XCMS: processing mass spectrometry data for metabolite profiling using nonlinear peak alignment, matching, and identification. Analytical Chemistry, 2006. 78(3): p. 779 - 787.*
111. *Fitzgibbon, M., et al., Open-Source Platform for the Analysis of Liquid Chromatography-Mass Spectrometry (LC-MS) Data. 2008. p. 369-381.*
112. *Pasa-Tolic, L., et al., Proteomic analyses using an accurate mass and time tag strategy. Biotechniques, 2004. 37(4): p. 621-4, 626-33, 636 passim.*
113. *Norbeck, A.D., et al., The utility of accurate mass and LC elution time information in the analysis of complex proteomes. J Am Soc Mass Spectrom, 2005. 16(8): p. 1239-49.*
114. *Shen, Y., et al., Making Broad Proteome Protein Measurements in 1¹/₂ min Using High-Speed RPLC Separations and High-Accuracy Mass Measurements. Analytical Chemistry, 2005. 77(23): p. 7763-7773.*
115. *Shen, Y., et al., Ultrahigh-Throughput Proteomics Using Fast RPLC Separations with ESI-MS/MS. Analytical Chemistry, 2005. 77(20): p. 6692-6701.*
116. *Kriz, W., Kaissling, B, Structural Organization of the Mammalian Kidney. The Kidney: Physiology and Pathophysiology, 2008. 4th Ed(Chapter 29): p. 479-564.*
117. *Biber, J., et al., Regulation of phosphate transport in proximal tubules. Pflugers Arch, 2009. 458(1): p. 39-52.*
118. *Bobulescu, I.A. and O.W. Moe, Luminal Na(+)/H (+) exchange in the proximal tubule. Pflugers Arch, 2009. 458(1): p. 5-21.*
119. *Kenny, A.J. and S. Maroux, Topology of microvillar membrane hydrolases of kidney and intestine. Physiol Rev, 1982. 62(1): p. 91-128.*

120. *Del Valle, P.L., et al., Characterization of glucose transport by cultured rabbit kidney proximal convoluted and proximal straight tubule cells. In Vitro Cell Dev Biol Anim, 2002. 38(4): p. 218-27.*
121. *Curthoys, N.P. and O.H. Lowry, The distribution of glutaminase isoenzymes in the various structures of the nephron in normal, acidotic, and alkalotic rat kidney. J Biol Chem, 1973. 248(1): p. 162-8.*
122. *Curthoys, N.P. and T. Kuhlenschmidt, Phosphate-independent glutaminase from rat kidney. Partial purification and identity with gamma-glutamyltranspeptidase. J Biol Chem, 1975. 250(6): p. 2099-105.*
123. *Minamide, L.S. and J.R. Bamberg, A filter paper dye-binding assay for quantitative determination of protein without interference from reducing agents or detergents. Anal Biochem, 1990. 190(1): p. 66-70.*
124. *McIntyre, T.M. and N.P. Curthoys, Comparison of the hydrolytic and transfer activities of rat renal gamma-glutamyltranspeptidase. J Biol Chem, 1979. 254(14): p. 6499-504.*
125. *Craig, R. and R.C. Beavis, TANDEM: matching proteins with tandem mass spectra. Bioinformatics, 2004. 20(9): p. 1466-7.*
126. *Fenyo, D. and R.C. Beavis, A method for assessing the statistical significance of mass spectrometry-based protein identifications using general scoring schemes. Anal Chem, 2003. 75(4): p. 768-74.*
127. *Elias, J.E. and S.P. Gygi, Target-decoy search strategy for increased confidence in large-scale protein identifications by mass spectrometry. Nat Methods, 2007. 4(3): p. 207-14.*
128. *Kall, L., et al., Assigning significance to peptides identified by tandem mass spectrometry using decoy databases. J Proteome Res, 2008. 7(1): p. 29-34.*
129. *Sokol, R.R., Rohlf, F.J., in Biometry: The principles and practice of statistics in biological research. 1994. 3rd Ed.*
130. *Zhang, B., et al., Detecting differential and correlated protein expression in label-free shotgun proteomics. J Proteome Res, 2006. 5(11): p. 2909-18.*

131. *Benjamini, Y. and D. Yekutieli, The control of the false discovery rate in multiple testing under dependency. Annals of Statistics, 2001. 29: p. 1165-1188.*
132. *Beissbarth, T., et al., Statistical modeling of sequencing errors in SAGE libraries. Bioinformatics, 2004. 20 Suppl 1: p. i31-9.*
133. *Dennis, G., Jr., et al., DAVID: Database for Annotation, Visualization, and Integrated Discovery. Genome Biol, 2003. 4(5): p. P3.*
134. *Huang da, W., B.T. Sherman, and R.A. Lempicki, Systematic and integrative analysis of large gene lists using DAVID bioinformatics resources. Nat Protoc, 2009. 4(1): p. 44-57.*
135. *Paoletti, A.C. and M.P. Washburn, Quantitation in proteomic experiments utilizing mass spectrometry. Biotechnol Genet Eng Rev, 2006. 22: p. 1-19.*
136. *Ronco, P., et al., Distribution of enkephalinase (membrane metalloendopeptidase, E.C. 3.4.24.11) in rat organs. Detection using a monoclonal antibody. Lab Invest, 1988. 58(2): p. 210-7.*
137. *Vekaria, R.M., et al., Immunolocalization of ectonucleotidases along the rat nephron. Am J Physiol Renal Physiol, 2006. 290(2): p. F550-60.*
138. *Furriols, M., et al., rBAT, related to L-cysteine transport, is localized to the microvilli of proximal straight tubules, and its expression is regulated in kidney by development. J Biol Chem, 1993. 268(36): p. 27060-8.*
139. *Burch, H.B., et al., The location of glutamine synthetase within the rat and rabbit nephron. Biochem Biophys Res Commun, 1978. 82(2): p. 498-505.*
140. *Lu, M., et al., Interaction between aldolase and vacuolar H⁺-ATPase: evidence for direct coupling of glycolysis to the ATP-hydrolyzing proton pump. J Biol Chem, 2001. 276(32): p. 30407-13.*
141. *Lu, M., et al., The glycolytic enzyme aldolase mediates assembly, expression, and activity of vacuolar H⁺-ATPase. J Biol Chem, 2004. 279(10): p. 8732-9.*

142. Lu, M., et al., *Physical interaction between aldolase and vacuolar H⁺-ATPase is essential for the assembly and activity of the proton pump. J Biol Chem, 2007. 282(34): p. 24495-503.*
143. Yanez, A.J., et al., *Nuclear localization of liver FBPase isoenzyme in kidney and liver. FEBS Lett, 2003. 550(1-3): p. 35-40.*
144. Ovadi, J. and P.A. Srere, *Macromolecular compartmentation and channeling. Int Rev Cytol, 2000. 192: p. 255-80.*
145. Gerich, J.E., et al., *Renal gluconeogenesis: its importance in human glucose homeostasis. Diabetes Care, 2001. 24(2): p. 382-91.*
146. Iynedjian, P.B., F.J. Ballard, and R.W. Hanson, *The regulation of phosphoenolpyruvate carboxykinase (GTP) synthesis in rat kidney cortex. The role of acid-base balance and glucocorticoids. J Biol Chem, 1975. 250(14): p. 5596-603.*
147. Rasmussen, M., et al., *Glutamatergic or GABAergic neuron-specific, long-term expression in neocortical neurons from helper virus-free HSV-1 vectors containing the phosphate-activated glutaminase, vesicular glutamate transporter-1, or glutamic acid decarboxylase promoter. Brain Res, 2007. 1144: p. 19-32.*
148. Sastrasinh, M. and S. Sastrasinh, *Effect of acute pH change on mitochondrial glutamine transport. Am J Physiol, 1990. 259(6 Pt 2): p. F863-6.*
149. Wright, P.A. and M.A. Knepper, *Glutamate dehydrogenase activities in microdissected rat nephron segments: effects of acid-base loading. Am J Physiol, 1990. 259(1 Pt 2): p. F53-9.*
150. Wright, P.A. and M.A. Knepper, *Phosphate-dependent glutaminase activity in rat renal cortical and medullary tubule segments. Am J Physiol, 1990. 259(6 Pt 2): p. F961-70.*
151. Schoolwerth, A.C., et al., *Changes in mRNAs for enzymes of glutamine metabolism in kidney and liver during ammonium chloride acidosis. Am J Physiol, 1994. 267(3 Pt 2): p. F400-6.*

152. *Preisig, P.A. and R.J. Alpern, Chronic metabolic acidosis causes an adaptation in the apical membrane Na/H antiporter and basolateral membrane Na(HCO₃)₃ symporter in the rat proximal convoluted tubule. J Clin Invest, 1988. 82(4): p. 1445-53.*
153. *Weiner, I.D. and J.W. Verlander, Molecular physiology of the Rh ammonia transport proteins. Curr Opin Nephrol Hypertens, 2010. 19(5): p. 471-7.*
154. *Bishop, J.M., et al., Role of the Rhesus Glycoprotein, Rh B Glycoprotein, in Renal Ammonia Excretion. Am J Physiol Renal Physiol, 2010. 299: p. F1087-1093.*
155. *Biver, S., et al., A role for Rhesus factor Rhcg in renal ammonium excretion and male fertility. Nature, 2008. 456(7220): p. 339-43.*
156. *Gunaratne, R., et al., Quantitative phosphoproteomic analysis reveals cAMP/vasopressin-dependent signaling pathways in native renal thick ascending limb cells. Proc Natl Acad Sci U S A, 2010. 107(35): p. 15653-8.*
157. *Sachs, A.N., et al., LC-MS/MS analysis of differential centrifugation fractions from native inner medullary collecting duct of rat. Am J Physiol Renal Physiol, 2008. 295(6): p. F1799-806.*
158. *Rinschen, M.M., et al., Quantitative phosphoproteomic analysis reveals vasopressin V2-receptor-dependent signaling pathways in renal collecting duct cells. Proc Natl Acad Sci U S A, 2010. 107(8): p. 3882-7.*
159. *Da Silva, N., et al., Proteomic analysis of V-ATPase-rich cells harvested from the kidney and epididymis by fluorescence-activated cell sorting. Am J Physiol Cell Physiol. 298(6): p. C1326-42.*
160. *Goldstrohm, D.A., et al., Importance of manual validation for the identification of phosphopeptides using a linear ion trap mass spectrometer. J. Biomolec Techniq., 2011. in press.*
161. *Khositseth, S., et al., Quantitative protein and mRNA profiling shows selective post-transcriptional control of protein expression by vasopressin in kidney cells. Mol Cell Proteomics, 2010. 10(1): p. M110 004036.*

162. Xie, L., et al., *Quantitative analysis of aquaporin-2 phosphorylation. Am J Physiol Renal Physiol*, 2010. 298(4): p. F1018-23.
163. Hwang, S., et al., *Vasopressin increases phosphorylation of Ser84 and Ser486 in Slc14a2 collecting duct urea transporters. Am J Physiol Renal Physiol*, 2010. 299(3): p. F559-67.
164. Walmsley, S.J., et al., *Proteomic analysis of brush-border membrane vesicles isolated from purified proximal convoluted tubules. Am J Physiol Renal Physiol*, 2010. 298(6): p. F1323-31.
165. Doctor, R.B., et al., *Distribution of epithelial ankyrin (Ank3) spliceoforms in renal proximal and distal tubules. Am J Physiol*, 1998. 274(1 Pt 2): p. F129-38.
166. Vinay, P., A. Gougoux, and G. Lemieux, *Isolation of a pure suspension of rat proximal tubules. Am J Physiol*, 1981. 241(4): p. F403-11.
167. Keller, A., et al., *Empirical Statistical Model To Estimate the Accuracy of Peptide Identifications Made by MS/MS and Database Search. Analytical Chemistry*, 2002. 74(20): p. 5383-5392.
168. Nesvizhskii, A.I., et al., *A statistical model for identifying proteins by tandem mass spectrometry. Anal Chem*, 2003. 75(17): p. 4646-58.
169. Paoletti, A.C., et al., *Quantitative proteomic analysis of distinct mammalian Mediator complexes using normalized spectral abundance factors. Proc Natl Acad Sci U S A*, 2006. 103(50): p. 18928-33.
170. Polpitiya, A.D., et al., *DAnTE: a statistical tool for quantitative analysis of omics data. Bioinformatics*, 2008. 24(13): p. 1556-8.
171. Ashburner, M., et al., *Gene ontology: tool for the unification of biology. The Gene Ontology Consortium. Nat Genet*, 2000. 25(1): p. 25-9.
172. Shiozawa, M., et al., *A monoclonal antibody against human kidney gamma-glutamyl transpeptidase: preparation, immunochemical, and immunohistochemical characterization. J Histochem Cytochem*, 1989. 37(7): p. 1053-61.

173. *Walmsley, S.J., et al., Proteomic analysis of brush-border membrane vesicles isolated from purified proximal convoluted tubules. Am J Physiol Renal Physiol. 298(6): p. F1323-31.*
174. *Dass, P.D. and T.C. Welbourne, Adaptation of gamma-glutamyltransferase to acidosis. Life Sci, 1980. 26(23): p. 1985-90.*
175. *Zhang, Y., et al., Effect of Dynamic Exclusion Duration on Spectral Count Based Quantitative Proteomics. Analytical Chemistry, 2009. 81(15): p. 6317-6326.*
176. *MacGregor, E.A., S. Janecek, and B. Svensson, Relationship of sequence and structure to specificity in the [alpha]-amylase family of enzymes. Biochimica et Biophysica Acta (BBA) - Protein Structure and Molecular Enzymology, 2001. 1546(1): p. 1-20.*
177. *Gao, J., et al., Changes in the Protein Expression of Yeast as a Function of Carbon Source. Journal of Proteome Research, 2003. 2(6): p. 643-649.*
178. *Vallon, V., Molecular determinants of renal glucose reabsorption. Focus on "Glucose transport by human renal Na⁺/D-glucose cotransporters SGLT1 and SGLT2". Am J Physiol Cell Physiol, 2011. 300(1): p. C6-8.*
179. *Paroder, V., et al., Na⁺/monocarboxylate transport (SMCT) protein expression correlates with survival in colon cancer: Molecular characterization of SMCT. Proceedings of the National Academy of Sciences, 2006. 103(19): p. 7270-7275.*
180. *Wade, J.B., et al., Localization and interaction of NHERF isoforms in the renal proximal tubule of the mouse. Am J Physiol Cell Physiol, 2003. 285(6): p. C1494-503.*
181. *Levi, M., Role of PDZ Domain-Containing Proteins and ERM Proteins in Regulation of Renal Function and Dysfunction. Journal of the American Society of Nephrology, 2003. 14(7): p. 1949-1951.*
182. *Pagliari, A.S. and A.D. Goodman, Relation of renal cortical gluconeogenesis, glutamate content, and production of ammonia. J Clin Invest, 1970. 49(11): p. 1967-74.*

183. *Roobol, A. and G.A. Alleyne, Control of renal cortex ammoniogenesis and its relationship to renal cortex gluconeogenesis. Biochim Biophys Acta, 1974. 362(1): p. 83-91.*
184. *Harris, S.J. and D.J. Winzor, Interactions of glycolytic enzymes with erythrocyte membranes. Biochimica et Biophysica Acta (BBA) - Protein Structure and Molecular Enzymology, 1990. 1038(3): p. 306-314.*
185. *Yun, C.H., et al., cAMP-mediated inhibition of the epithelial brush border Na⁺/H⁺ exchanger, NHE3, requires an associated regulatory protein. Proc Natl Acad Sci U S A, 1997. 94(7): p. 3010-5.*
186. *McDonough, A.A., Motoring down the microvilli. Focus on "PTH-induced internalization of apical membrane NaPi2a: role of actin and myosin VI". Am J Physiol Cell Physiol, 2009. 297(6): p. C1331-2.*
187. *Blaine, J., et al., PTH-induced internalization of apical membrane NaPi2a: role of actin and myosin VI. Am J Physiol Cell Physiol, 2009. 297(6): p. C1339-46.*
188. *Croizet-Berger, K., et al., The endocytic catalysts, Rab5a and Rab7, are tandem regulators of thyroid hormone production. Proceedings of the National Academy of Sciences of the United States of America, 2002. 99(12): p. 8277-8282.*
189. *Huang, F., et al., Analysis of Clathrin-mediated Endocytosis of Epidermal Growth Factor Receptor by RNA Interference. Journal of Biological Chemistry, 2004. 279(16): p. 16657-16661.*
190. *Strittmatter, E.F., et al., Proteome analyses using accurate mass and elution time peptide tags with capillary LC time-of-flight mass spectrometry. Journal of the American Society for Mass Spectrometry, 2003. 14(9): p. 980-991.*
191. *May, D., et al., Peptide sequence confidence in accurate mass and time analysis and its use in complex proteomics experiments. J Proteome Res, 2008. 7(12): p. 5148-56.*
192. *Krokhin, O.V., et al., An Improved Model for Prediction of Retention Times of Tryptic Peptides in Ion Pair Reversed-phase HPLC. Molecular & Cellular Proteomics, 2004. 3(9): p. 908-919.*

193. Xia, Q., et al., *Differential quantitative proteomics of Porphyromonas gingivalis by linear ion trap mass spectrometry: non-label methods comparison, q-values and LOWESS curve fitting. Int J Mass Spectrom, 2007. 259(1-3): p. 105-116.*
194. Cramer, S.C., et al., *Colocalization of GLUT2 glucose transporter, sodium/glucose cotransporter, and gamma-glutamyl transpeptidase in rat kidney with double-peroxidase immunocytochemistry. Diabetes, 1992. 41(6): p. 766-70.*
195. Dominguez, J.H., et al., *Glucose transporters of rat proximal tubule: differential expression and subcellular distribution. Am J Physiol, 1992. 262(5 Pt 2): p. F807-12.*
196. Nanni, P., et al., *Differential proteomic analysis of HT29 Cl.16E and intestinal epithelial cells by LC ESI/QTOF mass spectrometry. Journal of Proteomics, 2009. 72(5): p. 865-873.*
197. Nanni, P., et al., *A label-free nano-liquid chromatography-mass spectrometry approach for quantitative serum peptidomics in Crohn's disease patients. Journal of Chromatography B, 2009. 877(27): p. 3127-3136.*